Universitetet
i Stavanger

FACULTY OF SCIENCE AND TECHNOLOGY

MASTER'S THESIS

Study programme/specialisation: Offshore Technology/ Marine and Subsea Technology	Spring / ~~Autumn semester,~~ 2018.. Open/~~Confidential~~
Author: Akinlawon Oluwafemi Adejuwon	Akin Adejuwon ..... (signature of author)

Programme coordinator:
Professor Daniel Karunakaran, University of Stavanger and Subsea7

Supervisor(s):
Professor Daniel Karunakaran

Title of master's thesis:

Ultra-Deep water High Pressure Riser Concept Offshore Brazil

Credits: 30

Keywords: Steel Lazy Wave Risers, Spread Moored FPSO, Ultra-Deep water, Strength and Fatigue Response Analysis, X65, X80, X90	Number of pages: .....105..... + supplemental material/other: ..19..... Stavanger,...June 15, 2018..... date/year

University of Stavanger

subsea 7

Ultra-Deepwater High Pressure Riser Concept Offshore Brazil

A thesis presented to the University of Stavanger
for the award of Degree of Master of Science

Akinlawon Oluwafemi Adejuwon
Student Number: 238207
Offshore Technology/ Marine and Subsea Technology
Spring 2018

Abstract

Since the 1950s, risers have continued to be an important part of an oil and gas producing field. As the primary equipment that conveys fluids to and from the topside vessel, it is important that a riser is designed to withstand all conditions it will be subjected to during its lifetime. With hydrocarbon exploration activities moving into ultra-deep water, research related to the structural integrity of a riser deployed in ultra-deep water has become necessary.

The ultra-deep water region considered in this thesis work is the Santos Basin located about $300km$ offshore Brazil. The Santos Basin is a benign environment that is not characterized by hurricanes, typhoons or extreme weather conditions. However, oil producing activities in this region would require a vessel that has storage capabilities due to the distance the region is from shore. With this requirement in mind, different floaters were evaluated and a spread-moored Floating Production, Storage and Offloading (FPSO) vessel was selected for this thesis work.

The selection of the spread-moored FPSO presented a new challenge; high motion sensitivity. Since FPSOs are high motion vessels, risers connected to them will experience fatigue damage in their touchdown zone. However, after evaluation of different riser concepts, the Steel Lazy Wave Riser(SLWR) was selected because it has the ability to decouple its touchdown zone from vessel motions due to the presence of buoyancy modules fitted along the lower section of the riser.

With the selection of spread-moored FPSO and a SLWR, material selection for the SLWR was carried out. For ultra-deep water deployment, a riser's material should posses ultra-high strength, good weldability, high collapse resistance, high operating pressure and excellent low-temperature toughness. These material properties are found in the API 5L X65,X80 and X90 carbon steel grade material. Hence, they were the selected material used for the SLWRs in this thesis work. Dynamic and fatigue response analysis was conducted on the SLWRs made of each material and it was observed that all the three materials met the requirements of the DNV-OS-F201 reference standard with the X65 riser having the worst dynamic response, followed by the X80 riser, followed by the X90 riser.

Also in past SLWR deployments with spread-moored FPSOs, risers were usually connected to hang-off points along the port side of the vessel. In this thesis work,

the SLWRs were connected to hang-off points both along the port side of the vessel and along the middle of the vessel. The purpose of doing this was to investigate if buoyancy can be saved by connecting a riser along the middle of the vessel rather than the along the port side. From the results of the investigation, it was observed that about 7.5% of buoyancy could be saved by connecting a riser to the middle of the vessel rather than to the port side of the vessel. In addition, it was observed that risers connected to the middle of the vessel showed an increase of at least 246% in the minimum fatigue life observed.

Overall, all the riser materials considered in this study all meet the dynamic and fatigue response criteria. Therefore, further work should be carried out as given in the recommendations of this thesis work to select the most suitable material for deployment in the ultra-deep water region of the Santos Basin, offshore Brazil.

Acknowledgement

I would like to thank the almighty God who has given me the grace and strength to complete this thesis work.

I would like to thank my parents and siblings for the support, encouragement and guidance they have given to me up to this point in my life.

I would like to thank Professor Daniel Karunakaran for given me the opportunity to write my thesis under his guidance. His insightful knowledge and great understanding of my thesis work pushed me in the right direction and I will forever be grateful to him for this opportunity.

I am very grateful to Subsea7 AS Stavanger, for providing me with desk space and all the necessary resources that made this thesis work a success.

My sincere gratitude goes to Dr. Adekunle Orimolade for the valuable contributions, advice and even motivation you gave to me through out this thesis work. I can not thank you enough for the assistance you gave me during the strength and fatigue analysis conducting in this thesis work.

My heartfelt appreciation goes to Oystein Doskeland for the excellent help you gave me with your programing skills. This thesis work would have taken a lot longer to complete without your help.

To the whole Hydrodynamics and Ocean Technology group at Subsea7 AS, Stavanger, I say a very big thank you.

Finally, to Venkatesan Elumalai AKA the man, the myth, the legend, thank you very much for being the best desk mate I could have asked for.

Table of Contents

List of Figures

List of Tables

Abbreviations

ALS	Accidental Limit State
BSR	Buoy Supported Riser
COBRA	Catenary Offset Buoyant Riser Assembly
DDF	Deep Draft Floater
DP	Dynamic Positioning
FLIP	Floating Instrument Platform
FLS	Fatigue Limit State
FPDSO	Floating Production Drilling Storage and Offloading
FPS	Floating Production System
FPSO	Floating Production Storage and Offloading
FPU	Floating Production Unit
FSO	Floating Storage and Offloading
GoM	Gulf of Mexico
HRT	Hybrid Riser Tower
RAOs	Response Amplitude Operators
SCF	Stress Concentration Factor
SCR	Steel Catenary Riser
SHR	Single Hybrid Riser
SLOR	Grouped Single Line Offset Riser
SLS	Serviceability Limit State

SLWR	Steel Lazy Wave Catenary Riser
SS	Semisubmersible
TCR	Tethered Catenary Riser
TDP	Touch Down Point
TLP	Tension Leg Platform
TTR	Top Tensioned Riser
UK	United Kingdom
ULS	Ultimate Limit State

Chapter 1

Introduction

1.1 Background

Kerr McGee birthed the offshore industry in 1947 when he installed a platform out of sight in the GoM at a water depth of about 6 meters. Seventy-one years later, the demand for more energy has led to the exploration of offshore regions with challenging water depths. Water depth offshore is classified as shallow, deep or ultra-deep. In this thesis, shallow water, deep water and ultra-deepwater will be defined as water depths ranging from 0-600m, 601-2199m, $\geq$2200m respectively.

Figure 1.1 shows various deep and ultra-deepwater developments by Shell Global over the past forty years. It is also observed from Figure 1.1 that at water depths greater than 450m, the choice of production platform changes from a fixed platform to a floating platform because fixed platforms are not economically and structurally feasible beyond this depth. However, the use of floating platforms presented a new challenge; the dynamic loading of connected equipment.

The primary equipment connected to the floating platform is a large-diameter pipe called a riser. It connects the floating platform to the subsea infrastructure. Risers, developed in the 1950s, were first used for drilling purposes offshore of California. Today, risers are used for four main purposes (Sparks, 2007):

- Drilling
- Completion/workover
- Production/injection
- Export lines

The focus of interest in this thesis is on risers used for production purposes. A production riser is used during the production phase of a field to convey fluids to and from the platform. However, the design of a production riser is very complex (Bai & Bai, 2005).

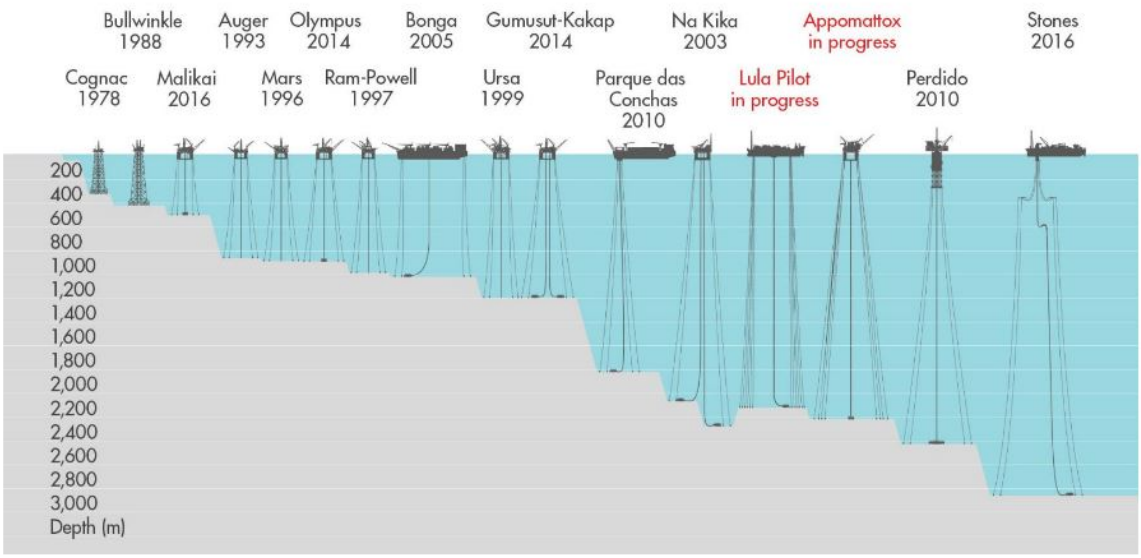

Figure 1.1: A history of deep and ultra deep water developments (Shell Global, 2016)

Risers are also grouped in terms of their physical properties. Based on physical properties, there are three major types of risers; steel risers, flexible risers and hybrid risers. Of these three types of risers, steel risers are most commonly used in deep and ultra-deep water developments because of their economic and structural feasibility at these great water depths. The first application of a steel riser as a production riser was on the Shell Auger Tension Leg Platform(a low motion vessel) in 1993. It was installed in a catenary shape hence it was called a Steel Catenary Riser (SCR).

Though the SCR is an attractive configuration for deep and ultra-deepwater developments, it has a poor dynamic performance when used with high motion vessels. This flaw lead to the development of a new configuration by Karunakaran et al (1996) called the Low Long Wave configuration with a better dynamic performance when compared to the SCR. To further improve the dynamic performance of the Low Long Wave configuration, buoyancy elements where added to riser region before the Touch Down Zone (TDZ) to help decouple the TDZ from vessel motions.

The Low Long Wave configuration, now referred to as the Steel Lazy Wave Riser configuration, was deployed for the first time in 2008 by Shell Global at the Parque das Conchas Field in Brazil at a water depth of 1800m. It was also deployed in the Caesar Tonga field in 2012 at a water depth of about 1500m. The most recent deployment was in the Stones Field in 2016 at a world record depth of approximately 2900m.

1.2 Research Objectives and Scope

The main objective of this thesis is to investigate the deployment of Steel Lazy Wave Risers in ultra-deep water regions offshore of Brazil. The thesis aims to:

- Evaluate and assess different floaters and determine their applicability in this region.
- Evaluate and assess different riser concepts, factors affecting the selection of riser concepts and also aim to justify the use of the SLWR concept for this region.
- Investigate and compare the dynamic performance of different riser hang-off points on the FPSO.
- Investigate and compare the strength and fatigue response of SLWRs made up of X65, X80 and X90 carbon steel.
- Suggest a suitable riser hang-off point and carbon steel material to be used for the deployment of the SLWR in this region.

1.3 Research Justification

At the commencement of this study, the SLWR has been deployed Offshore of Brazil only at a water depth of approximately 1800 meters. This water depth falls in the range of deep water according to the ranges of water depth defined by this thesis. Therefore, there is a need to investigate the performance of the SLWR in ultra-deep water offshore of Brazil as there are oil field blocks in this region that will be developed in the nearest future.

Chapter 2

Overview of Deepwater Floaters

2.1 Introduction

The economic and structural limits of fixed platforms have restrained their applications to only shallow waters. In deep and ultra-deepwater, floating platforms, also known as floaters, are suspended by buoyancy and not by a supporting structure that extends to the seabed as is the case for fixed platforms. Therefore, an increase in water depth increases the cost and weight of a floating platform linearly and a fixed platform exponentially. Hence, floaters have become the preferred choice of application in deep and ultra-deepwater.

There are different types of floaters used in deep and ultra deepwater developments. They include the following:

- Tension Leg Platform (TLP)(Deep water)
- Spar Platforms
- Semisubmersible
- Floating Production, Storage and Offloading (FPSO)
- Floating Production Drilling Storage and Offloading (FPDSO)

2.2 Tension Leg Platforms

The ever-growing need to conduct drilling and producing operations in deeper waters led to the development of the TLP concept in 1975. Afterwards, a prototype TLP named the Deep Oil X-1, was successfully installed offshore of California and was found to be exceptionally stable in the severe storms of the region (Brewer, 1975). However, it was not until 1984 that the first TLP was installed to develop the Hutton Field located at a water depth of 144m, 130km northeast of the Shetland Islands, UK North Sea.

Since then, TLPs have been deployed at various deepwater fields at different locations. Table 2.1 gives information on the deepest TLPs installed to the best knowledge of the author as at the time of writing this thesis.

Name of Field	**Location**	**Operator**	**Water Depth(m)**
Magnolia	GoM	Conoco	1425
Marco Polo	GoM	Anadarko	1310
Neptune	GoM	BHB Billiton	1295
Kizomba	Angola	Exxon	1177
Ursa	GoM	Shell	1158
Allegheny	GoM	Eni	1021
West Seno	Indonesia	Chevron	1005

Table 2.1: The deepest TLPs installed

TLPs are built of either steel or concrete, and they consist of a hull anchored to the seafloor by vertically-oriented tension cables hence, the name "Tension Leg Platforms". These tension cables virtually eliminate the heave, pitch and roll motions of the platform and also act as a restoring or station-keeping force when weather causes the platform to surge, sway, and yaw.

According to Brewer (1975), TLPs have several advantages when compared to fixed platforms in that:

- They are well suited for use in earthquake zones since they are not rigidly attached to the seafloor. Seismic excitation of the anchors would be attenuated through the long anchor cables.
- They may be easily relocated. They can be easily moved if a few delineation wells indicate that the platform should have been located in a different position
- They have applicability to a wide range of uses and locations in that the same basic platform could be re-outfitted for different applications.
- The time required for field development could be reduced since its fabrication is possible prior to field discovery. After field discovery, the proper length of tension leg cables could be obtained, outfitting completed, and the platform installed.

TLPs are not used as storage units because they are very sensitive to payloads as a result of the tensioning effects of the vertical cables that anchor them to the sea floor. They usually need pipeline infrastructure or FSOs to export produced oil (Paik & Thayamballi, 2007).

2.3 Spar Platforms

The concept of the Spar platform can be traced back to the Floating Instrument Platform (FLIP) built in 1962 for oceanographic measurements (F. Fisher & Spiess, 1963). However, in the 1970s, Shell pioneered the use of this concept in the offshore industry with the construction of the Brent spar for oil storage and offloading in the North Sea (Bax, de Werk, et al., 1974). In 1996, the first Spar built for production, the Ornyx Neptune Spar, was installed at a water depth of 588m in the GoM.

Table 2.2 presents different Spar platforms that have been installed at deep and ultradeep water depths.

Spar Name	Location	Operator	Water Depth(m)
Perdido	GoM	Shell	2450
Lucius	GoM	Anadarko	2164
Horn Mountain	GoM	BP	1645
Heidelberg	GoM	Anadarko	1620
Red Hawk	GoM	Anadarko	1615
Constitution	GoM	Anadarko	1524
Diana	GoM	ExxonMobil	1432

Table 2.2: Spar Platforms installed in deep and ultra deepwater

Technically, a spar consists of a vertical cylinder which provides buoyancy to support facilities above the water surface. Its stability is derived from the fact that the location of its centre of gravity is below the location its center of buoyancy. Station keeping of a Spar is provided by lateral, catenary anchor lines which may be attached to the hull near its center of pitch for low dynamic loadings(Halkyard, 1996).

The most obvious features of a Spar are its extreme draft, straight sides, large centrewell and large displacement which make it a very competitive candidate for deep and ultra-deep water applications(Glanville, Paulling, Halkyard, Lehtinen, et al., 1991). Glanville et al. (1991) discussed the following advantages of a Spar platform:

- Simplicity of design
- Favorable motion characteristics
- Insensitivity to water depth
- Possibility of supporting high deck load
- Centrewell provides protection for risers from wave loads
- Risers can be supported in tension by means of flotation

- Low cost shipyard construction
- Availability of oil storage capacity
- Can be easily relocated

2.4 Semi-submersibles

Semi-submersibles were initially used for drilling purposes in the early 1960s. The first SS used for production was the Argyll FPU. It was converted from the Transocean58 drilling semi-submersible and used in the Argyll oil field, UK North Sea in 1975. Over the next decade, more semi-submersibles such as the P-09, P-15, P-12, P-21, all owned by Petrobras, were converted from drilling rigs into production platforms. However, in 1986, the first production purpose semi-submersible was built for the Balmoral field located at a water depth of 150m, in the UK North Sea.

As years went by, technologically sophisticated semi-submersibles were built to operate at even greater water depths. Table 2.3 shows some semi-submersibles operating in deep water.

Semi-submersible Name	**Location**	**Operator**	**Water Depth(m)**
Atlantis PQ	GoM	BP	2156
Blind Faith	GoM	ChevronTexaco	1980
Nakika	GoM	BP	1936
P-52	Brazil	Petrobras	1795
Thunder Hawk	GoM	Murphy	1740
P-55	Brazil	Petrobras	1707
P-36	Brazil	Petrobras	1360

Table 2.3: Semi-submersiblesoperating in deepwater.

A semi-submersible unit has submerged ballasted pontoons that provide most of its buoyancy. These pontoons are connected to the platform deck located well above the sea level by ring or rectangular columns. Chain-or-Wired mooring systems are usually used for the station-keeping of semi-submersibles(Paik & Thayamballi, 2007). Typically, the draft of a semi-submersible is about 25 meters. However, when stability needs to be increased, the draft may be increased to achieve better motion response.

Semi-submersibles have become a favourable choice for operations in benign deep water environment because their natural periods are above the natural wave periods except for waves in extreme sea states. Some advantages and disadvantages of semi-submersibles were discussed by Barltrop (1998) and they include the following:

Advantages of Semi-submersibles

- They have a good and stable response to wave action
- They allow for a large number of flexible risers because there is no weathervaning system

Disadvantages of Semi-submersibles

- Pipeline infrastructure or other means is required to export produced oil.
- Only a limited number of (rigid) risers can be supported because of the bulk of the tensioning systems required.
- Considering that most semi-submersible production systems are converted from drilling rigs, the topside weight capacity or a converted semi-submersible is usually limited
- Building schedules for semi-submersibles are usually longer than those for ship-shaped offshore structures.

2.5 FPSOs

Floating Production, Storage and Offloading systems as the name implies, have the combined ability to produce, store and offload oil and gas. Since the first FPSO was built for Shell in 1977, over 260 FPSOs have been built and deployed worldwide in shallow, deep and ultra deepwater. FPSOs are very competitive in remote locations where oil reserves are too small to justify the construction of a purpose platform or when it will be too expensive to install long distance pipelines to an onshore terminal. FPSOs are easy to install, relocate, and can carry heavy deckload.

As at the time of this study, the Egina FPSO is the biggest FPSO in the world with a storage capacity of 2.3 million barrels of oil. In addition, the Turritela FPSO (see Figure 2.1) is the world's deepest FPSO operating in the GoM at a water depth of 2900m.

FPSOs are majorly ship-shaped vessels and are held up by their buoyancy. For station-keeping, they are anchored to the seabed with either the use of chain-or-wired mooring lines or thrusters. The difference in the mode of station-keeping of FPSOs gives birth to three different types of FPSOs namely:

- Spread Moored FPSOs
- Turret Moored FPSOs
- Dynamic Positioned FPSOs

Figure 2.1: The Turritela FPSO
(Shell Global, 2016)

2.5.1 Spread Moored FPSOs

In spread moored FPSOs, the mooring lines are connected to the bow and stern of the vessel are independent of risers. Risers are hung off the side of the vessel, and there is little practical limit to the number of risers that can installed. Spread moored FPSOs are usually deployed in benign environments or in locations dominated by one wind or wave direction. They are most often less expensive than turret moored FPSO. Figure 2.2 by England et al. (2001) shows an illustration of the spread moored FPSO.

2.5.2 Turret-Moored FPSOs

The turret moored FPSO is a weathervaning vessel as a result of the presence of a turret that integrates the FPSO's mooring system, the installation equipment for the anchor legs and the risers, the fluid-transfer system including riser support, manifold, pig launching and receiving, metering, chemical injection, and subsea control systems into one compact, self-contained module (England et al., 2001). It is usually deployed in harsh environments due to its weathervaning properties.

Turrets can be grouped into two major types: permanent and disconnectable turret system. The permanent turret system is categorized based on the location of the turret; internal and external turret system. In the internal turret system, the turret is mounted within the hull while in the external turret system, the turret is mounted on an extended structure cantilevered off the vessel bow. Figure 2.3 and 2.4 give an illustration of internal and external mooring systems.

In a disconnectable turret system, a part of the system usually a buoy, has

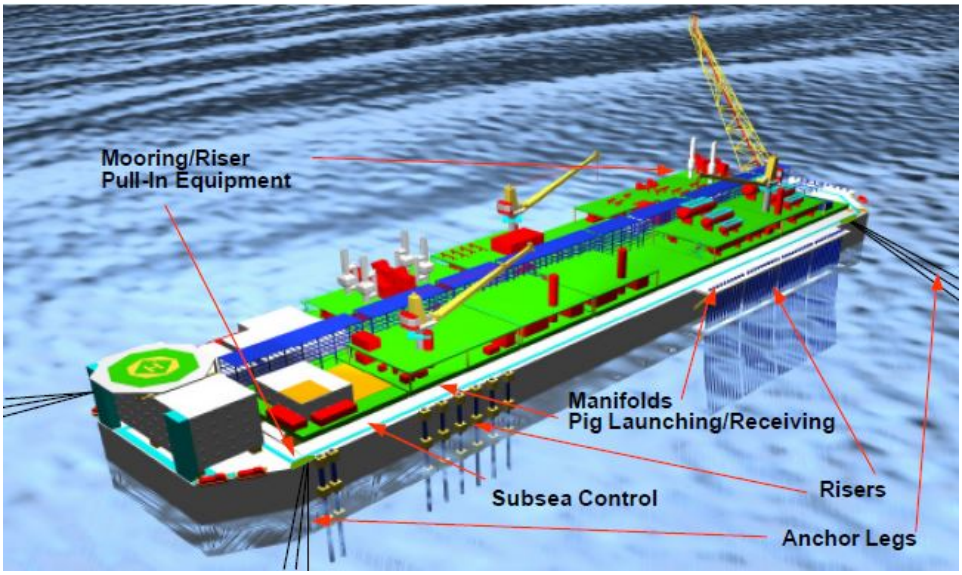

Figure 2.2: Spread Moored FPSO
(England et al., 2001)

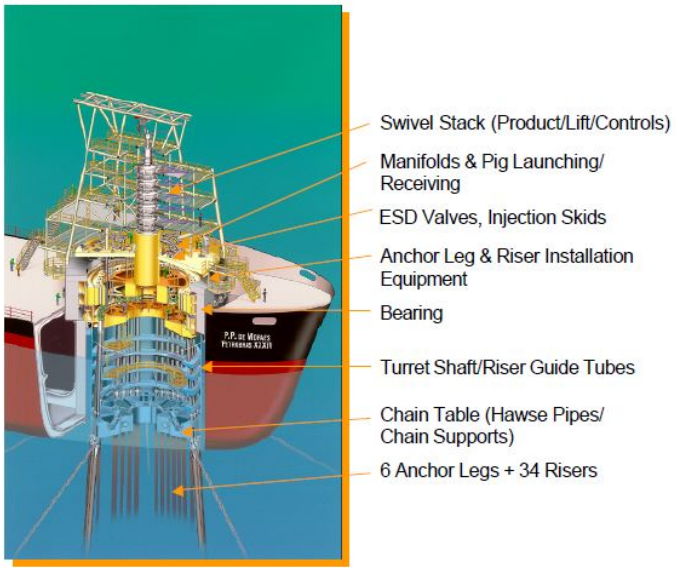

Figure 2.3: Internal Turret Mooring System
(England et al., 2001)

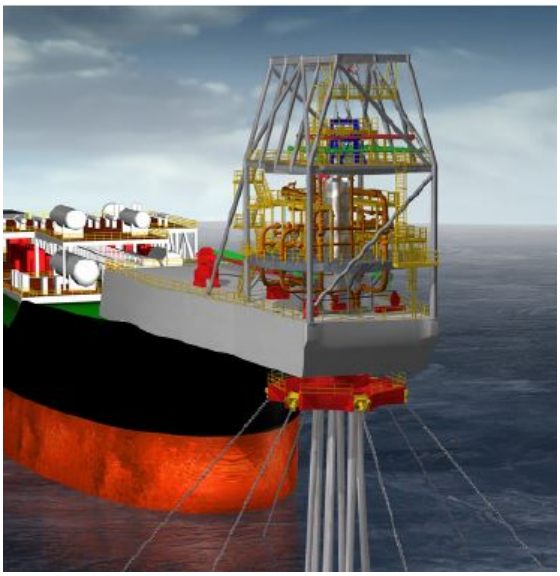

Figure 2.4: External Turret Mooring System
(England et al., 2001)

disconnectable attributes in the event that extreme environmental conditions approach e.g. a Hurricane. The FPSO disconnects from the buoy and sails to safety. This makes it clear that the environmental conditions of field are a major factor in deciding the type of turret mooring system to use. An example of an FPSO that uses a disconnectable turret system is the FPSO Turritela deployed in the Stones oil and gas field, GoM.

2.5.3 Dynamically Positioned FPSOs

The Dynamic Positioning(DP) technology was originally used by drillships in the early 1960s operating in deep and ultra deepwater. Decades later, the FPSO Seillean became the first dynamically positioned FPSO constructed for the offshore industry.

Dynamically Positioned FPSOs use azimuth or transverse tunnel thrusters located at the front, back and sides of the vessel for station keeping. Unlike, turret and spread moored FPSOs, they do not require anchor cables or mooring lines to maintain their positions. In environments characterized by typhoons and hurricane occurrences such as the South China Sea and GoM, they are used in combination with a disconnectable turret system that enables quick disconnection of the riser system from the vessel during extreme weather conditions.

The basic principle applied during the design of a DP FPSO is that a single failure shall not lead to a critical situation caused by loss of position or heading (Lopez-Cortijo, Duggal, Van Dijk, Matos, et al., 2003). Hence, it is important that a DP FPSO fulfills all reliability requirements before deployment as a failure could

lead to a catastrophic disaster.

DP FPSOs are generally more expensive than spread and turret moored FPSOs in operating expenditure as a result of the fuel requirements of the DP system.

2.6 Selection of Floater Concept

Several technical factors including environmental conditions, riser concepts, topsides loads, storage capacity, floater motion characteristics as well as commercial and risk factors including technology maturity, local content, market requirements, shipyards capacities help to determine the most suitable floater concept for a field development (Toro et al., 2015).

In the previous sections, Tension Leg Platforms, Spars, Semi-submersibles and FPSOs have all being reviewed. However, for the ultra-deep water region(Santos Basin) that will be considered in this thesis, TLPs are not feasible. Spars have been used in ultra-deep water regions (e.g The Perdido Spar) in the past in the GoM but they are yet to be used offshore Brazil. Therefore, the Spar platform concept is not a proven technology in this region.

This presents two final options; a Semi-submersible and a FPSO unit. Since the region in consideration 300 km away from shore, there is a need for the floater to have storage capacity. The limited storage capacity of a Semi-submersible makes it an undesirable concept for this region making the FPSO the winning floater concept. Although the FPSO has been selected to be the winning floater concept, the type of FPSO to be used still has to be determined.

Environmental conditions majorly determine the type of FPSO to be used. Offshore Brazil is a benign environment that is not characterized by hurricanes, typhoons or extreme weather conditions. Therefore, there is little or no need for a turret moored FPSO leaving the spread moored and dynamic positioned FPSO as the remaining options. Most of the FPSOs Offshore Brazil as observed by this study are spread moored. The high capital and operating expenditure of a dynamic positioned FPSO makes the spread moored FPSO a more attractive option and the selected floater for this thesis.

Chapter 3

Overview of Deepwater Riser Systems

3.1 Introduction

As established in the chapter 2, the spread moored FPSO is selected as the floater concept for this thesis. In this chapter, various riser concepts will be reviewed with the intention of selecting the most suitable concept to be used in combination with the Spread Moored FPSO in this Study.

Following from the discussion in Chapter 1, the primary equipment that connects the floater to the subsea infrastructure is called a riser and it serves four main purposes; drilling, completion/workover, production/injection and export lines.

According to DNV (2010c),

- Drilling risers provide fluid transportation to and from the well; support auxiliary lines, guide tools, and drilling strings; serve as a running and retrieving string for the BOP.
- Completion/workover risers are temporary risers used for completion and workover operations and include any equipment between the subsea tree/tubing hanger and the workover floaters tensioning system.
- Production risers transport fluids produced from the reservoir. Injection risers transport fluids to the producing reservoir or a convenient disposal or storage formation.
- Export risers transfer the processed fluids from/to the floater/structure to/from another facility, which may include another platform/floater or pipeline.

Based on physical properties, there are three main types of risers namely flexible risers, steel(rigid) risers and hybrid risers which are combinations of both flexible and steel risers. They will be discussed in the following sections.

3.2 Flexible Risers

Flexible risers have been used since the 1970s and they have found applications in shallow and deep waters in Brazil, North Sea, GoM and West Africa. However, with oil exploration and production moving into ultra-deep water, the use of flexible risers has become technologically and economically challenging.

Flexible risers are made up of several layers (see Figure 3.1) that perform different functions. As a result of this, they take up large motions and combine low bending stiffness with high axial tensile stiffness by use of helical or tensile armouring and polymer sealing layers (DNV, 2010a). There are two main types of flexible risers; the bonded flexible riser and the unbonded flexible riser. In a bonded flexible riser, the layers of the riser are free to move while in an unbonded flexible riser, the layers are locked together with the use of a polymer material.

The deployment of flexible risers in ultra-deep water is restricted by the capabilities of the risers to withstand the high external hydrostatic pressures they will experience at these depths (Carter, Ronalds, et al., 1998). However, in recent times, the flexible riser technology has been qualified for water depths of up to 3000m as a result of the use of composite materials such as carbon fibre and innovative solutions to resist corrosive fluids, potentially combined with high temperature and high pressure fluid (Luppi, Cousin, O'Sullivan, et al., 2014).

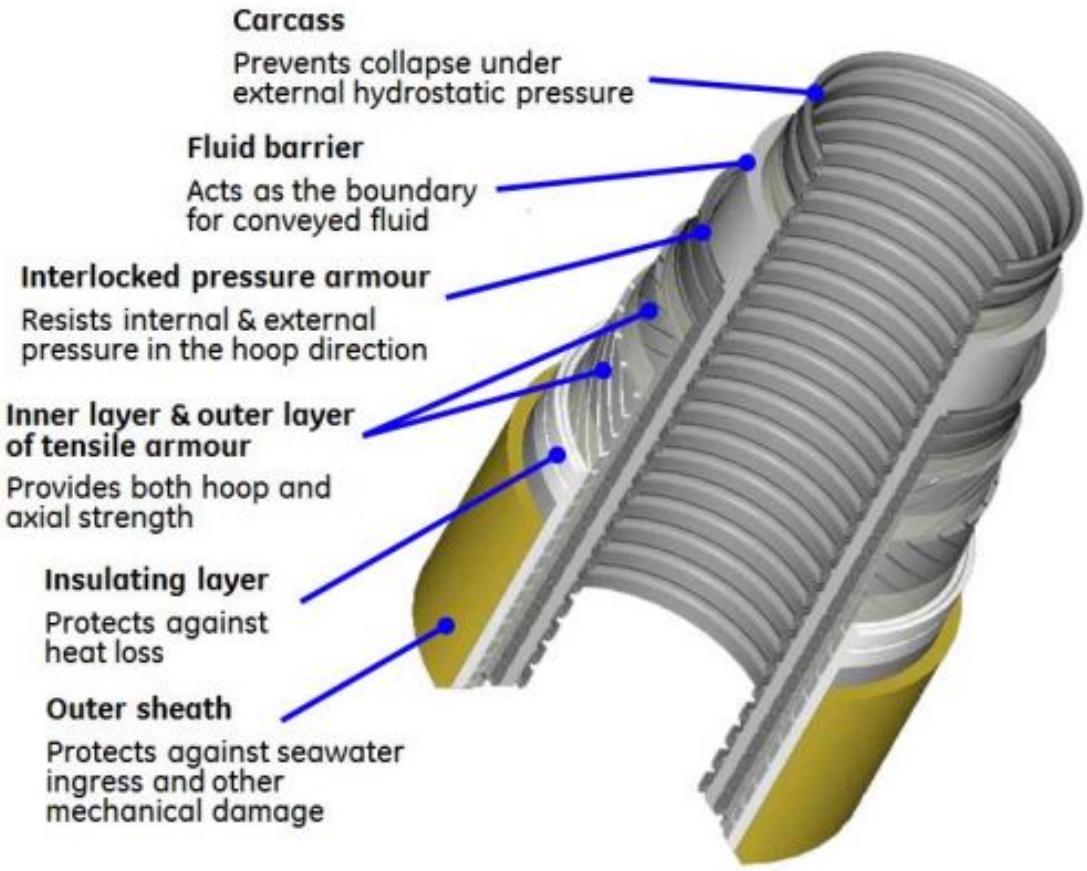

Figure 3.1: A typical flexible riser (Jha et al., 2013)

3.3 Rigid Steel Risers

Steel risers, mainly made from low carbon steel such as X60, X65 and X70, have been used in various deep and ultra deepwater field developments. They are relatively cheap and available in larger diameters when compared to flexible risers. They also have higher axial strength than flexible risers which gives them the ability to be effectively suspended at great water depths (Huang & Hatton, 1996).

Steel risers can be configured in different ways and in this study, the focus will be on the SCR and SLWR configuration.

3.3.1 Steel Catenary Riser Configuration

Since the first SCR was installed on the Shell Auger TLP in 1993, SCRs have gained acceptability and have been deployed in deep and ultra deepwater regions. They

have been used in combination with all the floaters discussed in chapter 2 of this thesis in benign environments such as GoM, West Africa and Brazil.

SCRs are cheap, available in large diameters, have the ability to withstand high temperatures and pressure, easy to install and maintain, and have very simple designs. A typical SCR configuration is illustrated in Figure 3.2.

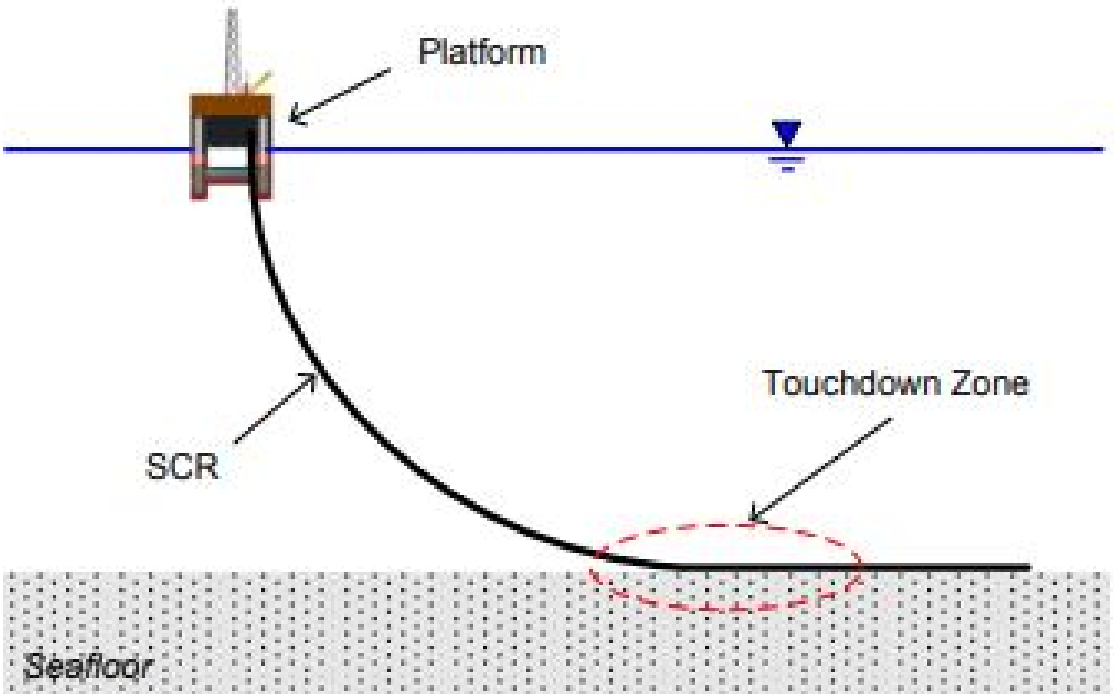

Figure 3.2: Steel Catenary Riser Configuration (You et al., 2008)

The major drawback of the SCR is its poor dynamic performance, especially when combined with high motion vessels such as semi-submersibles and FPSOs. These vessels induce large dynamic loads thus generating a significant amount of fatigue particularly at the hang-off and touchdown zone of the SCR. Karunakaran et al. (2002) improved the dynamic performance of SCRs by using coatings with different densities which varied weight along the riser. The study of karunakaran et al. (2013) also showed that the attachment of weights such as ballast modules above the Touch Down Point(TDP) and buoyancy wraps at the TDP improved the fatigue response of SCRs.

3.3.2 Steel Lazy Wave Riser Configuration

The fatigue problems of SCRs lead to the development of the SLWR configuration by Karunakaran et al (1996). In a SLWR configuration, buoyancy modules are added along the length of the riser just before the touchdown region. These modules create an uplift force that generates a lazy wave configuration which helps decouple the vessel motions from the touchdown zone and improve the strength and fatigue performance of the riser in the touch down zone.

The SLWR configuration is a field-proven concept and it was first deployed in the Parques das Conchas field, Brazil in 2008 by Shell. Recently, the SLWR was also used in the Stones oil and gas field by Shell in the GoM which happens to be the deepest field development in the world at a water depth of approximately 2900m.

Geometrically, the SLWR has four sections namely the upper catenary section, buoyancy section, lower catenary section and the bottom section. Figure 3.3 gives an illustration of the SLWR configuration.

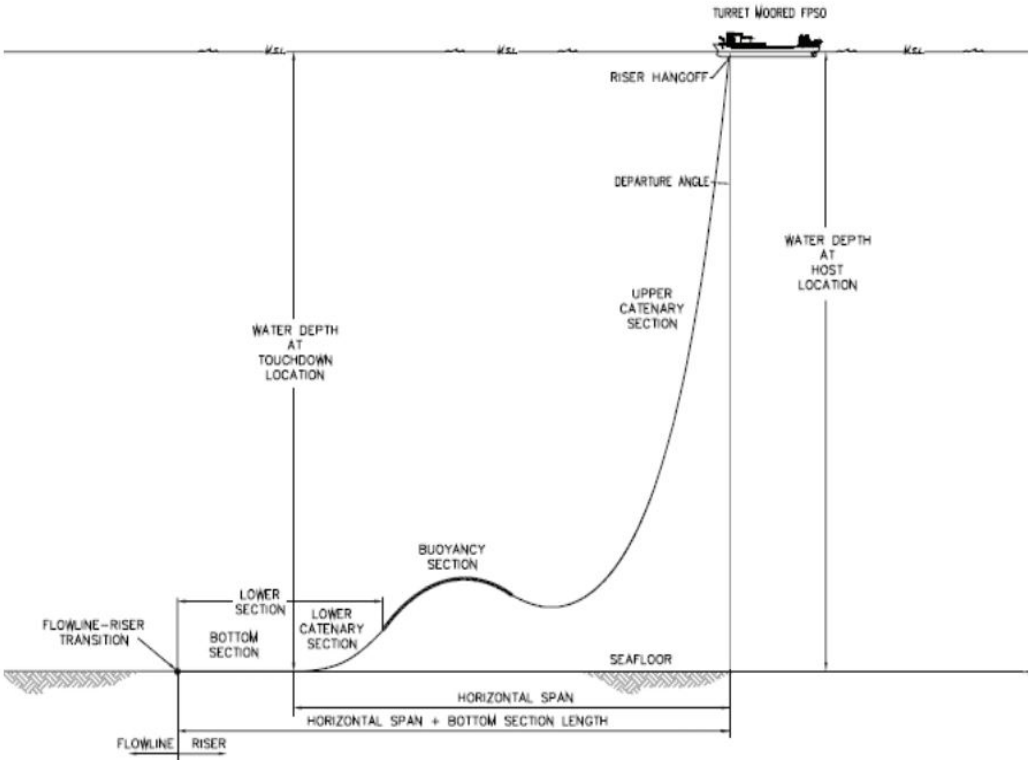

Figure 3.3: Steel Lazy Wave Riser Configuration (Hoffman et al., 2010)

The geometry of these sections are not easily determined. However, Cheng et al. (2013) introduced a design approach based on intuitive observation to define the

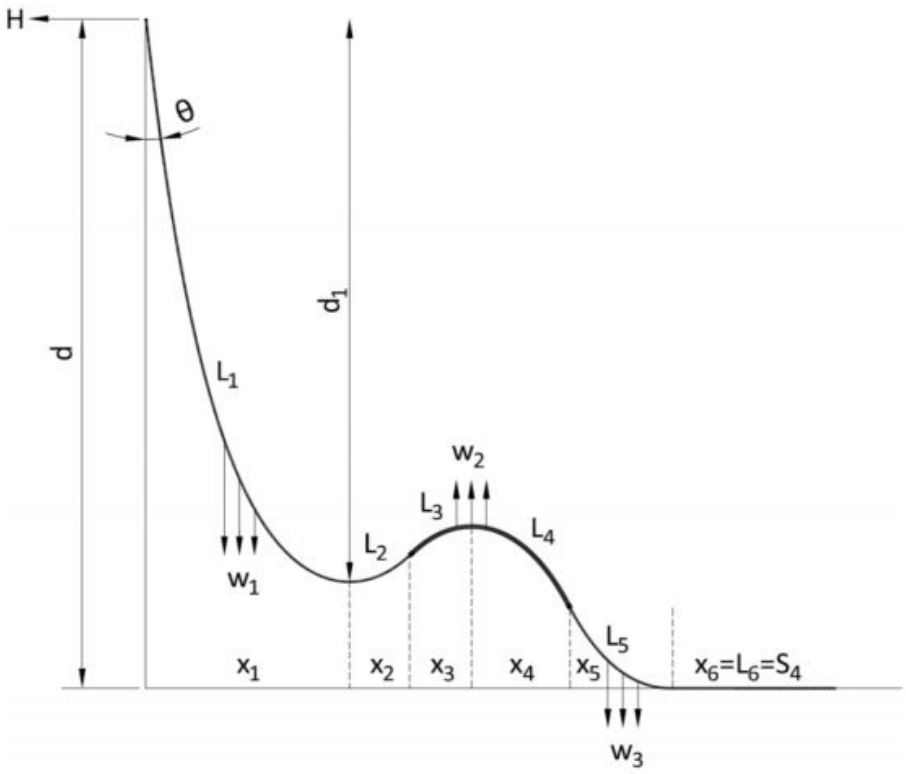

Figure 3.4: Geometry of a Steel Lazy Wave Riser Configuration (Cheng & Cao, 2013)

initial static geometry of the SLWR. The initial static geometry is of significant importance because it directly affects the results of the dynamic analysis of the SLWR. In Figure 3.4, the sections of the SLWR are labeled with parameters and variables that can be inputted into equations to obtain the initial static geometry of the SLWR shape. The parameters include:

d	Water depth
H	The horizontal force for SLWR system
w_1	The submerged weight for upper catenary section
w_2	The submerged weight of the middle buoyancy section
w_3	The submerged weight of the lower catenary section
$L_i(i = 1, 2, 3, ..., 6)$	Segment length for each segment
$x_i(i = 1, 2, 3, ..., 6)$	Scope for each segment
$S_1 = L_1 + L_2$	The upper catenary section length
$S_3 = L_5$	The submerged weight of the lower catenary section

variables include:

d_1	Equivalent riser payload water depth
θ	Departure Angle
$S_2 = L_3 + L_4$	The middle buoyancy section length

The equations proposed by Cheng include the following:

$$a_1 \sinh\left(\frac{x_1}{a_1}\right) + a_1 \sinh\left(\frac{x_3}{a_2}\right) = L_1 + L_2 = S_1 \tag{3.1}$$

$$a_2 \sinh\left(\frac{x_3}{a_2}\right) + a_2 \sinh\left(\frac{x_5}{a_3}\right) = L_3 + L_4 = S_2 \tag{3.2}$$

$$a_1 \cosh\left(\frac{x_1}{a_1}\right) - (a_1 + a_2) \cosh\left(\frac{x_3}{a_2}\right) + (a_2 + a_3) \cosh\left(\frac{x_5}{a_3}\right) = a_3 + d \tag{3.3}$$

Where $a_1 = \frac{H}{w_1}$; $a_2 = \frac{H}{w_2}$; $a_3 = \frac{H}{w_3}$ are the minimum local radii of curvature at the sag bend, arch bend, and touchdown locations, respectively. The buoyancy ratio is also an important design parameter and is defined as:

$$\text{Buoyancy ratio} = 1 + \frac{w_2}{w_1} = 1 + \frac{a_1}{a_2} \tag{3.4}$$

The equations above can be solved if the values for the departure angle, equivalent payload water depth, and buoyancy section length are known. These equations also indicate the balance of weight and buoyancy. The net buoyancy of segment L_3 lifts the weight of segment L_2, the net buoyancy of segment L_4 lifts the weight of segment L_5; therefore the riser payload equals to the weight of segment L_1 part of the upper catenary riser, which is governed by d_1 (Cheng & Cao, 2013).

3.4 Hybrid Risers

The first installation of a hybrid riser concept was in 1988 at the Placid Green Canyon Block 29 Project (Fisher & Berner, 1988). The three decades that followed witnessed

the development of various hybrid riser concepts which were developed and applied in fields located in deepwater regions (see Table 2.3). These concepts include the Single Hybrid Riser (SHR), Hybrid Riser Tower (HRT) and the Buoy Supported Riser (BSR) concepts. Other hybrid riser concepts that have been developed include the Tethered Catenary Riser (TCR), Catenary Offset Buoyant Riser Assembly (COBRA) and the Grouped Single Line Offset Riser (SLOR) concept. However, these concepts are yet to be field-proven at the time of this writing.

Name of Field	**Location**	**HR Concept**	**Water Depth(m)**
Guara-Lula	Brazil	BSR	2153
Girassol	Angola	HRT	1350
Kizomba	Angola	SHR	1349
Placid Green Canyon	GoM	HRT	469

Table 3.1: Field Proven Hybrid Riser Concepts

Generally, a hybrid riser concept consists of flexible jumpers, a buoyancy tank, tethers/tendon, upper riser assembly, steel riser, lower riser assembly, bottom rigid spool, and a suction anchor. The functions of these components as documented by Brouard et al (2016), are presented below:

- Flexible Jumper(s): Acts as a connection from the buoyancy tank to the floater on the sea surface.
- Buoyancy Tank: Provides uplift load to the risers. It also absorbs floater motions thereby limiting the transfer of dynamic stresses to the risers.
- Tethers and Tendon: Holds the submerged buoyancy tank to the seabed.
- The Upper Riser Assembly: Terminates the riser pipe/bundle section and allow the transfer of mechanical load from the buoyancy tank to the riser pipe/bundle and ensures the connection of the risers to the flexible jumpers. In the case of the HRT concept, it is called the Upper Riser Tower Assembly (URTA).
- The Rigid Riser/Riser Bundle: Consists of a riser pipe as in the SHR or a group of risers which are arranged around a central structural pipe as in the HRT concept. Other hybrid riser concepts use SCRs or SLWRs.
- The Lower Riser Assembly: Allows the transfer of mechanical loads from the riser pipe/bundle to the suction anchor through Flexible Joints and ensures the connection of the risers to the Flowlines at the bottom through the Rigid Spool. In the case of the HRT concept, it is called the Lower Riser Tower Assembly.
- The Bottom Rigid Spool: Connects the risers or risers in the bundle to the Flowlines on the seabed.

- The Suction Anchor: Anchors the HRT, SLOR and SHR to the seabed.

The use of hybrid risers in field developments offers advantages such as the possibility of pre-installation prior to floater arrival, little or no dynamic excitation of risers leading to longer fatigue life, reduced riser loads on the floater, ultra-deep water applications (COBRA and BSR). However, the cost of hybrid risers falls between the cost of SCRs and flexible risers (Sworn, 2005).

3.4.1 Hybrid Riser Tower

The (HRT) concept was first installed in the Placid Green Canyon Block 29 project back in 1988 in the GoM (Fisher & Berner, 1988). It can be defined as a bundled, free-standing vertical riser with near surface flexible connections. It is basically configured, as illustrated in Figure 3.5, with the following elements from bottom up:seabed foundation, flexible joint/flowline jumpers, riser bundle, buoyancy tank, flexible jumpers (Sworn, 2005).

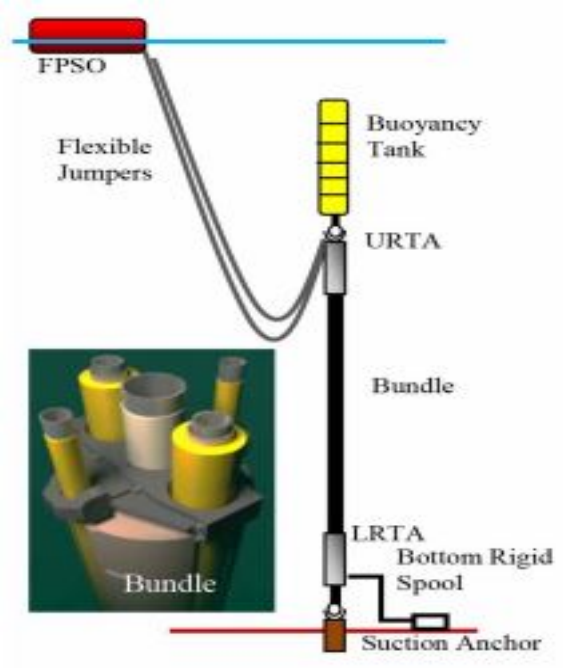

Figure 3.5: Hybrid Riser Tower Configuration (Brouard et al., 2016)

Benefits of the HRT concept includes the following:

- Subsea footprint is minimal since risers all converge at the base of the tower.
- The design of individual product lines can be changed without major impact on dynamic performance of the system.

- The payload on the floater is reduced.
- Installation can be carried out before the floater is in place.
- They are applicable in deepwater fields

3.4.2 Buoy Supported Riser

A Buoy Supported Riser (BSR) concept consists of a subsurface buoy that is submerged and connected with steel risers coming from the wells on one side and flexible jumpers connected to the floater on the surface on the other side. The buoy is moored to the seabed with multiple tethers and absorbs the motions of the floater thereby limiting the transfer of dynamic stresses to the risers (Hiller, Karunakaran, Cruz, Tadeu, et al., 2015).

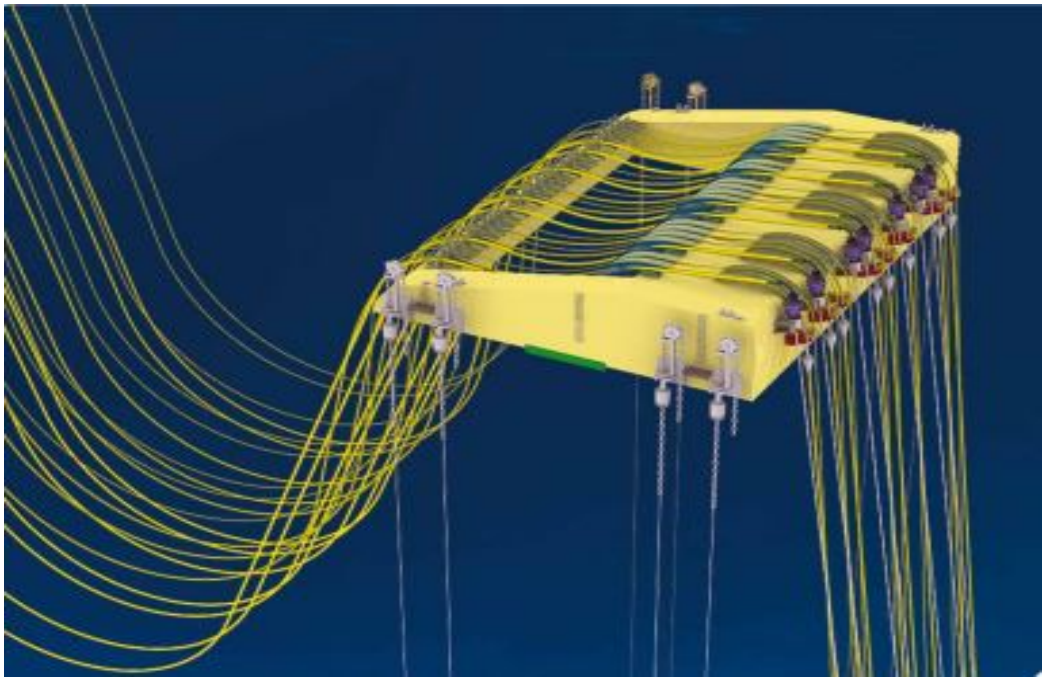

Figure 3.6: The Buoy used in the Guara-Lula Project Project by Subsea7 for Petrobras

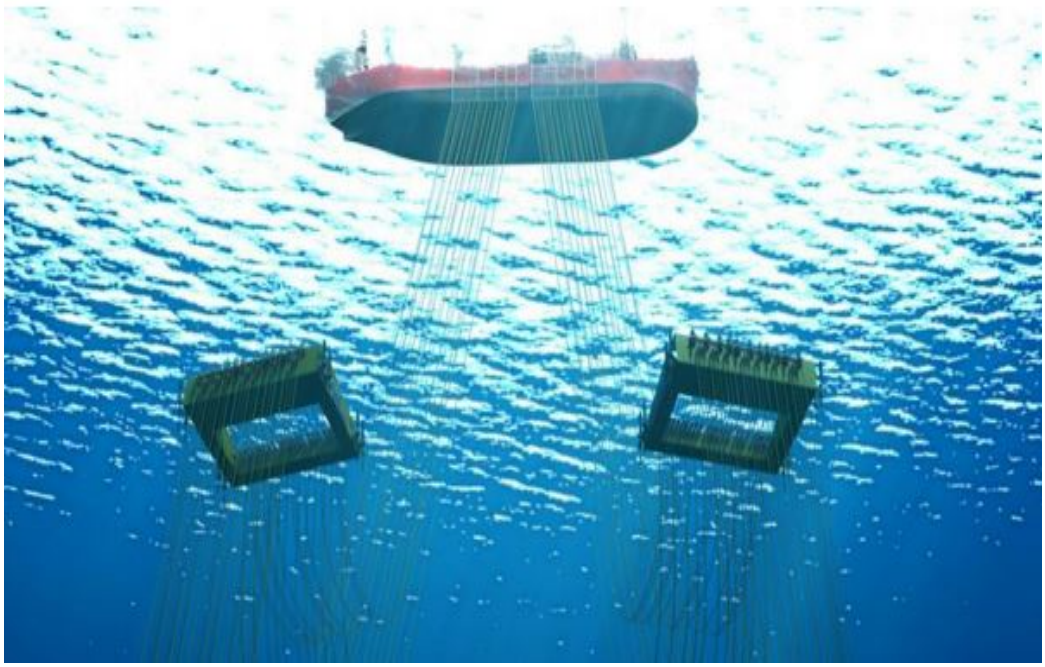

Figure 3.7: Buoy Supported Riser Concept in Guara-Lula Project by Subsea7 for Petrobras

Subsea7 pioneered the installation of a large scale BSR system for Petrobras in the Sapinhoa-Lula NE field at a water depth of about 2200m in the Santos Basin, offshore Brazil. In this BSR system, the Buoy was moored to the seabed by 8 tethers(2 at each end) and supports 27 SCRs. An illustration of the size of the buoy used in the sapinhoa-lula field development is given in Figure 3.6.

3.4.3 Tethered Catenary Riser

Proposed by Subsea7, the Tethered Catenary Riser (TCR) concept is an attractive concept for deepwater developments all over the world. It consists of a number of SCRs supported by a subsurface buoy which is tethered down to the seabed by means of a single pipe tendon and anchored by means of a suction pile which makes it different from a BSR. The floater and the buoy are then connected by flexible jumpers. It is advantageous in that the flexible jumpers absorb the motions of the floaters thereby limiting the dynamic excitation of the rigid risers (Legras, 2013). See Figure 3.8 for an illustration of the Tethered Catenary Riser concept.

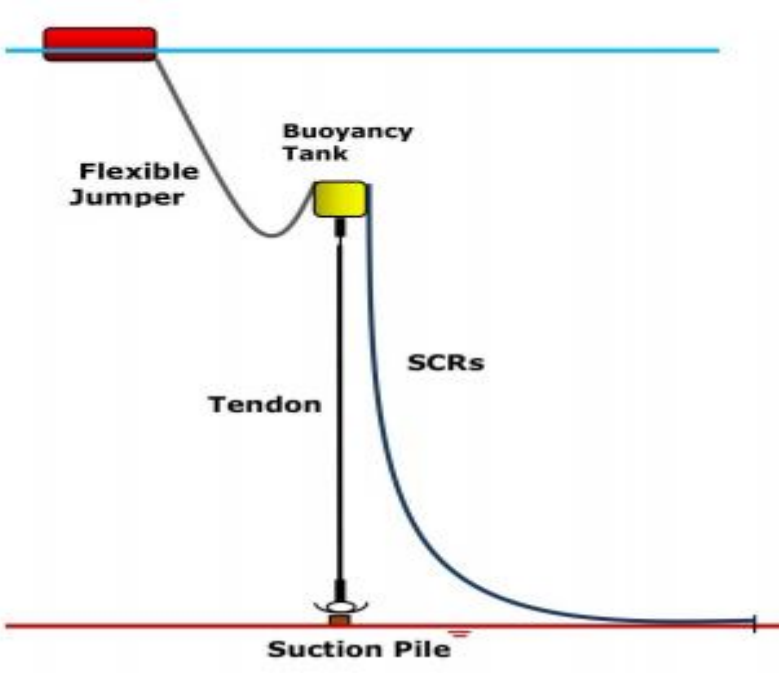

Figure 3.8: The Tethered Catenary Riser concept (Brouard et al., 2016)

3.4.4 Catenary Offset Buoyant Riser Assembly

The Catenary Offset Buoyant Riser Assembly (COBRA) concept, developed for a water depth of up to 3000m in benign and harsh environments, combines the simplicity and economical features of the SCR with the motion handling capabilities of a hybrid riser tower. As a variation to the Catenary Bundle Riser developed by Subsea7, the COBRA consists of a catenary riser section with a long, slender buoyancy module which is tethered to the seabed. The buoyancy module is then connected to the floater through a flexible a jumper (Karunakaran & Baarholm, 2013). An illustration of the COBRA concept is given in Figure 3.9.

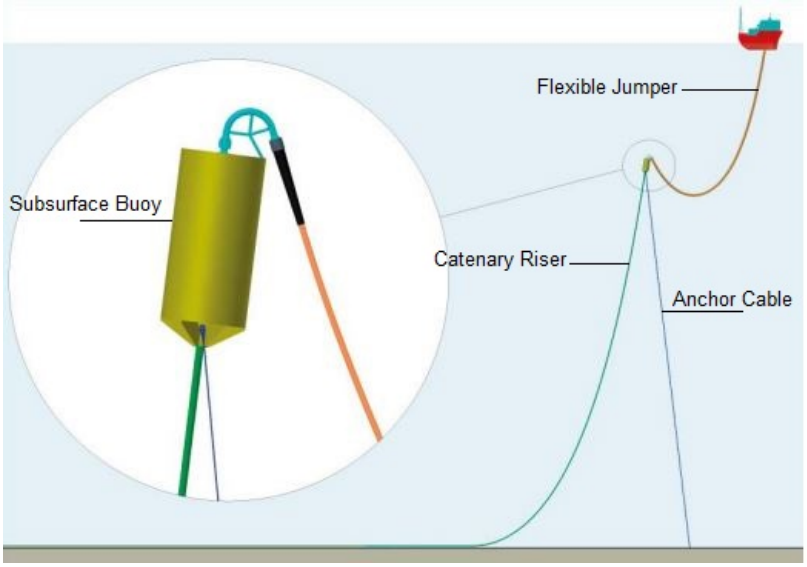

Figure 3.9: The COBRA concept (Karunakaran & Baarholm, 2013)

3.5 On the Selection of the SLWR Concept

Apparent from the above write-up is the review of different deep water and ultra-deep water riser systems. The ultra-deep water region that will be considered in this study eliminates the use of flexible risers since they are not able to withstand the high external hydrostatic pressure at this water depth.

With the hybrid riser concepts, the water depth challenge is eliminated. However, the costs and complexity of design and installation do not make them an attractive option for the purpose of this thesis.
SCRs have poor dynamic performances with high motion vessels like the FPSO. Since the FPSO is the selected floater for this study, the SCR option is eliminated. As a result of this, the SLWR is the selected riser concept for this study because of its great dynamic performance and fatigue response.

Chapter 4

Applicable Riser Design Codes and Standards

4.1 Introduction

Over the years, various international codes and standards have been developed to ensure that a riser is designed, manufactured, fabricated, installed, operated and maintained with the safety of personnel and protection of the environment in mind.

The pioneer standard for the design of production risers was the API-RP-2RD: Design of Risers for Floating Production Systems and Tension Leg Platforms published in 1998. In 2001, Det Norske Veritas (DNV) published another riser design standard, the DNV-OS-F201: Dynamic Risers Offshore Standard, with a new design approach in addition to the suggested approach of the API-RP-2RD.

Since the DNV-OS-F201 (now referred to as DNVGL-ST-F201 as of January 2018) contains the two riser design approaches, it will be the selected standard used for the design of the SLWR in this study. In the next section, a review of the design philosophy, design principles and design approaches of the DNV-OS-F201 will be presented.

4.2 DNV-OS-F201

The DNV-OS-F201 standard gives criteria, requirements and guidance on structural design and analysis of an offshore dynamic riser. According to DNV-OS-F201, a riser should be designed, manufactured, fabricated, operated and maintained in such a way that:

- with acceptable probability, it will remain fit for its intended use, having due regard to its service life and its cost, and

- with appropriate degree of reliability, it will sustain all foreseeable load effects and other influences likely to occur during the service life and have adequate durability in relation to maintenance costs.

The DNV-OS-F201 recommends two design approaches for riser design. These approaches include the Load Resistance Factor Design(LRFD) Approach and the Working Stress Design(WSD) Approach.

4.2.1 DNV-OS-F201: LFRD Approach

A riser is exposed to both static and dynamic loads throughout its lifetime. These static and dynamic loads are further categorized into pressure, functional, environmental and accidental loads(see Table 4.1) and a riser should be design to withstand their effects. However, these effects have uncertainties.

In the LFRD approach, the uncertainties of the effects of these loads are accounted for with the use of partial safety factors. The general LRFD safety format can be expressed as (DNV, 2010c):

$$g(S_p; \gamma_F \cdot S_F; \gamma_E \cdot S_E; \gamma_A \cdot S_A; R_k; \gamma_{sc}; \gamma_m; \gamma_c; t) \leq 1 \tag{4.1}$$

where:

S_p	Pressure loads
S_F	Load effect from functional loads
S_E	Load effect from environmental loads
S_A	Load effect from accidental loads
γ_F	load effect factor for functional loads
γ_E	load effect factor for environmental loads
γ_A	load effect factor for accidental loads
R_k	Generalized resistance
γ_{sc}	Resistance factor to take into account the safety class (i.e failure consequence)
γ_m	Resistance factor to account for material and resistance uncertainties.
γ_c	Resistance factor to account for special conditions
t	Time

If Equation 4.1 is greater 1, the design is safe. If it is less than 1, failure will occur.

According to Katla (2001), the design objective of the LRFD approach is to keep the failure probability (i.e. probability of exceeding a Limit State) below a certain value for all relevant failure modes of a riser. A Limit State is the state beyond which the riser or part of the riser no longer satisfies the requirements laid down to its performance or operation. The DNV-OS-F201 standard recommends that risers should be designed with the following Limit States in mind:

Functional loads	Environmental loads	Pressure loads	Accidental loads
Weight of riser	Current	External hydrostatic pressure	Tensioner failure
Weight of coatings, attachments and tubing	Waves	Internal fluid pressure	Small objects dropped
Weight of tubing contents and annulus fluid	Vessel motions induced by waves wind and current	Water levels	Normal Handling Impacts
Installation induced residual loads or pre-stressing	Ice		Partial loss of station-keeping
Pre-load of connectors	Earthquake		Flow induced impact between risers
Applied displacements and guidance loads, including active positioning of support floater			
Thermal loads			
Soil pressure on buried risers			
Differential settlements			
Loads from drilling operations			
Construction loads and loads caused by tools			

Table 4.1: Riser Loads, (DNV, 2010c)

- Serviceability Limit State (SLS)
- Ultimate Limit State (ULS)
- Fatigue Limit State (FLS)
- Accidental Limit State (ALS)

4.2.1.1 Serviceability Limit State (SLS)

The SLS requires that a riser must be able to remain in service and operate properly. It sets the requirements for normal operating conditions. Relevant failure modes as a result of exceeding this state include clearance, angular response, top displacement, ovalization and mechanical function. The most relevant of these failure modes is excessive ovalization and the criteria is given as (DNV, 2010c):

$$f_o = \frac{D_{max} - D_{min}}{D_o} \leq 0.03 \tag{4.2}$$

where:

f_o	ovality
D_{max}	maximum diameter
D_{min}	minimum diameter
D_o	initial diameter

4.2.1.2 Ultimate Limit State (ULS)

The ULS requires that the riser must remain intact and avoid rupture, but not necessarily be able to operate. For operating condition, this limit state corresponds to the maximum resistance to applied loads with 10^{-2} annual exceedence probability. Relevant failure modes include (DNV, 2010c):

- bursting
- hoop buckling
- propagating buckling
- gross plastic deformation and local buckling
- gross plastic deformation, local buckling and hoop buckling

The design criteria, according to DNV-OS-F201, against these failure modes are presented below:

Bursting Criterion

Bursting occurs due to net internal over pressure and the riser should be designed to satify the following criterion:

$$(P_{li} - P_e) \leq \frac{P_b(t_1)}{\gamma_m \cdot \gamma_{sc}} \tag{4.3}$$

The burst resistance P_b is given by

$$P_b(t) = \frac{2}{\sqrt{3} \cdot \frac{2 \cdot t}{D-t} \cdot min\left(f_y; \frac{f_u}{1.15}\right)} \tag{4.4}$$

where:

P_{li}	local incidental pressure
P_e	external pressure
P_b	burst resistance
t	dummy variable to be substituted by t_1 or t_2 where relevant
γ_m	material resistance factor
γ_{sc}	safety class resistance factor
D	nominal pipe outer diameter
f_y	yield strength
f_u	tensile strength

Hoop Buckling or Collapse Criterion

Hoop buckling or collapse occurs due to net external overpressure and the riser should be designed to satisfy the following criterion:

$$(P_e - P_{min}) \leq \frac{P_c(t_1)}{\gamma_m \cdot \gamma_{sc}} \tag{4.5}$$

The resistance for external pressure $P_c t$ is given by

$$(P_c(t) - P_{el}(t)) \cdot \left(P_c^2(t) - P_p^2(t)\right) = P_c(t) \cdot P_{el}(t) \cdot P_p(t) \cdot f_o \cdot \frac{D}{t} \tag{4.6}$$

The elastic collapse pressure(instability) $P_{el}(t)$ of the pipe is given by:

$$P_{el}(t) = \frac{2 \cdot E \cdot \left(\frac{t}{D}\right)^3}{1 - v^2} \tag{4.7}$$

The plastic collapse pressure $P_p(t)$ of the pipe is given by:

$$P_p(t) = 2\frac{t}{D} \cdot f_y \cdot \alpha_{fab} \tag{4.8}$$

where:

P_e	external pressure
P_{min}	minimum internal pressure
$P_c t$	resistance for external pressure(hoop buckling)
$P_{el}(t)$	elastic collapse pressure (instability) of a pipe
$P_p(t)$	plastic collapse pressure
f_o	initial ovality
α_{fab}	fabrication factor

Propagating Buckling Criterion

Even if the hoop buckling criterion above is satisfied, hoop buckling may still be initiated at a lower pressure by accidental means. In order to ensure that the buckle does not propagate, the riser is designed to satisfy the criterion given below:

$$(P_e - P_{min}) \leq \frac{P_{pr}}{\gamma_c \cdot \gamma_m \cdot \gamma_{sc}} \tag{4.9}$$

where:

P_{pr}	the resistance against buckling propagation
γ_c	1.0 if no buckling is allowed and 0.9 if buckling is allowed to travel a short distance

The resistance against buckling propagation P_{pr} is given by:

$$P_{pr} = 35 \cdot f_y \cdot \alpha_{fab} \cdot \left(\frac{t_2}{D}\right)^{2.5} \tag{4.10}$$

The definition of the parameters of the equation have been given above.

A riser designed to meet the propagation criterion also meets the buckling criteria because the propagation criterion results in a design that may be too conservative due to a significant increase in wall thickness. In practical application, buckle arrestors could be used if the propagation criterion is not met.

Gross Plastic Deformation and Local Buckling Criterion

Gross plastic deformation and local buckling occurs due to the combination of effective tension, bending moment and net internal overpressure. The riser should be designed to meet this criterion:

$$(\gamma_{sc} \cdot \gamma_m) \left[\left(\frac{|M_d|}{M_k}\right) \cdot \sqrt{1 - \left(\frac{P_{ld} - P_e}{P_b(t_2)}\right)^2} + \left(\frac{T_{ed}}{T_k}\right)^2 \right] + \left(\frac{P_{ld} - P_e}{P_b(t_2)}\right)^2 \leq 1 \tag{4.11}$$

The design bending moment is given by:

$$M_d = \gamma_F \cdot M_F + \gamma_E \cdot M_E + \gamma_A \cdot M_A \tag{4.12}$$

The plastic bending moment resistance M_k is given by:

$$M_k = f_y \cdot \alpha_c \cdot (D - t_2)^2 \cdot t_2 \tag{4.13}$$

The design effective tension is given by:

$$T_{ed} = \gamma_F \cdot T_{eF} + \gamma_E \cdot T_{eE} + \gamma_A \cdot T_{eA} \tag{4.14}$$

The plastic axial force resistance is given by:

$$T_k = f_y \cdot \alpha_c \cdot \pi \cdot (D - t_2) \cdot t_2 \tag{4.15}$$

where:

M_d	design bending moment
M_k	plastic bending moment resistance
P_{ld}	local internal design pressure
P_e	local external pressure
T_{ed}	design effective tension
T_k	plastic axial force resistance
γ_F	functional load factor
γ_E	environmental load factor
γ_A	accidental load factor
M_F	Bending moment from functional load
M_E	Bending moment from environmental load
M_A	Bending moment from accidental load
T_{eF}	effective tension from functional loads
T_{eE}	effective tension from environmental loads
T_{eA}	effective tension from accidental loads
α_c	parameter accounting for strain hardening and wall thinning

Gross Plastic Deformation, Local Buckling and Hoop Buckling Criterion

Gross plastic deformation, local buckling and hoop buckling occurs due to the combination of bending moment, effective tension and net external overpressure. A riser should be designed to meet this criterion:

$$(\gamma_{sc} \cdot \gamma_m)^2 \left[\left(\frac{|M_d|}{M_k} \right) + \left(\frac{T_{ed}}{T_k} \right)^2 \right]^2 + (\gamma_{sc} \cdot \gamma_m)^2 \left(\frac{P_e - P_{min}}{P_c(t_2)} \right)^2 \leq 1 \tag{4.16}$$

4.2.1.3 Fatigue Limit State(FLS)

The FLS of a riser is an ultimate limit state from accumulated excessive fatigue crack growth or damage under cyclic loading.

The standard lists two fatigue assessment methods that can be used to verify the fatigue resistance of the riser. These two assessment methods are based on S-N curves and fatigue crack propagation respectively.

In the **S-N curves Fatigue Assessment Method**, the following fatigue criterion should be satisfied:

$$D_{fat} \cdot DFF \leq 1 \tag{4.17}$$

where:

D_{fat}	accumulated fatigue damage
DFF	design fatigue factor given by Table 4.3

Design Fatigue Factors		
Safety Class		
Low	Normal	High
3	6	10

Table 4.2: Design Fatigue Factors

In the **Fatigue Crack Propagation Method**, the riser should be designed to satisfy the following criterion:

$$\frac{N_{tot}}{N_{cg}} \cdot DFF \leq 1 \tag{4.18}$$

where:

N_{tot}	total number of applied stress cycles during service or to in-service inspection
N_{cg}	Number of stress cycles necessary to increase the defect from the initial to the critical defect size
DFF	as previously defined

4.2.1.4 Accidental Limit State(ALS)

The DNV-OS-F201 defines the accidental limit state as a limit state due to accidental loads or events. These accidental events have an annual frequency or probability of occurrence less than 10^{-2}. Accidental loads may include:

- fires and explosions
- impact/collisions such as infrequent riser interference, impact from dropped objects and anchors, impact from floater
- hook/snag loads
- failure of support systems
- exceedence of incidental internal overpressure
- environmental events such as earthquakes, tsunamis, icebergs

For more information of the accidental limit state, refer to section 5 of the DNV-OS-F201.

4.2.2 DNV-OS-F201: WSD Approach

In the WSD approach, the uncertainties in the effects of the loads and resistance are accounted for by the use of a single safety or usage factor.The general WSD design format according to DNV-OS-F201 can be expressed as:

$$g(S, R_k, \eta, t) \leq 1 \tag{4.19}$$

where:

S	Total load effect
R_k	Resistance
η	Usage factor
t	Time

If Equation 4.19 is less than 1, the design is safe and if it is greater than 1, the design will fail.

The total load effect S is due to a combined action from pressure, functional, environmental and accidental loads relevant for the actual limit states and load case.

The Limit States considered in the WSD approach are the same as those considered in the LFRD approach. Of importance in the WSD approach according to DNV-OS-F201 are the gross propagation and local buckling, gross propagation, local buckling and hoop buckling criteria. These criteria are presented below.

Gross Propagation and Local Buckling Criterion

Gross propagation and local buckling occurs due to the combined effect of bending moment, effective tension, and net internal overpressure. The riser should be designed to satisfy the criterion:

$$\left[\left(\frac{|M|}{M_k}\right)\cdot\sqrt{1-\left(\frac{P_{ld}-P_e}{P_b(t_2)}\right)^2}+\left(\frac{T_{ed}}{T_k}\right)^2\right]+\left(\frac{P_{ld}-P_e}{P_b(t_2)}\right)^2\leq\eta^2 \tag{4.20}$$

where:

η usage factor

The other parameters of Equation 4.20 have been previously defined.

Gross Propagation, Local Buckling and Hoop Buckling Criterion

Gross Propagation, Local Buckling and Hoop Buckling occurs due to the combined effect of bending moment, effective tension and net external overpressure. The riser should be designed to satisfy the criterion:

$$\left[\left(\frac{|M|}{M_k}\right)+\left(\frac{T_{ed}}{T_k}\right)^2\right]^2+\left(\frac{P_e-P_{min}}{P_c(t_2)}\right)^2\leq\eta^4 \tag{4.21}$$

where the parameters of Equation 4.21 have been previously defined.

4.2.3 Safety Classes

The safety class concept in the DNV-OS-F201 is used to rate the failure consequences of a riser. The safety class of a riser depends on (DNV, 2010c):

- the hazard potential of the fluid in the riser i.e fluid category
- the location of the part of the riser that is being designed
- the state of the riser i.e whether the riser is in operating or temporary state

The categories of fluids and classifications of the locations of the part of the riser are presented in Table 4.3 and 4.4 respectively.

Category	Description
A	Typical non-flammable water-based fluids
B	Flammable and/or toxic substances which are liquids at ambient temperature and atmospheric pressure conditions
C	Non-flammable substances which are gases at ambient temperature and atmospheric pressure conditions
D	Non-toxic, single-phase gas
E	Flammable and toxic substances, which are gases at ambient temperature and atmospheric pressure conditions and which, are conveyed as gases or liquids

Table 4.3: Fluid Classification (DNV, 2010c)

Location	Description
1	Area where no frequent human activity is anticipated
2	The part of the riser in the near platform (manned) area or in areas with frequent human activity

Table 4.4: Location Classification (DNV, 2010c)

Based on these, three safety classes are introduced and they are presented in Table 4.5

Safety Class	Definition
Low	where failure implies low risk of human injury and minor environmental consequences
Normal	for conditions where failure implies risk of human injury, significant environmental pollution or very high economic or political consequences
High	for operating conditions where failure implies high risk of human injury, significant environmental pollution or very high economic or political consequences

Table 4.5: Safety Class Classification (DNV, 2010c)

Chapter 5

Methodology and Design Premise

5.1 Introduction

In this chapter, the methodology and design data used in this study are presented. The design data presented includes the FPSO dimensions and motion characteristics, operational and accidental design conditions, environmental conditions, riser and buoyancy modules properties and internal fluid data.
Based on these presented data, the SLWR was modeled and extreme strength and fatigue response analysis was carried out in OrcaFlex to verify that the modeled SLWR met the acceptance criteria specified by the reference standards given below:

- DNV-0S-F 101,2010: Submarine Pipeline Systems
- DNV-RP-C203,2012: Fatigue Design of Offshore Steel Structures
- API Specification 5L, 2018: Specification for a Line Pipe
- API RP 2SK,2007: Design and Analysis of Station-keeping Systems for Floating Structures
- NORSOK N-003,2017:Actions and Actions Effects

5.2 Data for Design and Analysis

5.2.1 FPSO Dimensions

In chapter 2, the spread-moored FPSO was selected as the most suitable vessel for SLWR deployment in the ultra-deepwater regions of the Santos Basin. The physical dimensions of the FPSO used in this study are presented in Table 5.1.

Parameter	**Unit**	**Value**
Length	m	332
Width	m	58
Height	m	31
Maximum Draught	m	22
Riser Hang-off Distance Above Vessel Base line	m	2.6

Table 5.1: FPSO Dimensions

In OrcaFLex, the FPSO was set to 195^o in clockwise direction from the North because of the environmental conditions in the Santos Basin. The direction and local coordinates of the FPSO as modeled in OrcaFlex are illustrated by Figure 5.1.

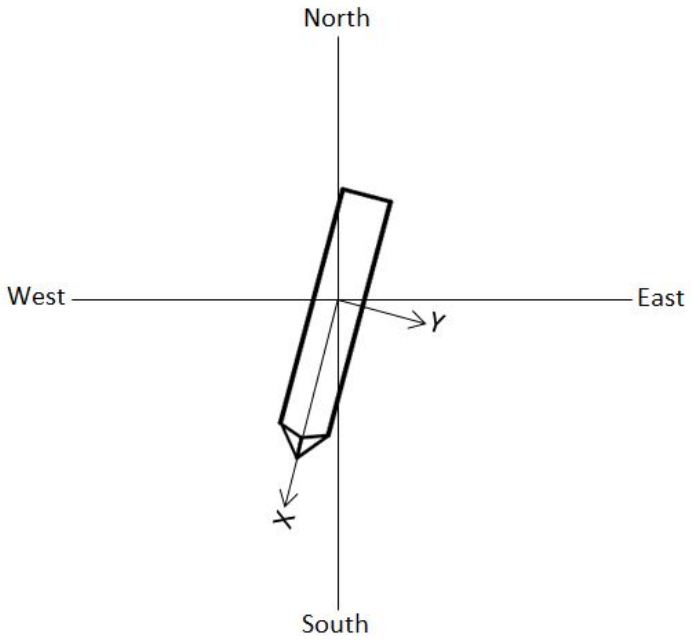

Figure 5.1: Local FPSO Coordinate System and Vessel Heading

5.2.2 FPSO Motion Data

In the design of risers, the FPSO motion data required includes the following (DNV, 2010c):

- FPSO Static Offsets
- Wave Frequency Motions
- Low Frequency Motions

5.2.2.1 FPSO Static Offsets

These are offsets a FPSO experiences due to the combination of steady waves, current and wind (API, 2005). In the design of risers, the most critical situations considered are when these offsets occur in the same direction as the riser.

When the FPSO offset is towards the subsea connection, it is called a near offset and when it is away from the subsea connection, it is called a far offset. The near and far offsets are illustrated in Figure 5.2.

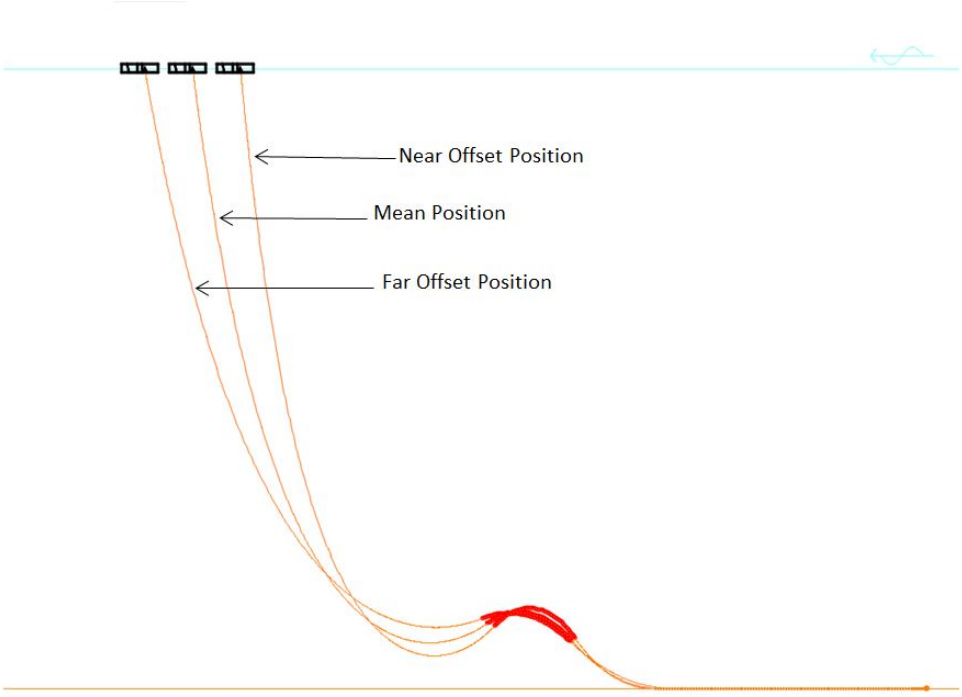

Figure 5.2: FPSO Offset Positions

5.2.2.2 Wave Frequency Motions

Wave frequency motions are motions induced by first order wave forces acting directly on the FPSO. They have periods ranging from 3-25 seconds and are described by the

Response Amplitude Operators (RA0s) of the FPSO (DNV, 2010c). The RAOs data of the FPSO used in this study is confidential and is therefore not presented.

5.2.2.3 Low Frequency Motions

Low frequency motions are motions induced by second order wave forces and wind gust loading. They occur at frequencies below wave frequencies and typically have periods between 30 to 300 seconds (DNV, 2010c).

5.2.3 Accidental and Operational Design Conditions

A spread-moored FPSO uses mooring lines terminated at its corners for station-keeping. For the strength analysis of risers connected to it, both the operational and accidental conditions of these mooring lines should be considered.

According to API-RP-2SK reference code, during normal operational conditions, all mooring lines should be intact. For this study, the maximum FPSO offset allowed under normal operational conditions is 154m either towards(near) or away(far) from the subsea connection. It should be noted that 154m corresponds to 7% of 2200m(water depth considered this study).

The breakage of one of the mooring lines used for station-keeping is considered an accidental condition by API-RP-2SK. If this occurs, the maximum FPSO offset allowed is 176m which corresponds to 8% of the water depth considered in this study.

5.2.4 Environmental Data

5.2.4.1 Wave and Current

A riser should be designed to withstand the worst environmental condition it can be subjected to during its lifetime. This condition is usually driven by a combination of a 100-year wave with an associated 10-year current found in the region the riser will be installed in. For this study, this condition was determined by conducting a vessel response analysis process which is discussed in details in Section 6.2.

5.2.4.2 Riser-Soil Interaction

Due to an FPSO's high sensitivity to motion, the riser is continuously subjected to oscillatory loads during its lifetime which causes it to move out of its own plane. These loads develop oscillatory stresses which causes metal fatigue to develop in the riser especially at the touch down point as a result of stress concentration in the welded joints of the riser (Sen, Hesar, et al., 2007).

Therefore, it is important to account for the complex pipe-soil interaction that occurs to accurately capture the fatigue life of the touch down zone of the riser.

The riser-soil interaction parameters used in this study are given below:

- Normal Friction Coefficient - 0.5
- Axial Friction Coefficient- 0.5
- Normal Stiffness - 50 $kN/m/m^2$
- Shear Stiffness- 200 $kN/m/m^2$

5.2.5 Riser Properties

For a riser to be deployed in ultra-deepwater, its material should have the following properties:

- Ultra high strength
- Excellent low-temperature toughness
- High collapse resistance
- Good weldability
- High operating pressure

These properties are found in the API 5L X65, X80 and X90 carbon steel grade and their strength and fatigue performances are compared together in this study. Since 3 carbon steel grade materials are considered, 3 SLWRs made of each material is modeled in OrcaFlex with the parameters presented in Tables 5.2, 5.3 and 5.4.

Parameter	**Value**
Internal Diameter(in/mm)	10/254
Riser Wall Thickness(mm)	30
Steel Material Density(kg/m^3)	7850
Specified Minimum Yield Strength (MPa)	448,2
Specified Minimum Tensile Strength(MPa)	530.9
Design Pressure (MPa)	75
Elastic Modulus(GPa)	207
Poisson Ratio	0.3
Internal Cladding Thickness(mm)	3
Internal Cladding Density (kg/m^3)	8440
External Coating Thickness(mm)	40
External Coating Density	850

Table 5.2: API 5L X65 Carbon Steel Grade Riser Parameters

Parameter	**Value**
Internal Diameter(in/mm)	10/254
Riser Wall Thickness(mm)	25
Steel Material Density(kg/m^3)	7850
Specified Minimum Yield Strength (MPa)	551,6
Specified Minimum Tensile Strength(MPa)	620,6
Design Pressure (MPa)	75
Elastic Modulus(GPa)	207
Poisson Ratio	0.3
Internal Cladding Thickness(mm)	3
Internal Cladding Density (kg/m^3)	8440
External Coating Thickness(mm)	40
External Coating Density	850

Table 5.3: API 5L X80 Carbon Steel Grade Riser Parameters

Parameter	Value
Internal Diameter(in/mm)	10/254
Riser Wall Thickness(mm)	22
Steel Material Density(kg/m^3)	7850
Specified Minimum Yield Strength (MPa)	625
Specified Minimum Tensile Strength(MPa)	695
Design Pressure (MPa)	75
Elastic Modulus(GPa)	207
Poisson Ratio	0.3
Internal Cladding Thickness(mm)	3
Internal Cladding Density (kg/m^3)	8440
External Coating Thickness(mm)	40
External Coating Density	850

Table 5.4: API 5L X90 Carbon Steel Grade Riser Parameters

5.2.6 Design Life

The design life for the SLWRs in this study is considered to be 25 years. Since they are all production risers, a safety factor of 10 is used based on the recommendations of the DNV-OS-F201. Therefore, for the wave induced fatigue analysis, the minimum required fatigue life for the SLWRs is 250 years.

5.2.7 Marine Growth and Hydrodynamic Data

In the design of a SLWR, it is important to account for the presence of marine growth because of the effect it has on the diameter of a riser(Li, 2012). When marine growth is present, the diameter of the SLWR increases. This causes an increase in the mass, top tension and hydrodynamic loading of the riser.

According to DNV-OS-F201, the hydrodynamic loading of the SLWR can be expressed by the Morison equation in terms of the relative fluid-structure velocities and accelerations. The Morison equation is given by:

$$f_n = \frac{1}{2}\rho C_{\mathrm{D}}^{\mathrm{n}} D_h |v_n - \dot{r}_n|(v_n - \dot{r}_n) + \rho\frac{\pi D_{\mathrm{b}}^2}{4} C_{\mathrm{M}}^{\mathrm{n}} \dot{v}_n - \rho\frac{\pi D_{\mathrm{b}}^2}{4}(C_{\mathrm{M}}^{\mathrm{n}} - 1)\ddot{r}_n \tag{5.1}$$

$$f_t = \frac{1}{2}\rho C_{\mathrm{D}}^{\mathrm{t}} D_h |v_t - \dot{r}_t|(v_t - \dot{r}_t) + \rho\frac{\pi D_{\mathrm{b}}^2}{4} C_{\mathrm{M}}^{\mathrm{t}} \dot{v}_t - \rho\frac{\pi D_{\mathrm{b}}^2}{4}(C_{\mathrm{M}}^{\mathrm{t}} - 1)\ddot{r}_t \tag{5.2}$$

where:

f_n	Force per unit length in normal direction
f_t	Force per unit length in tangential direction
ρ	Water density
D_b	Buoyancy diameter
D_h	Hydrodynamic diameter
$v_n, \dot{v}_n$	Fluid velocity and acceleration in normal direction
$\dot{r}_n, \ddot{r}_n$	Structural velocity and acceleration in normal direction
$C_{\mathrm{D}}^{\mathrm{n}}, C_{\mathrm{M}}^{\mathrm{n}}$	Drag and inertia coefficients in normal direction
$v_t, \dot{v}_t$	Fluid velocity and acceleration in tangential direction
$\dot{r}_t, \ddot{r}_t$	Structural velocity and acceleration in tangential direction.
$C_{\mathrm{D}}^{\mathrm{t}}, C_{\mathrm{M}}^{\mathrm{t}}$	Drag and inertia coefficients in tangential direction

The drag and inertia coefficients in the Morison equation depend on parameters such as the surface roughness of the body, Reynolds number and the Keulegan-Carpenter number.

A drag coefficient between 0.7 and 1.0 and an inertia coefficient of 2.0 is recommended by the DNV-OS-F201 reference standard when no marine growth is taken into consideration. NORSOK (2007) recommends a drag coefficient of at least 1.05 when marine growth is to be accounted for. However, in this study, a drag coefficient of 1.2 is selected and is assumed to be constant along the riser length to achieve a more conservative design.

5.2.8 Buoyancy Modules

The most important section of SLWR is the buoyancy section because it creates the lazy wave configuration that decouples the touch down zone of the riser from vessel motions. In this study, different buoyancy modules were used for each riser material due to their varying weight as a result of their variation in strength and wall thickness requirements. The properties of these modules are presented in Table 5.5.

Buoyancy Module Properties for X65 Riser		
Parameter	**Value**	**Unit**
Length	4.3	m
Inner Diameter	0.248	m
Outer Diameter	1.079	m
Material Density	395	kg/m^3
Clamp Weight	25	kg
Pitch	6	m
Buoyancy Module Properties for X80 Riser		
Parameter	**Value**	**Unit**
Length	4.3	m
Inner Diameter	0.248	m
Outer Diameter	0.987	m
Material Density	395	kg/m^3
Clamp Weight	25	kg
Pitch	7.36	m
Buoyancy Module Properties for X90 Riser		
Parameter	**Value**	**Unit**
Length	4.3	m
Inner Diameter	0.248	m
Outer Diameter	0.928	m
Material Density	395	kg/m^3
Clamp Weight	25	kg
Pitch	8.5	m

Table 5.5: Buoyancy Module Properties for X65, X80 and X90 Risers

5.2.9 Internal Fluid Data

For this study, the internal fluid considered has a density of 800 kg/m^3 and its associated design pressure at the seabed is set to 75 MPa.

5.3 Design Cases

As described in Chapter 1, one of the major objectives of this study is to compare the strength and fatigue performance of a SLWR hung off at two different hang-off points; one along the portside and the other along the middle of the FPSO. Another major objective is to compare the strength and fatigue performance of SLWRs made

of X65, X80 and X90 carbon steel. These objectives created six different design cases presented in Table 5.6.

Design Case	**Riser Material**	**Riser Hang-Off Point**
1	X65	Port Side
2	X65	Middle
3	X80	Port Side
4	X80	Middle
5	X90	Port Side
6	X90	Middle

Table 5.6: Design Cases

The strength and fatigue analysis was conducted for each design case and the following SLWR response characteristics were observed and discussed in Chapter 6:

- Maximum Effective Tension
- Maximum Bending Moment
- Maximum Utilization
- Minimum Fatigue Life

5.4 Wall Thickness

Due to the high external and internal pressure the SLWR will experience in this study, it was important that the riser wall thickness selected would ensure the riser does not fail when subjected to net external or internal overpressure.

The DNV Pipeline Engineering Tool was used to calculate the wall thickness selected in this study and the details of these calculations, for each riser material, are presented in Appendix A. Figure 5.3 presents the minimum wall thickness obtained from the calculations for the 3 riser material considered in this study with an operating pressure of 75MPa and at a water depth of 2200m.

From Figure 5.3, it can be observed that the required minimum wall thickness of a riser increases as the yield strength of the material reduces.

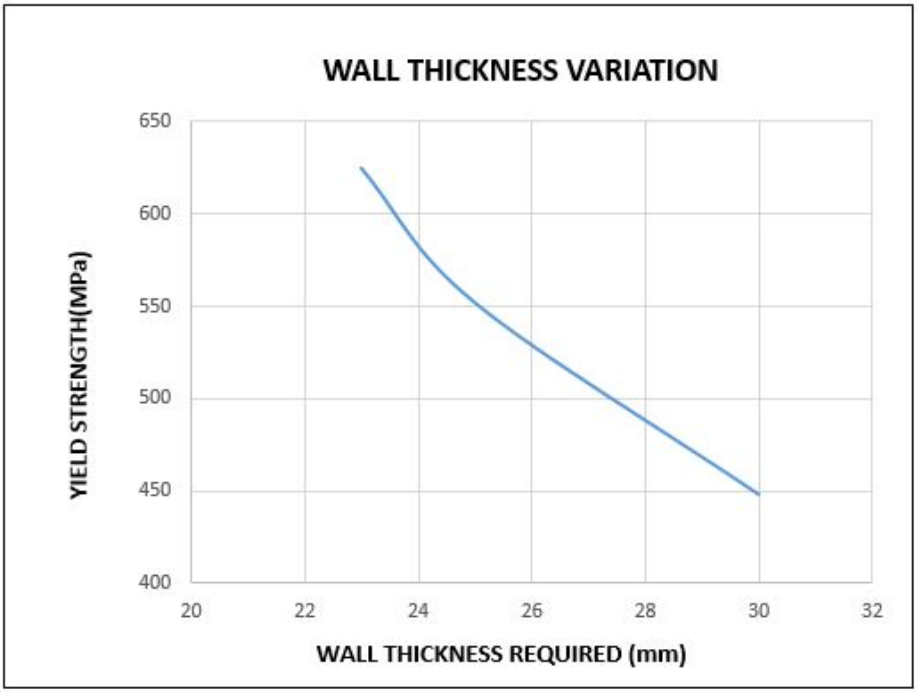

Figure 5.3: Yield Strength Vs Wall Thickness

5.5 SLWR Acceptance Criteria

In the design of SLWRs, several different configurations are possible for the same water depth. However, not all these configurations will meet the requirements of the reference standard(DNV-OS-F201) used in this study. For a configuration to be acceptable in any of the design cases listed in Table5.6 it must meet the following requirement:

- The DNV LRFD utilization function given by equation 5.2 below must be satisfied :

$$g(t) = g(M_d(t), T_{ed}(t), \Delta_p, R_k, \Lambda) \leq 1 \tag{5.3}$$

where:

M_d	Design bending moment
T_{ed}	Design effective tension
Δ_p	Local differential pressure
R_k	Vector of cross sectional capacities
Λ	Vector of safety factors

If $g(t) > 1$, the design will fail and the configuration is not accepted.

- Compression must be limited or completely avoided to prevent column buckling.

- A minimum fatigue life of 250 years must be achieved in the fatigue response analysis.

Chapter 6

Strength and Fatigue Analysis

6.1 Introduction

In this chapter, strength(static and dynamic) and fatigue analysis are conducted on the SLWRs. Focus is given to the top, sag-bend, hog-bend and touch down sections because these sections are considered critical by the DNV-OS-F201 reference standard.

All modelling and analysis in this chapter were performed solely with OrcaFlex and the approach adopted is summarised as follows:

- Determination of the worst sea state
- Selection of riser hang-off points based on the worst sea state.
- Determination of an acceptable static configuration for the SLWR
- Strength Analysis
- Fatigue Analysis

This approach is followed for each design case given in Table 5.6 and the results observed are presented and discussed.

6.2 Determination of the Worst Sea State

In this study, the worst sea state is defined as the combination of a 100-year wave and 10-year current that yields the maximum downward velocity on the riser hang-off points considered.

A total of six riser hang-off points were considered and they are presented in Figure 6.1.

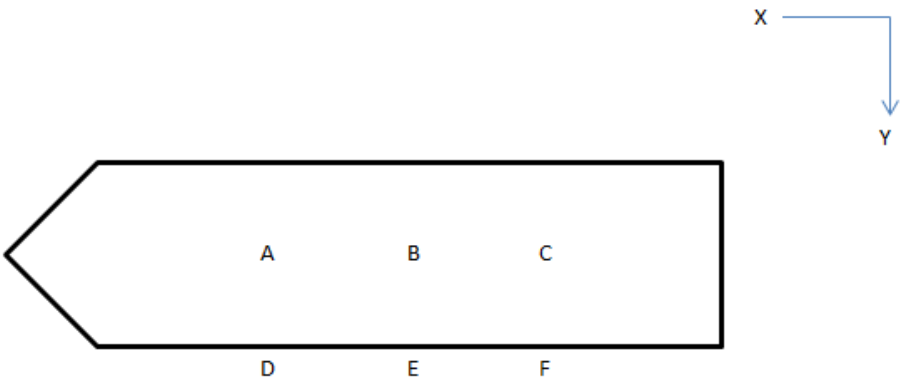

Figure 6.1: Riser Hang-off Points

To determine the worst sea state, the following steps were taken:

1. Metocean Data Study
2. Vessel Response Analysis

6.2.1 Metocean Data Study

The metocean data of the Santos Basin presents information about the 100-year wave and 10-year current for each direction. The 100-year wave contains different H_s and T_p combination. However, the maximum H_s and T_p values do not always yield the maximum downward velocity.

Therefore, a vessel response analysis that subjects the vessel to all the different H_s and T_p combinations for each wave direction needs to be conducted to identify the combination and wave direction that yields the maximum downward velocity.

6.2.2 Vessel Response Analysis

From the metocean data study, a total of 268 different H_s and T_p combinations are possible. Since 6 riser hang-off points were considered, a grand total of 1608 combinations were analyzed. Analyzing these combinations manually would have been very time-consuming. Therefore, a python script was written to make the analytical process semi-automatic. The results were fitted to a Gumbel distribution and the values at the 90% percentile were selected. A variation of the python script used is presented in Appendix B.

From the results of the analysis, it was observed that all the hang-off points experienced their maximum downward velocity when the 100-year wave and 10-year current was from the East-SouthEast direction as shown in Figure 6.2. However, an interesting observation was that it was not the same 100-year wave that caused the

maximum downward velocity in the hang-off points when the wave direction was East-SouthEast. Two different 100-year waves were responsible and their parameters are presented in Table 6.1.

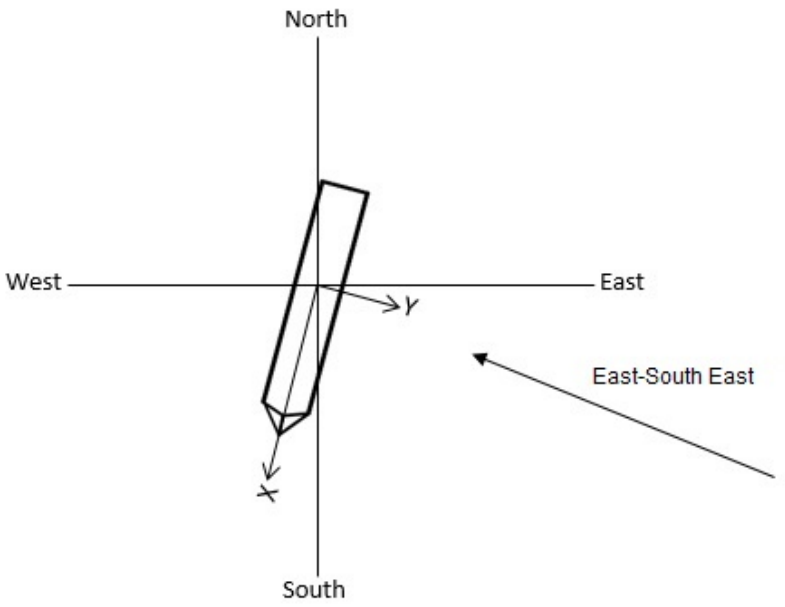

Figure 6.2: Worst 100-year Wave and 10-year Current Direction(Far Offset)

Riser Hang-off Point Location	**Hs(m)**	**Tp(s)**
Middle of the Vessel	6.5	11.5
Portside of the Vessel	6.3	14

Table 6.1: Parameters of Worst 100-Year Wave From East-SouthEast Direction

Due to the vessel heading, waves coming from the East-SouthEast and West-NorthWest directions(shown in Figures 6.2 and 6.3) will move the vessel to the far and near offset positions respectively. Hence, it was important to determine the 100 year-wave and 10-year current coming from the West-NorthWest direction that caused the maximum downward velocity in the hang-off points. This wave and current were determined and the parameters of the wave are presented in 6.2.

The associated 10-year current profiles that move the vessel into far or near offsets are shown in 6.4 and 6.5 respectively.

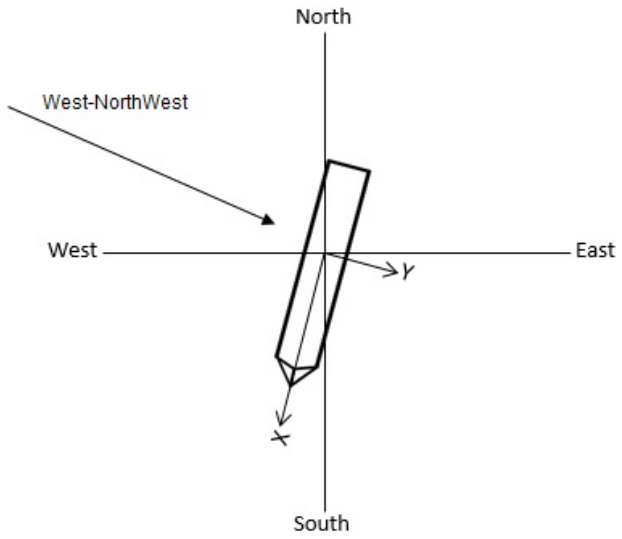

Figure 6.3: Worst 100-year Wave and 10-year Current Direction(Near Offset)

Riser Hang-off Point Location	**Hs(m)**	**Tp(s)**
Middle of the Vessel	4.8	10
Portside of the Vessel	4.8	10

Table 6.2: Parameters of Worst 100-Year Wave From West-NorthWest Direction

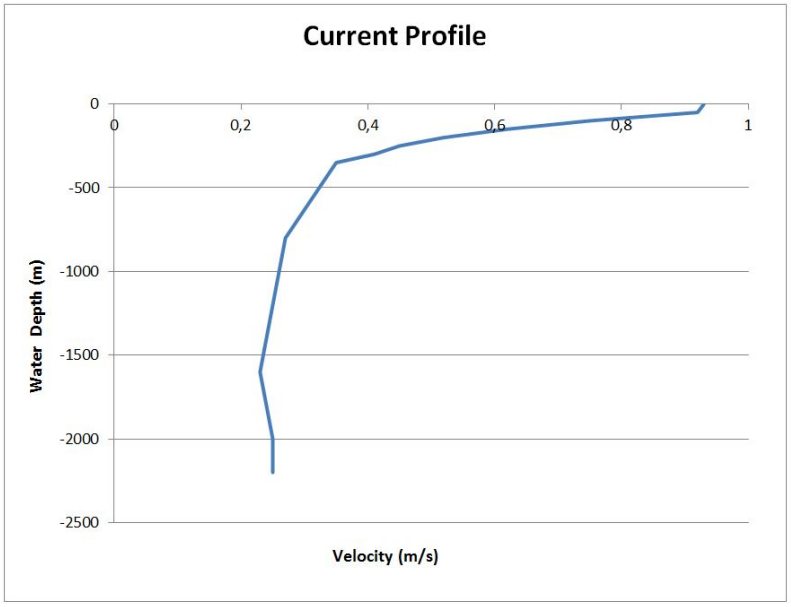

Figure 6.4: 10-Year Current Profile For Point A & D in Far Offset. Direction of Current is East-SouthEast

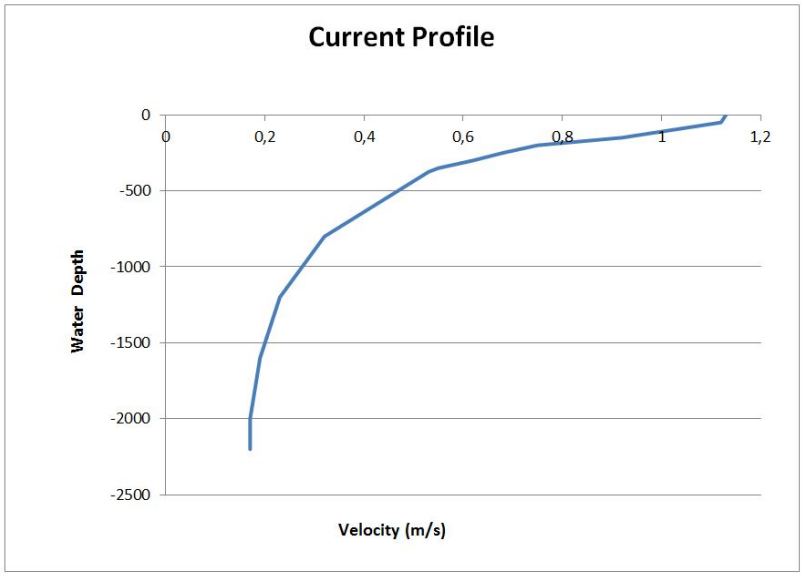

Figure 6.5: 10-Year Current Profile For Point A & D in Near Offset. Direction of Current is West-NorthWest

6.3 Selection of Riser Hang-off Points

The worst sea states that yield the maximum downward velocity at the riser hang-off points have been determined in Section 6.2. In this section, the hang-off points to be

used in the strength and fatigue analysis will be selected.

As one of the objectives of this thesis is to compare the strength and fatigue performance of a SLWR hung-off along the port side of the vessel with another hung-off along the middle of the vessel, two hang-off points need to be selected; one from the port side, and the other from the middle the vessel.

In Figure 6.1, the six hang-off points considered are shown; three along the middle of the vessel and three along the port side of the vessel. Therefore, the hang-off points were classified into two groups:

1. Group 1: Hang-off Point A, B and C
2. Group 2: Hang-off Point D, E and F

For a hang-off point to be selected from its group, it must have the largest maximum downward velocity in the group. In addition, the value of this velocity must not be greater than 6 m/s for this point to be eligible for SLWR application as suggested by the study of Gemilang and Karunakaran (2017).

To obtain adequate statistical confidence for the largest maximum downward velocity of a hang-off point, NORSOK (2007) recommends that at least 20-30 3hr dynamic simulations should be carried out. In these dynamic simulations, the vessel is subjected to the worst sea state determined in Section 6.2 and the wave seed component is varied for each simulation. In this study, 81 simulations were carried out and it should be noted that the number 81 has no significance. Any number that falls within the NORSOK (2007) recommended range could also have been selected.

Therefore, for the six hang off points considered, four hundred and eighty six(486) 3hr simulations were carried out. For each hang-off point, the obtained results of these simulations were fitted to a Gumbel distribution as shown in Figures 6.6,6.7,6.8,6.9 and the value at the 90% percentile was selected as the largest maximum downward velocity of that point.

This approach is in accordance with the NORSOK-N003:2007 for sea states with an annual exceedance probability of 10^{-2}. The obtained values at the 90% percentile of the Gumbel distribution are presented in Tables 6.3 and 6.4 and it can be seen that hang-off points A and D show the largest maximum downward velocity in their respective groups. Also, these values are below 6 m/s hence, the hang-off points A and D are well qualified for SLWR application.

Riser Hang-off Point	**Max Downward Velocity (m/s)**
A (30,0,11.6)	**-3.69**
B (0,0,11.6)	-3.67
C (-30,0,11.6)	-3.65
D (30,31,11.6)	**-4.98**
E (0,31,11.6)	-4.92
F (-30,31,11.6)	-4.90

Table 6.3: Maximum Downward Velocity of Riser Hang-off Points, Wave Direction:East-SouthEast

Riser Hang-off Point	**Max Downward Velocity(m/s)**
A(30,0,11.6)	**-2.32**
B(0,0,11.6)	-2.29
C(-30,0,11.6)	-2.27
D(30,31,11.6)	**-1.77**
E(0,31,11.6)	-1.75
F(-30,31,11.6)	-1.73

Table 6.4: Maximum Downward Velocity of Riser Hang-off Points, Wave Direction:West-NorthWest

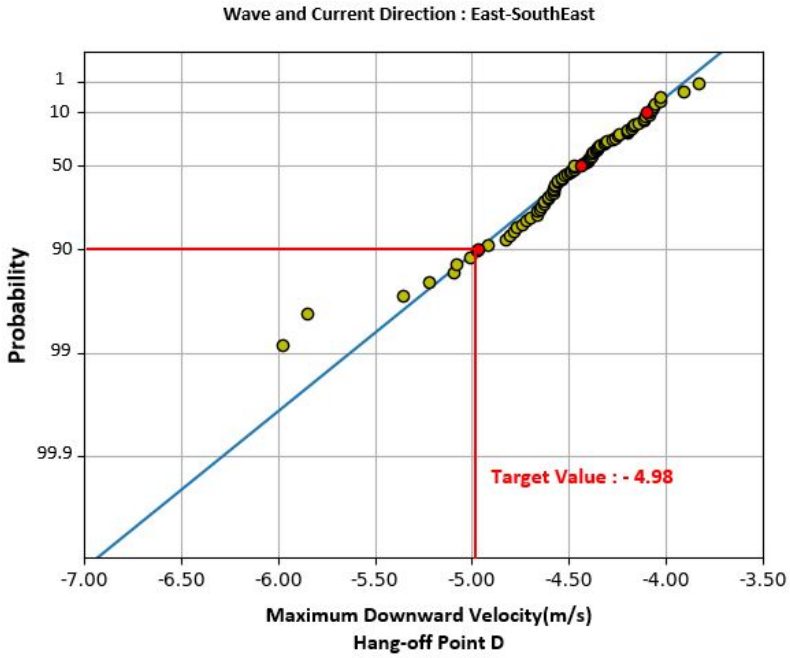

Figure 6.6: Linearized cumulative Gumbel distribution of Maximum Downward Velocities at Hang-off Point D, East-SouthEast

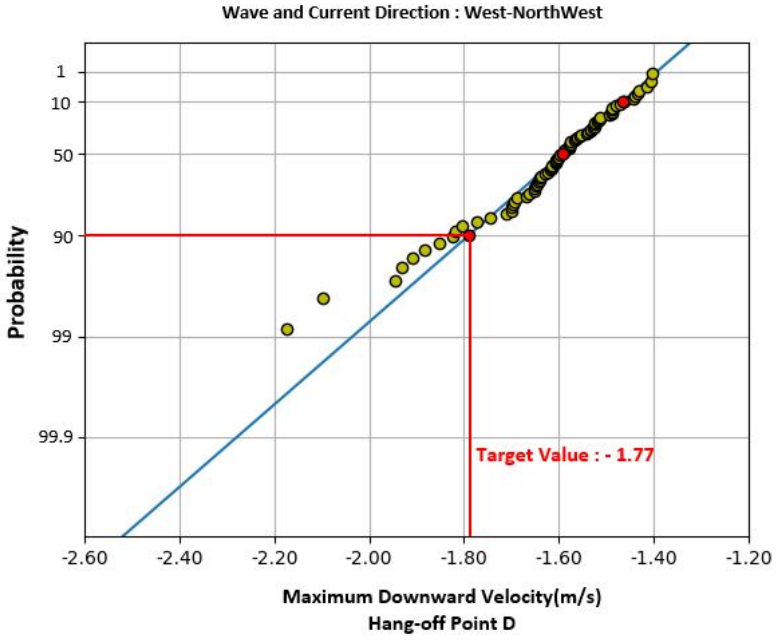

Figure 6.7: Linearized cumulative Gumbel distribution of Maximum Downward Velocities at Hang-off Point D, West-NorthWest

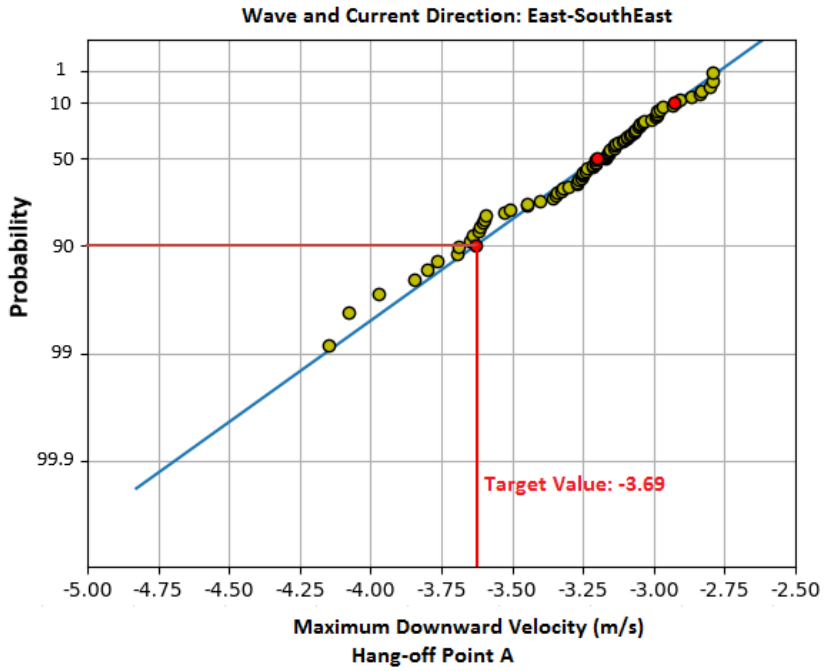

Figure 6.8: Linearized cumulative Gumbel distribution of Maximum Downward Velocities at Hang-off Point A, East-SouthEast

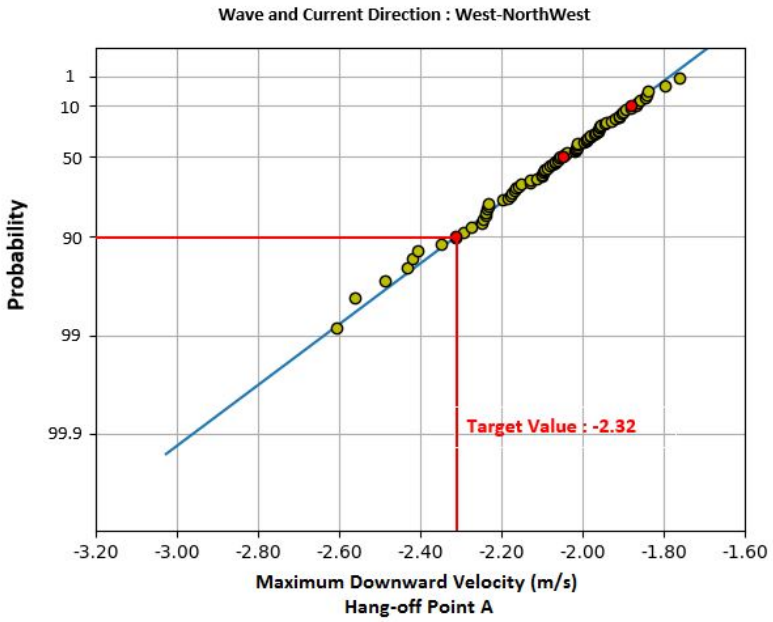

Figure 6.9: Linearized cumulative Gumbel distribution of Maximum Downward Velocities at Hang-off Point D, West-NorthWest

6.4 Determination of SLWR Static Configuration

With the worst sea states determined and riser hang-off points selected in the previous sections, a static SLWR configuration is determined in this section. A major objective of this study is to compare the strength and fatigue performance of SLWRs made of X65, X80 and X90 carbon steel grade. In order to have a reasonable comparison, each SLWR made of X65, X80, and X90 should have the same static shape.

To determine the static configuration, the following factors were considered:

- The DNV utilization criteria should be met by the configuration.
- Sufficient sag-bend height to ensure that there are no clashes with the seabed when the vessel moves the SLWR to the near offset position.
- Sufficient wave height i.e vertical distance between the sag-bend and the hog-bend to ensure that the SLWR configuration retains its wavy configuration when the vessel is in the far offset position.

Considering the above factors, an ideal static configuration was achieved for the X65, X80 and X90 SLWRs. The details of this configuration is presented in Table 6.5 and a graphical representation is shown in Figure 6.10. It should also be noted that for the initial analysis, the SLWR connected to the hang-off point at the port side has the same configuration as the one connected at the middle in order to make reasonable comparisons between the two hang-off points.

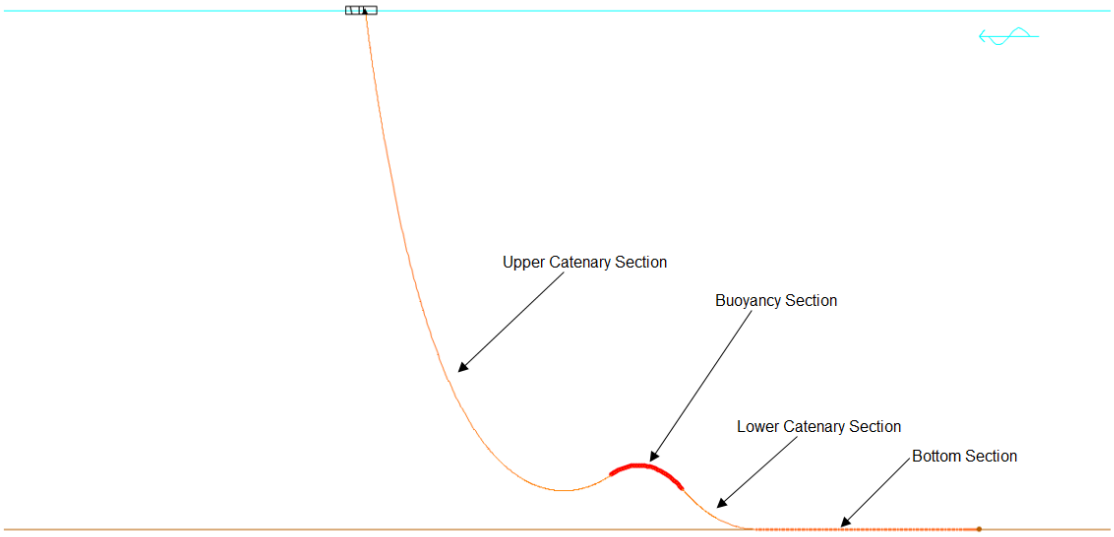

Figure 6.10: SLWR Static Configuration

Description	Value	Unit
Hang-off Angle	8	°
Total Riser Length	4275	m
Upper Catenary Length	2565	m
Buoyancy Section Length	350	m
Lower Catenary Length	380	m
Bottom Section Length	980	m
Sag-bend Height to Seabed	163	m
Hog-bend Height to Seabed	270	m
Lazy Wave Height	107	m
Net Buoyancy Force-X65 SLWR	173.2	kN
Net Buoyancy Force-X80 SLWR	141.9	kN
Net Buoyancy Force-X90 SLWR	123.3	kN

Table 6.5: Details of the SLWR Static Configuration

From Table 6.5, it can be seen that the net buoyancy required to achieve the same static configuration in the X65, X80 and X90 SLWR. This is because the X80 and X90 risers have lower wall thickness requirements which make them lighter than the X65 riser.

6.5 Strength Analysis

In this section, the static and dynamic analysis of the SLWR is conducted over the entire riser length and the maximum effective tension, maximum bending moment and maximum LRFD utilization observed in the critical sections of the SLWR i.e the top, sag-bend, hog-bend, and touch down, are presented.

6.5.1 Static Analysis

In the static analysis, only the functional loads described in Table 4.1 are considered because the SLWR is assumed to be in the mean position. Hence, environmental loads are not considered and the maximum effective tension, maximum bending moment and maximum DNV LRFD utilization observed along the entire length of the X65, X80 and X90 SLWRs are shown in Figures 6.11, 6.12 and 6.13 respectively. The values observed in the critical sections of the SLWR are presented in Table 6.6.

The results shown in Figures 6.11, 6.12 and 6.13 and presented in Table 6.6 are the same for the static analysis of the SLWRs connected either to the middle or the port side of the vessel. This is because no environmental loads are considered in this analysis.

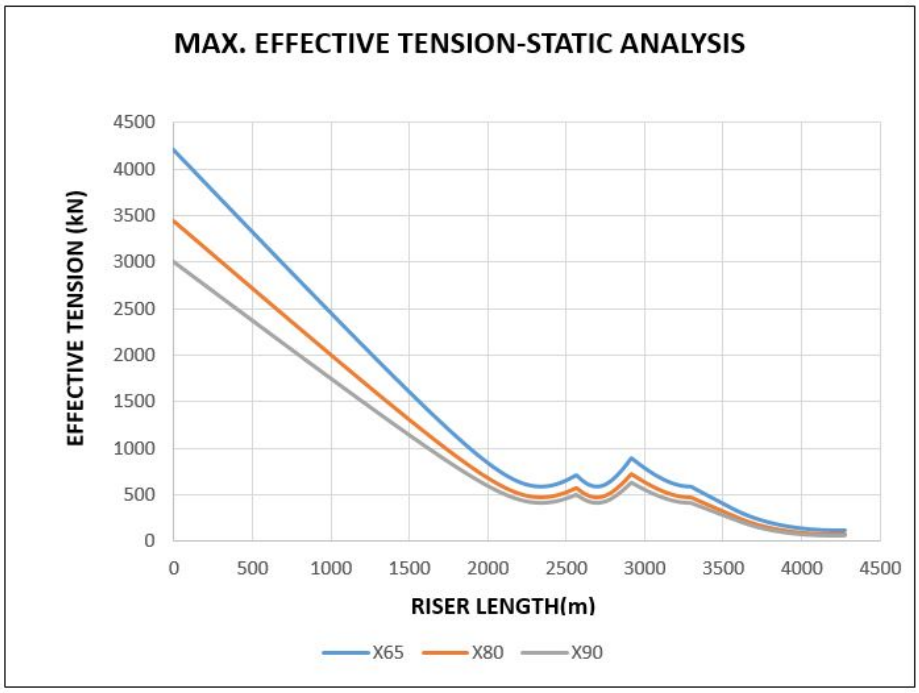

Figure 6.11: Maximum Effective Tension-Static Analysis

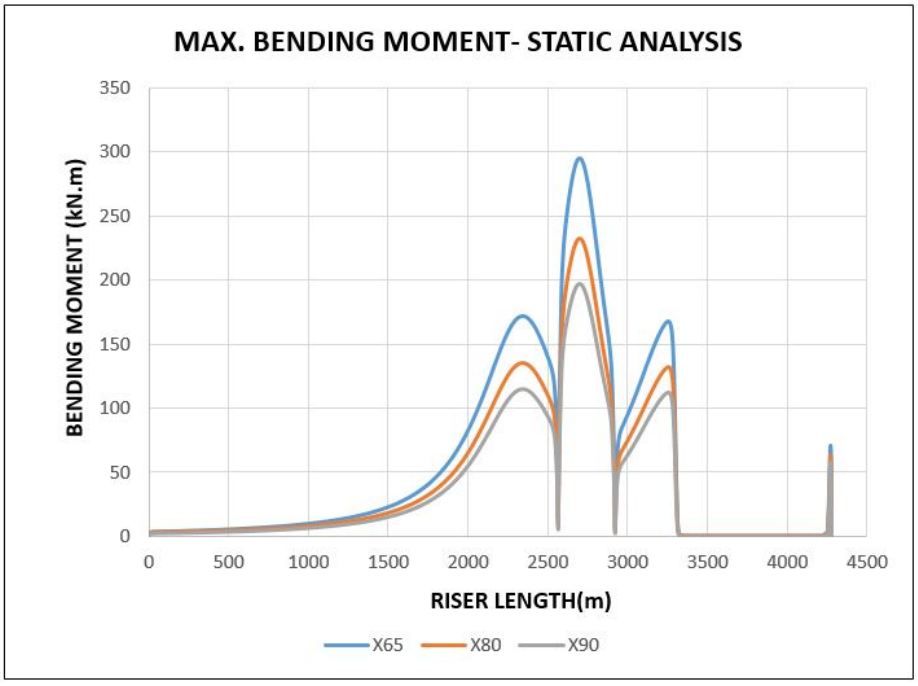

Figure 6.12: Maximum Bending Moment - Static Analysis

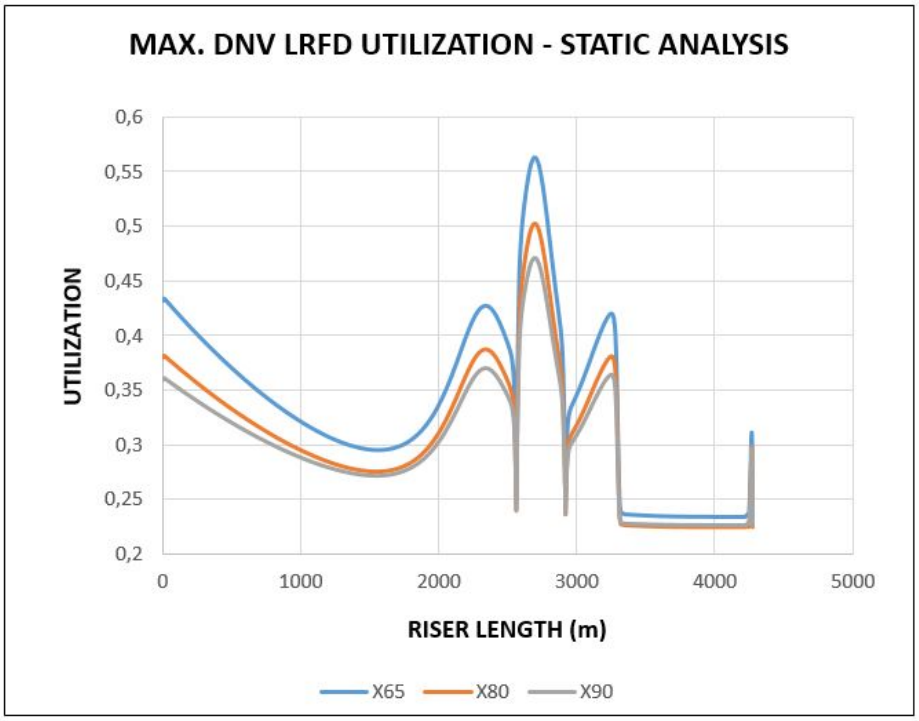

Figure 6.13: Maximum DNV LRFD Utilization-Static Analysis

Critical Section	**Top**		
Riser Material	**X65**	**X80**	**X90**
Maximum Effective Tension(kN)	4206	3443	2999
Maximum Bending Moment(kN.m)	0	0	0
Maximum DNV LRFD Utilization	0.43	0.38	0.36
Critical Section	**Sag-bend**		
Riser Material	**X65**	**X80**	**X90**
Maximum Effective Tension (kN)	708	580	505
Maximum Bending Moment(kN.m)	172	135	115
Max DNV LRFD Utilization	0.43	0.39	0.37
Critical Section	**Hog-bend**		
Riser Material	**X65**	**X80**	**X90**
Maximum Effective Tension (kN)	890	730	634
Maximum Bending Moment (kN.m)	295	233	197
Maximum DNV LRFD Utilization	0.56	0.50	0.47
Critical Section	**Touch Down Point**		
Riser Material	**X65**	**X80**	**X90**
Maximum Effective Tension (kN)	581	476	414
Maximum Bending Moment (kN.m)	54	45	33
Maximum DNV LRFD Utilization	0.30	0.28	0.27

Table 6.6: Static Analysis Results at Critical Sections of the SLWR

6.5.1.1 Discussion of the Static Analysis

The following observations were made from the results of the static analysis of the SLWRs:

1. The X65 SLWR has the largest maximum effective tension, maximum bending moment, and maximum DNV LRFD utilization in the group. This is because

the X65 SLWR has the lowest tensile and yield strength which invariably leads to the highest wall thickness requirements thereby making it the heaviest riser in the group.

2. The maximum effective tension occurs at the top of the riser. This is caused by the weight of the upper catenary section when filled with content and suspended at a height of approximately 2040m.

3. The maximum bending moment and maximum DNV LRFD Utilization occur at the hog-bend section of the SLWR. This caused by the geometric shape of the SLWR.

6.5.2 Dynamic Analysis

As previously established in Section 6.2, the worst sea state moves the vessel either to a far or near offset position depending on the direction of the wave and current in this sea state. This movement affects the geometrical shape of the SLWR which creates the need to verify the integrity of the riser in these new positions. Hence, dynamic analysis is conducted on the SLWR in these new positions. These new positions are extreme positions(both far and near) and in this study, they are taken to be 7% of water depth ($154m$) for the ULS and 8% of water depth ($176m$) for ALS.

Since two of the major objectives of this study is to show the comparison of the performance of a SLWR connected to two different hang-off points and also comparison of the performance of the X65, X80 and X90 carbon steel grade riser material, the results of the dynamic analysis are presented in the following order to avoid confusion:

1. First of all, the results of the dynamic analysis of the X65, X80 and X90 SLWR connected along the port side of the vessel in the ULS and ALS Far and Near Offset positions are presented and discussed.

2. Secondly, the results of the dynamic analysis of the X65, X80 and X90 SLWR connected along the middle of the vessel in the ULS and ALS Far and Near Offset positions are presented and discussed.

3. Thirdly, the maximum values obtained in each SLWR critical section in 1 and 2 are compared together to show the differences in the performance of the two hang-off points.

6.5.2.1 Dynamic Analysis Results in ULS and ALS Far and Near Offset, Port side of Vessel Hang-off Point

The results of the dynamic analysis in ULS and ALS far and near offset positions when the SLWR is connected to the hang-off point along the port side of the vessel are presented in Tables 6.7 and 6.8 respectively.

As highlighted in the Tables, the following has been observed in the ULS and ALS offset positions for the X65, X80 and X90 SLWRs:

1. The maximum effective tension occurs in the top section of the risers when it is in the ALS far offset position. For the X65, X80 and X90 SLWRs, the maximum effective tension observed are 6346 kN, 5336 kN, 4743 kN respectively. Therefore, changing the riser material from X65 to X80 reduces the maximum effective tension by 19% and from X80 to X90 reduces it 13% further.

2. The maximum bending moment occurs in the hog-bend section of the riser when it is in the ALS near offset position. For the X65, X80 and X90 SLWRs, the maximum bending moment observed are $427kN.m$, $340kN.m$ and $290kN.m$ respectively. Therefore, changing the riser material from X65 to X80 reduces the maximum bending moment tension by 26% and from X80 to X90 reduces it 17% further.

3. The maximum DNV LRFD Utilization occurs in the hog-bend section of the riser when it is in the ULS near offset position. For the X65, X80 and X90 SLWRs, the maximum DNV LRFD utilization observed are 0.7, 0.62, 0.58 respectively. Therefore, changing the riser material from X65 to X80 reduces the maximum DNV LRFD utilization by 13% and from X80 to X90 reduces it 7% further.

4. The maximum DNV LRFD utilization values observed meet the DNV LRFD utilization criteria. Hence, the design is safe.

5. No compressive forces are observed in any of the analysis.

Critical Section	**Top**					
Riser Material	**X65**		**X80**		**X90**	
Offset	**Far**	**Near**	**Far**	**Near**	**Far**	**Near**
Maximum Effective Tension (kN)	6301	4877	5297	4036	4708	3534
Maximum Bending Moment (kN.m)	0	0	0	0	0	0
Max DNV LRFD Utilization	0.66	0.50	0.57	0.43	0.52	0.40
Critical Section	**Sag Bend**					
Riser Material	**X65**		**X80**		**X90**	
Offset	**Far**	**Near**	**Far**	**Near**	**Far**	**Near**
Maximum Effective Tension (kN)	1690	666	1464	549	1335	479
Maximum Bending Moment (kN.m)	209	235	177	185	160	158
Max DNV LRFD Utilization	0.49	0.50	0.45	0.45	0.44	0.42
Critical Section	**Hog Bend**					
Riser Material	**X65**		**X80**		**X90**	
Offset	**Far**	**Near**	**Far**	**Near**	**Far**	**Near**
Maximum Effective Tension (kN)	1532	768	1327	630	1215	547
Maximum Bending Moment (kN.m)	355	414	295	329	260	281
Max DNV LRFD Utilization	0.66	0.70	0.60	0.62	0.57	0.58
Critical Section	**Touch Down Point**					
Riser Material	**X65**		**X80**		**X90**	
Offset	**Far**	**Near**	**Far**	**Near**	**Far**	**Near**
Maximum Effective Tension (kN)	1238	441	1089	360	1009	313
Maximum Bending Moment (kN.m)	123	114	99	93	86	71
Max DNV LRFD Utilization	0.39	0.36	0.36	0.34	0.34	0.31

Table 6.7: Dynamic Analysis Results: ULS Far and Near, PortSide Hang-off Point

Critical Section	**Top**					
Riser Material	**X65**		**X80**		**X90**	
Offset	**Far**	**Near**	**Far**	**Near**	**Far**	**Near**
Maximum Effective Tension (kN)	6346	4870	5336	4033	4743	3531
Maximum Bending Moment (kN.m)	0	0	0	0	0	0
Max DNV LRFD Utilization	0.57	0.45	0.49	0.39	0.45	0.37
Critical Section	**Sag Bend**					
Riser Material	**X65**		**X80**		**X90**	
Offset	**Far**	**Near**	**Far**	**Near**	**Far**	**Near**
Maximum Effective Tension (kN)	1770	657	1535	542	1399	472
Maximum Bending Moment (kN.m)	210	243	178	191	163	163
Max DNV LRFD Utilization	0.45	0.48	0.42	0.43	0.41	0.41
Critical Section	**Hog Bend**					
Riser Material	**X65**		**X80**		**X90**	
Offset	**Far**	**Near**	**Far**	**Near**	**Far**	**Near**
Maximum Effective Tension (kN)	1607	754	1399	618	1282	537
Maximum Bending Moment (kN.m)	355	427	296	340	262	290
Max DNV LRFD Utilization	0.59	0.66	0.54	0.59	0.52	0.55
Critical Section	**Touch Down Point**					
Riser Material	**X65**		**X80**		**X90**	
Offset	**Far**	**Near**	**Far**	**Near**	**Far**	**Near**
Maximum Effective Tension (kN)	1324	424	1166	347	1084	300
Maximum Bending Moment (kN.m)	115	95	98	77	85	58
Max DNV LRFD Utilization	0.35	0.33	0.33	0.31	0.32	0.29

Table 6.8: Dynamic Analysis Results: ALS Far and Near, PortSide Hang-off Point

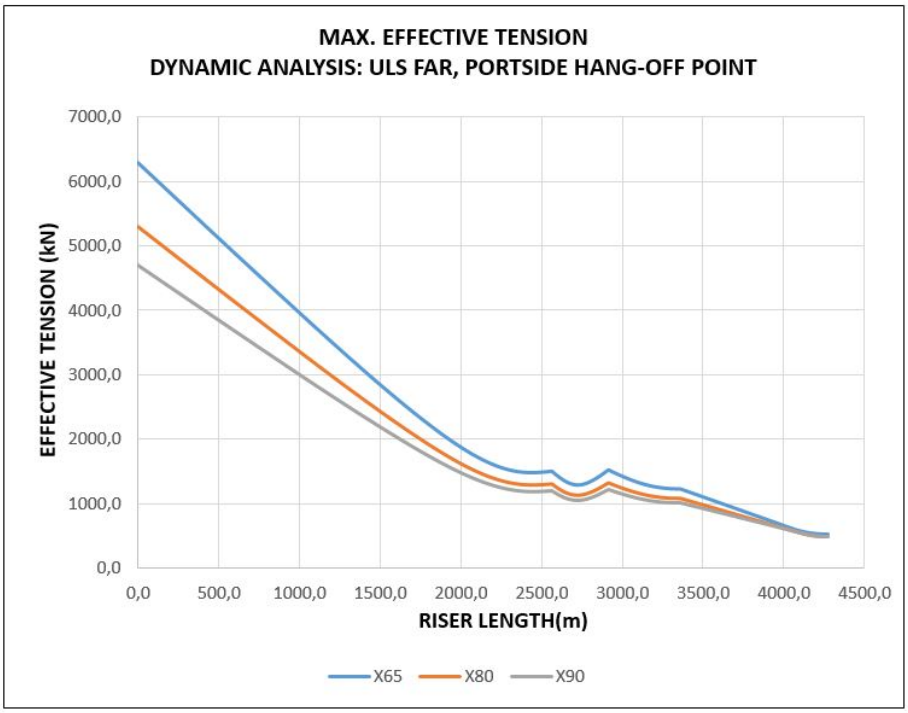

Figure 6.14: Maximum Effective Tension, Dynamic Analysis-ULS Far, PortSide Hang-off Point

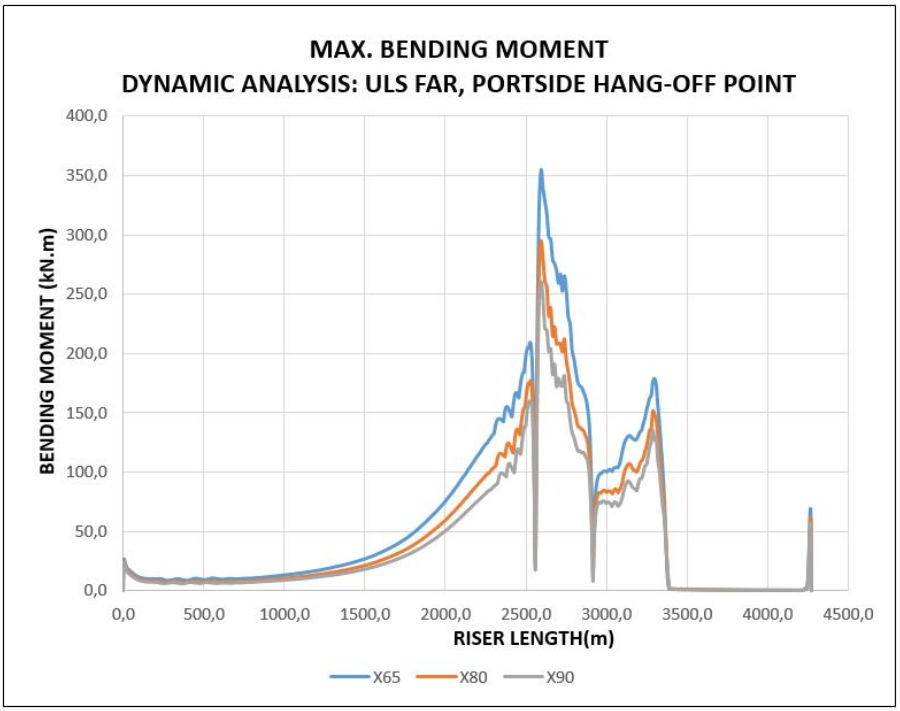

Figure 6.15: Maximum Bending Moment, Dynamic Analysis-ULS Far, PortSide Hang-off Point

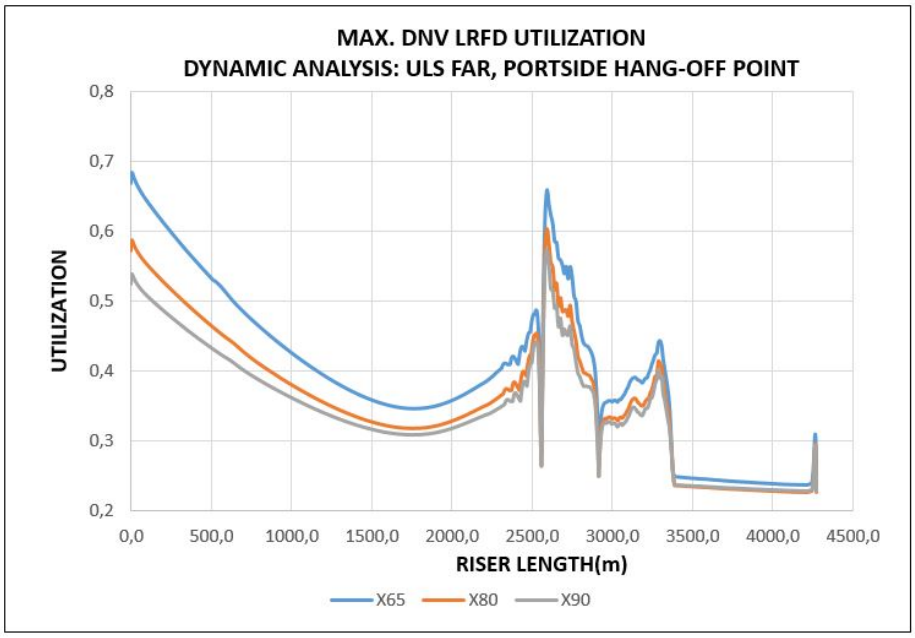

Figure 6.16: Maximum DNV LRFD Utilization, Dynamic Analysis-ULS Far, PortSide Hang-off Point

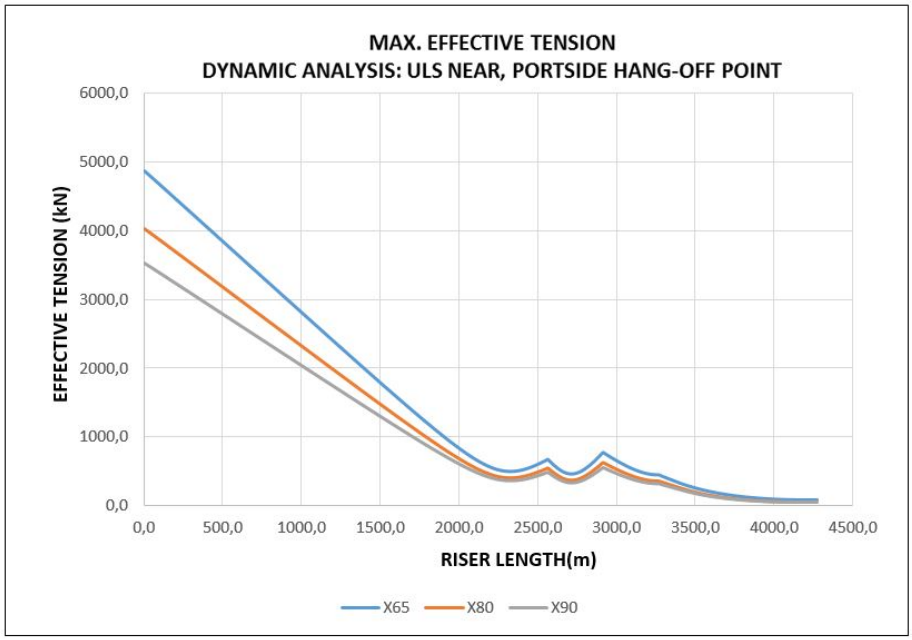

Figure 6.17: Maximum Effective Tension, Dynamic Analysis-ULS Near, PortSide Hang-off Point

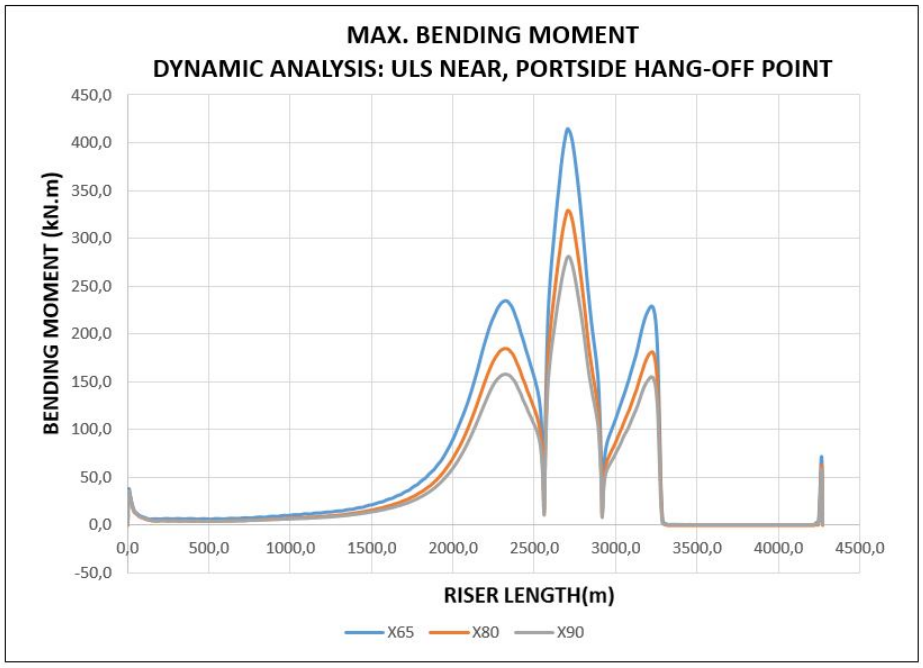

Figure 6.18: Maximum Bending Moment, Dynamic Analysis-ULS Near, PortSide Hang-off Point

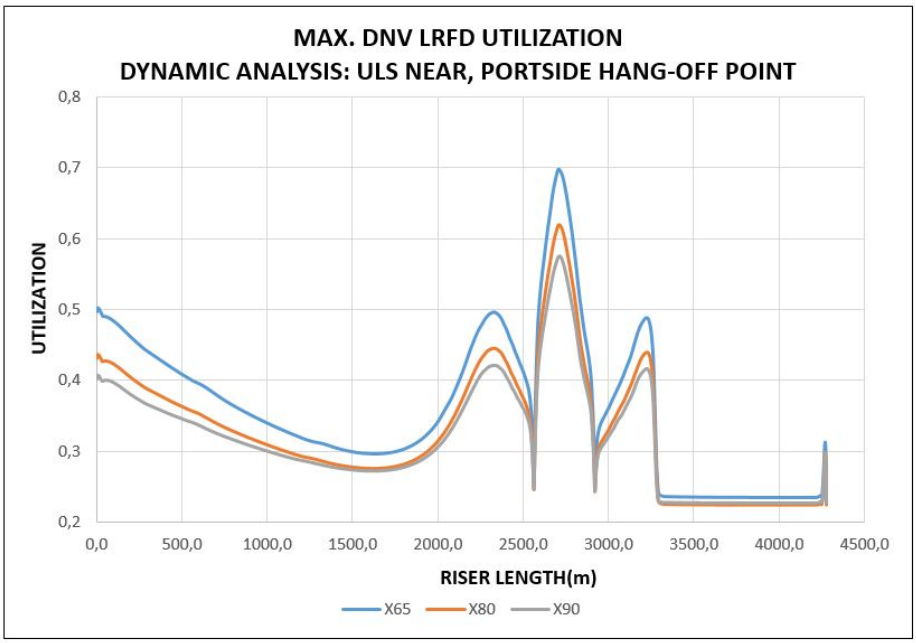

Figure 6.19: Maximum DNV LRFD Utilization, Dynamic Analysis-ULS Near, PortSide Hang-off Point

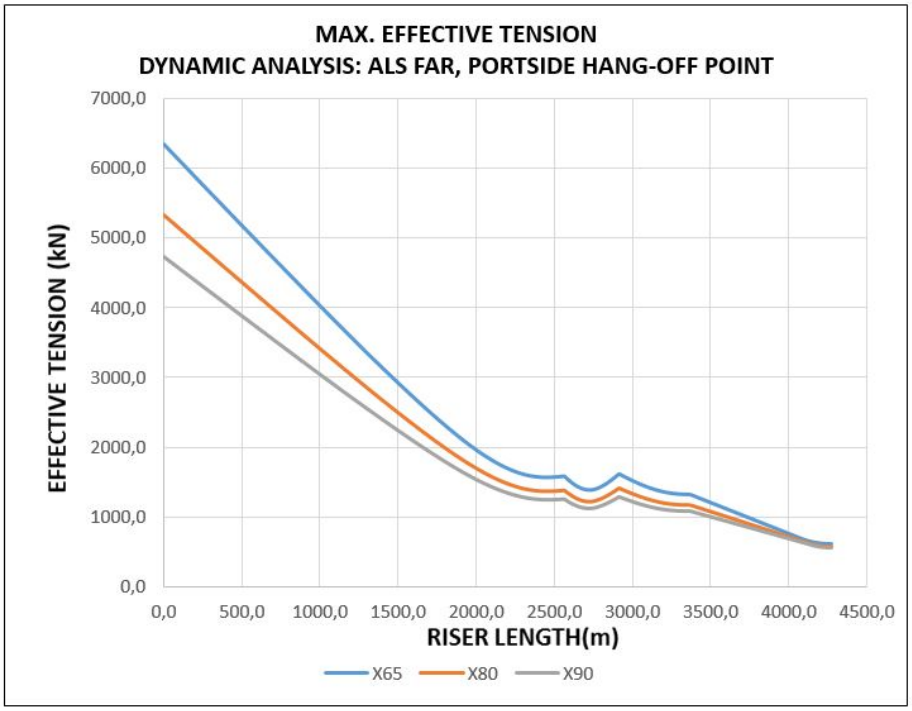

Figure 6.20: Maximum Effective Tension, Dynamic Analysis-ALS Far, PortSide Hang-off Point

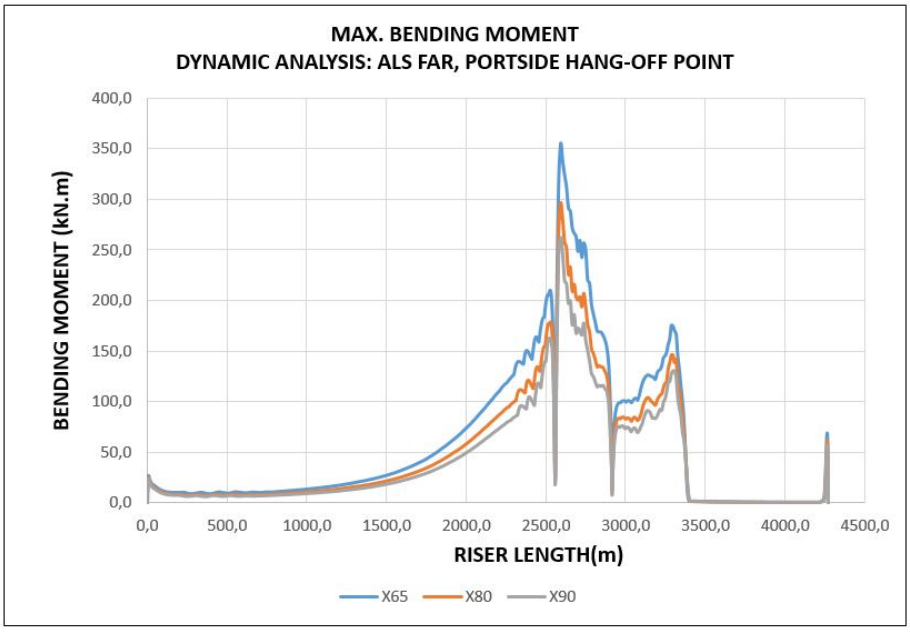

Figure 6.21: Maximum Bending Moment, Dynamic Analysis-ALS Far, PortSide Hang-off Point

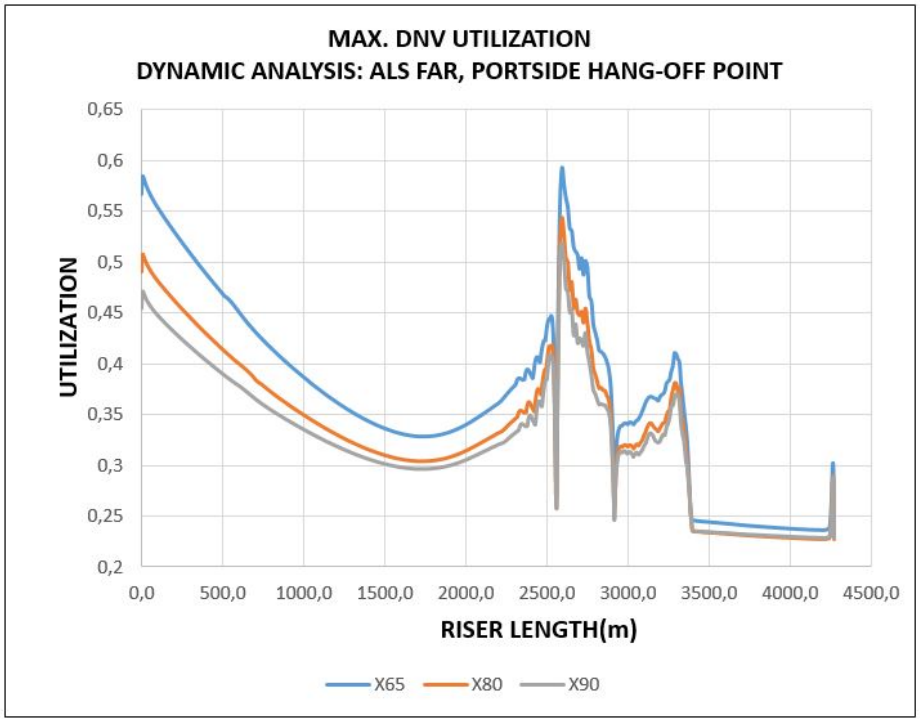

Figure 6.22: Maximum DNV LRFD Utilization, Dynamic Analysis-ALS Far, PortSide Hang-off Point

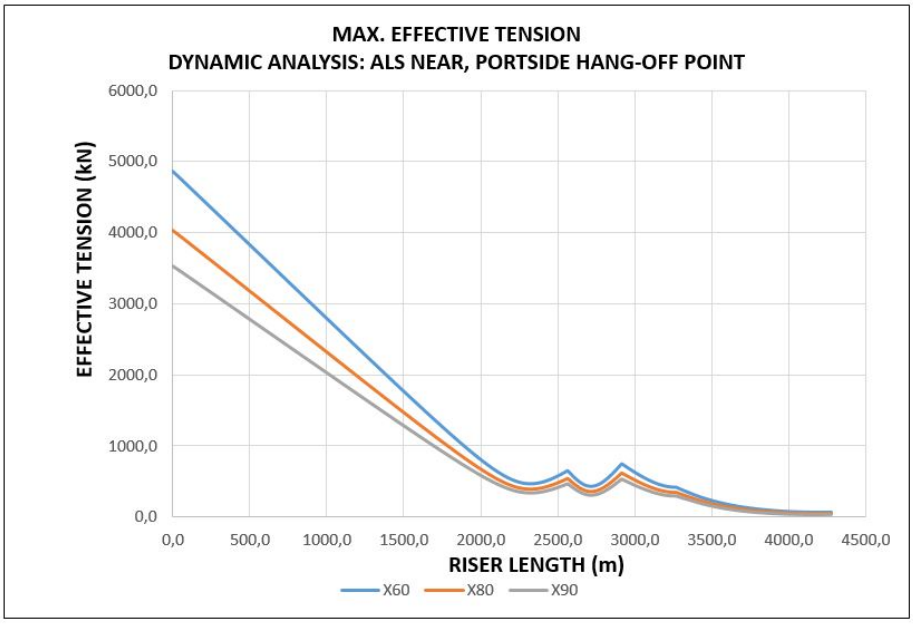

Figure 6.23: Maximum Effective Tension, Dynamic Analysis-ALS Near, PortSide Hang-off Point

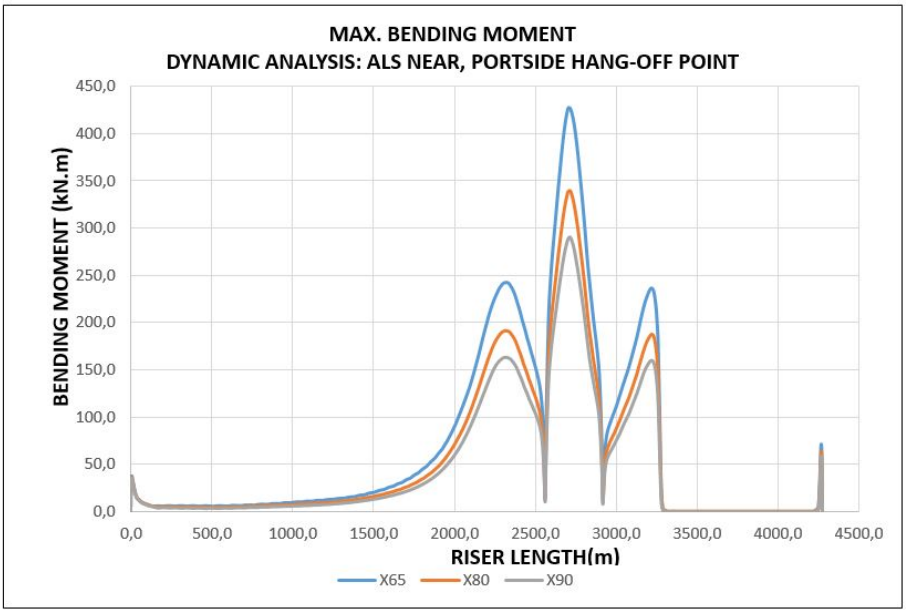

Figure 6.24: Maximum Bending Moment, Dynamic Analysis-ALS Near, PortSide Hang-off Point

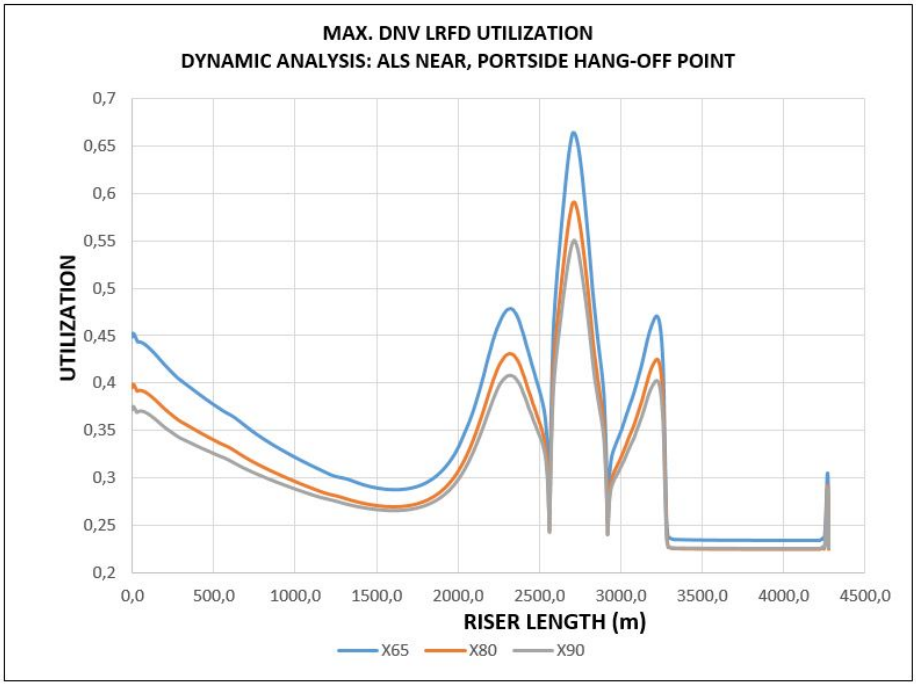

Figure 6.25: Maximum DNV LRFD Utilization, Dynamic Analysis-ALS Near, PortSide Hang-off Point

6.5.2.2 Dynamic Analysis Results in ULS and ALS Far and Near Offset, Middle of Vessel Hang-off Point

The results of the dynamic analysis in ULS and ALS far and near offset positions when the SLWR is connected to the hang-off point along the middle of the vessel are presented in Tables 6.9 and 6.10 respectively.

As highlighted in the tables, the following was observed in the ULS and ALS offset positions for the X65, X80 and X90 SLWRs:

1. The maximum effective tension occurs in the top section of the risers when it is in the ALS far offset position. For the X65, X80 and X90 SLWRs, the maximum effective tensions observed are 6139 kN, 5121 kN, 4530 kN respectively. Therefore, changing the riser material from X65 to X80 reduces the maximum effective tension by 19% and from X80 to X90 reduces it 13% further.

2. The maximum bending moment occurs in the hog-bend section of the riser when it is in the ALS near offset position. For the X65, X80 and X90 SLWRs, the maximum bending moment observed are $435kN.m$, $345kN.m$ and $295kN.m$ respectively. Therefore, changing the riser material from X65 to X80 reduces the maximum bending moment by 26% and from X80 to X90 reduces it 17% further.

3. The maximum DNV LRFD Utilization occurs in the hog-bend section of the riser when it is in the ULS near offset position. For the X65, X80 and X90 SLWRs, the maximum DNV LRFD utilization observed are 0.71, 0.63, 0.59 respectively. Therefore, changing the riser material from X65 to X80 reduces the maximum DNV LRFD utilization by 13% and from X80 to X90 reduces it 7% further.

4. The maximum DNV LRFD utilization values observed meet the DNV LRFD utilization criteria. Hence, the design is safe.

5. No compressive forces are observed in any of the analysis.

The above results show that the same percentage reduction is experienced when the riser materials are changed whether they are connected either to the hang-off point along the middle or the hang-off point along the port side.

Critical Section	**Top**					
Riser Material	**X65**		**X80**		**X90**	
Offset	**Far**	**Near**	**Far**	**Near**	**Far**	**Near**
Maximum Effective Tension (kN)	6106	5137	5095	4253	4505	3738
Maximum Bending Moment (kN.m)	0	0	0	0	0	0
Max DNV LRFD Utilization	0.64	0.52	0.54	0.45	0.50	0.42
Critical Section	**Sag Bend**					
Riser Material	**X65**		**X80**		**X90**	
Offset	**Far**	**Near**	**Far**	**Near**	**Far**	**Near**
Maximum Effective Tension (kN)	1418	689	1208	569	1087	499
Maximum Bending Moment (kN.m)	174	236	144	186	127	158
Max DNV LRFD Utilization	0.44	0.50	0.41	0.45	0.40	0.42
Critical Section	**Hog Bend**					
Riser Material	**X65**		**X80**		**X90**	
Offset	**Far**	**Near**	**Far**	**Near**	**Far**	**Near**
Maximum Effective Tension (kN)	1312	770	1110	632	992	549
Maximum Bending Moment (kN.m)	301	422	242	334	209	286
Max DNV LRFD Utilization	0.59	0.71	0.53	0.63	0.50	0.59
Critical Section	**Touch Down Point**					
Riser Material	**X65**		**X80**		**X90**	
Offset	**Far**	**Near**	**Far**	**Near**	**Far**	**Near**
Maximum Effective Tension (kN)	1012	441	867	361	780	314
Maximum Bending Moment (kN.m)	105	117	86	95	72	72
Max DNV LRFD Utilization	0.37	0.37	0.34	0.34	0.32	0.32

Table 6.9: Dynamic Analysis Results: ULS Far and Near, Middle of Vessel Hang-off Point

Critical Section	**Top**					
Riser Material	**X65**		**X80**		**X90**	
Offset	**Far**	**Near**	**Far**	**Near**	**Far**	**Near**
Maximum Effective Tension (kN)	6139	5130	5121	4249	4530	3733
Maximum Bending Moment (kN.m)	0	0	0	0	0	0
Max DNV LRFD Utilization	0.55	0.47	0.47	0.41	0.44	0.38
Critical Section	**Sag Bend**					
Riser Material	**X65**		**X80**		**X90**	
Offset	**Far**	**Near**	**Far**	**Near**	**Far**	**Near**
Maximum Effective Tension (kN)	1481	678	1262	560	1138	491
Maximum Bending Moment (kN.m)	174	244	144	192	127	164
Max DNV LRFD Utilization	0.41	0.48	0.38	0.43	0.37	0.41
Critical Section	**Hog Bend**					
Riser Material	**X65**		**X80**		**X90**	
Offset	**Far**	**Near**	**Far**	**Near**	**Far**	**Near**
Maximum Effective Tension (kN)	1374	742	1163	609	1040	529
Maximum Bending Moment (kN.m)	298	435	240	345	208	295
Max DNV LRFD Utilization	0.54	0.67	0.49	0.60	0.46	0.56
Critical Section	**Touch Down Point**					
Riser Material	**X65**		**X80**		**X90**	
Offset	**Far**	**Near**	**Far**	**Near**	**Far**	**Near**
Maximum Effective Tension (kN)	1073	424	920	347	830	301
Maximum Bending Moment (kN.m)	100	98	81	80	69	59
Max DNV LRFD Utilization	0.34	0.33	0.31	0.31	0.30	0.29

Table 6.10: Dynamic Analysis Results: ALS Far and Near, Middle of Vessel Hang-off Point

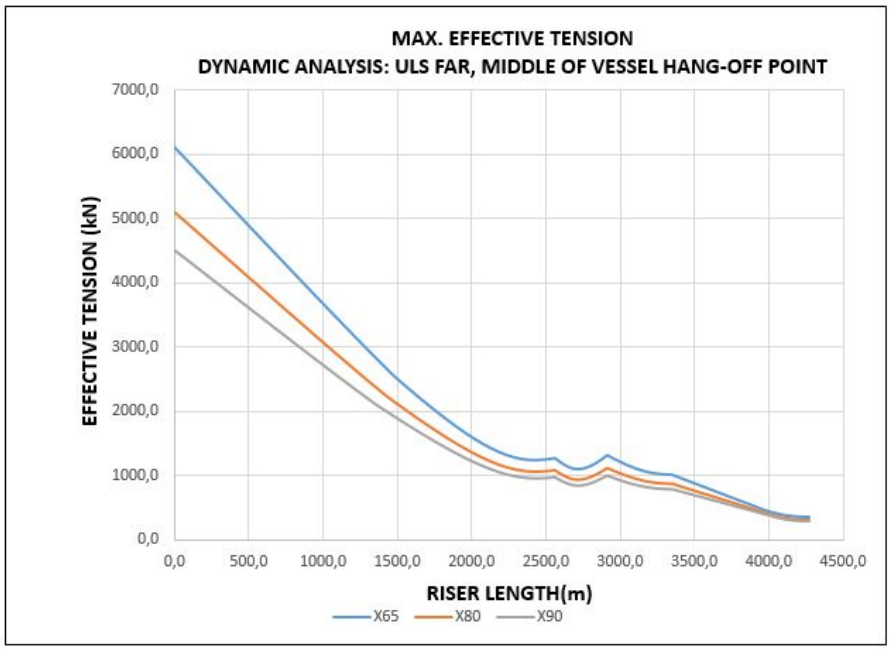

Figure 6.26: Maximum Effective Tension, Dynamic Analysis-ULS Far, Middle of Vessel Hang-off Point

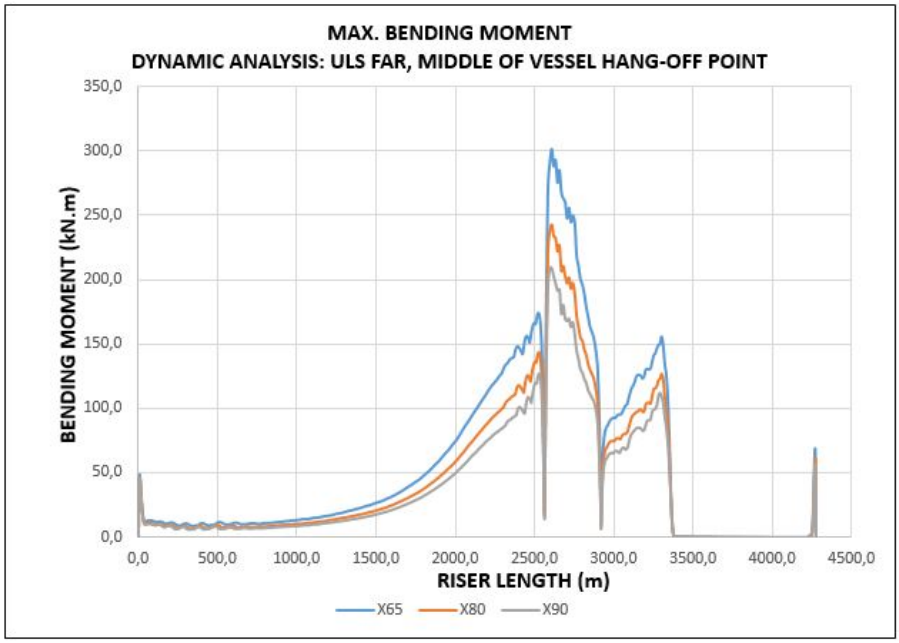

Figure 6.27: Maximum Bending Moment, Dynamic Analysis-ULS Far, Middle of Vessel Hang-off Point

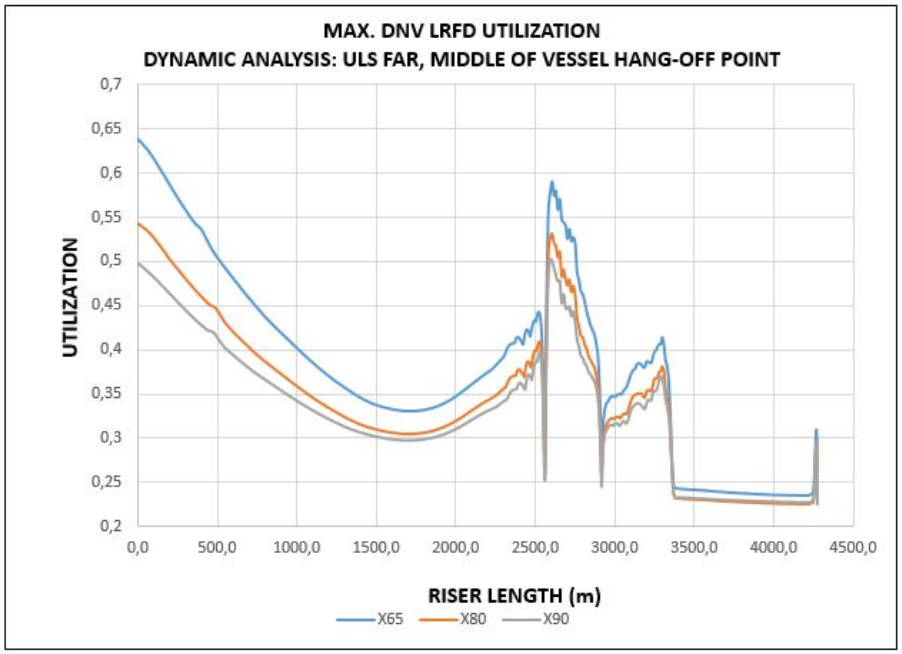

Figure 6.28: Maximum DNV LRFD Utilization, Dynamic Analysis-ULS Far, Middle of Vessel Hang-off Point

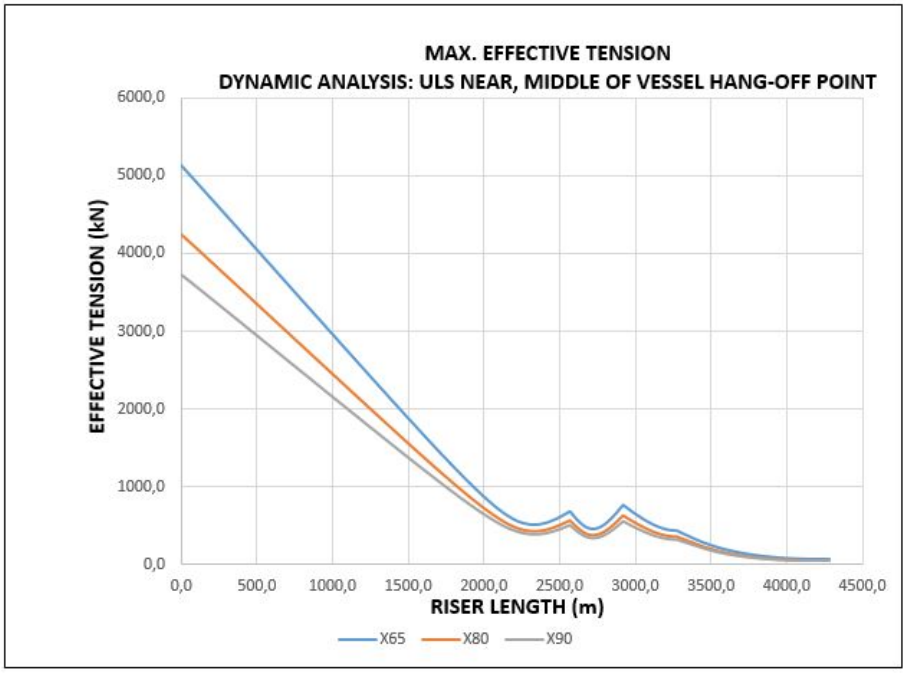

Figure 6.29: Maximum Effective Tension, Dynamic Analysis-ULS Near, Middle of Vessel Hang-off Point

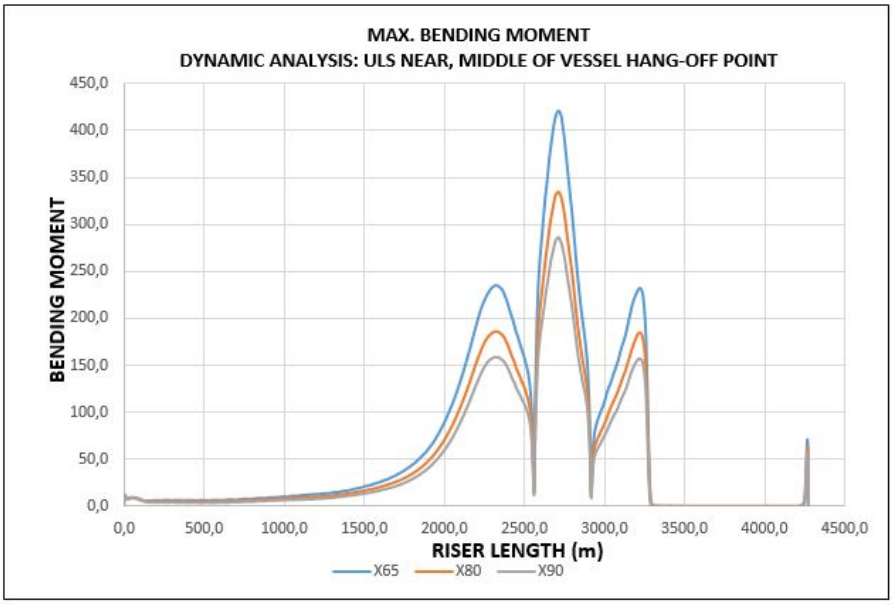

Figure 6.30: Maximum Bending Moment, Dynamic Analysis-ULS Near, Middle of Vessel Hang-off Point

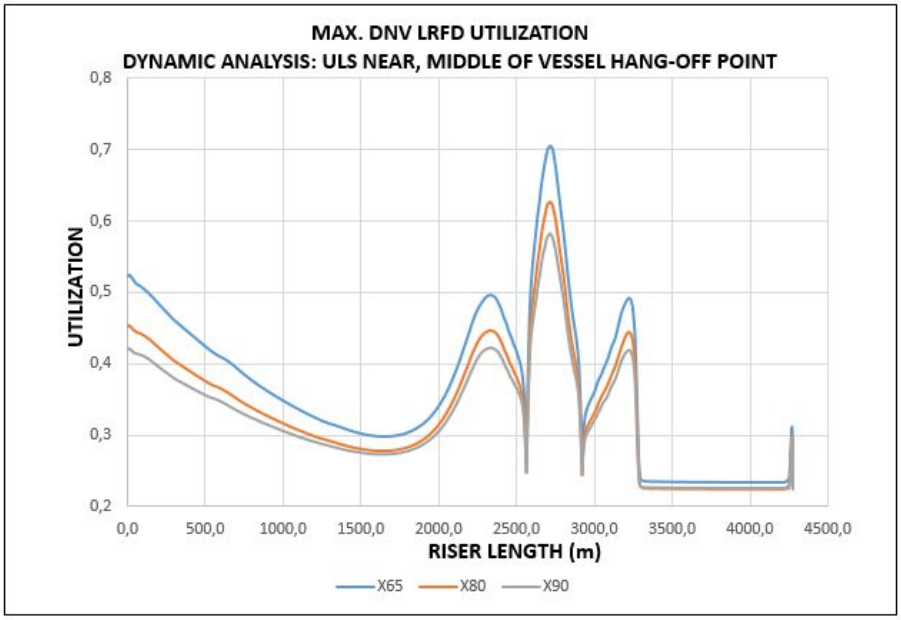

Figure 6.31: Maximum DNV LRFD Utilization, Dynamic Analysis-ULS Near, Middle of Vessel Hang-off Point

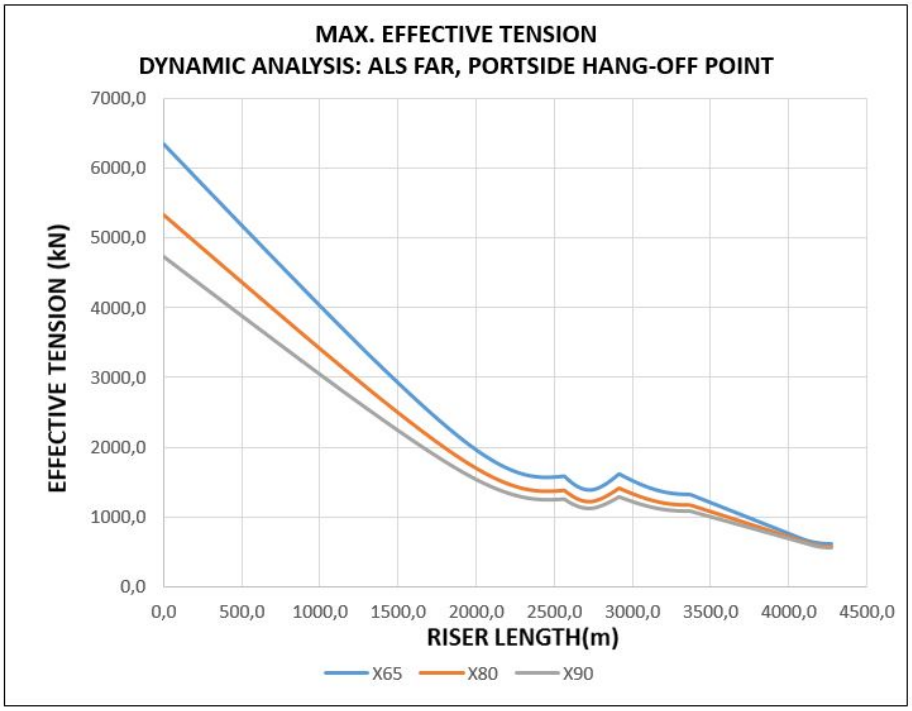

Figure 6.32: Maximum Effective Tension, Dynamic Analysis-ALS Far, Middle of Vessel Hang-off Point

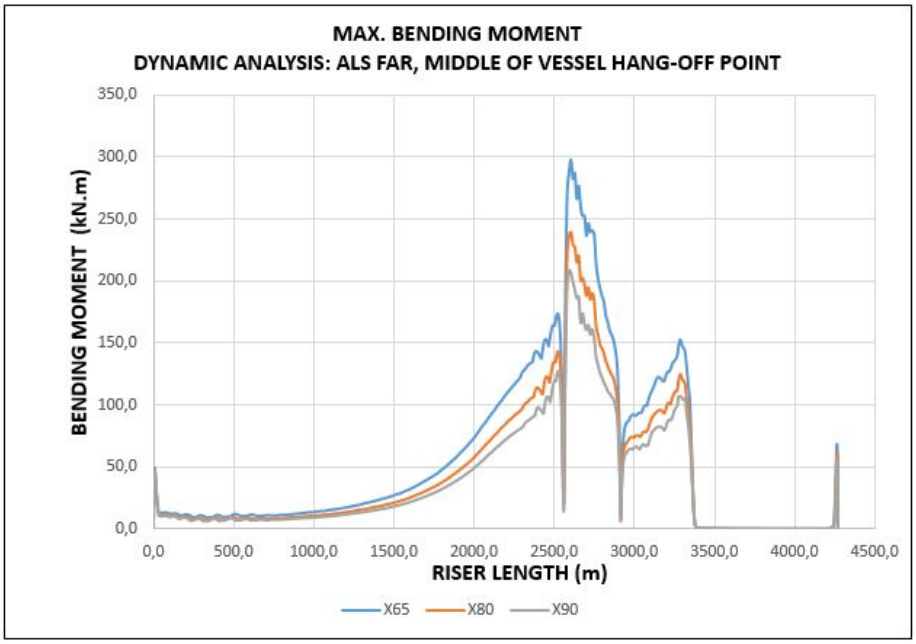

Figure 6.33: Maximum Bending Moment, Dynamic Analysis-ALS Far, Middle of Vessel Hang-off Point

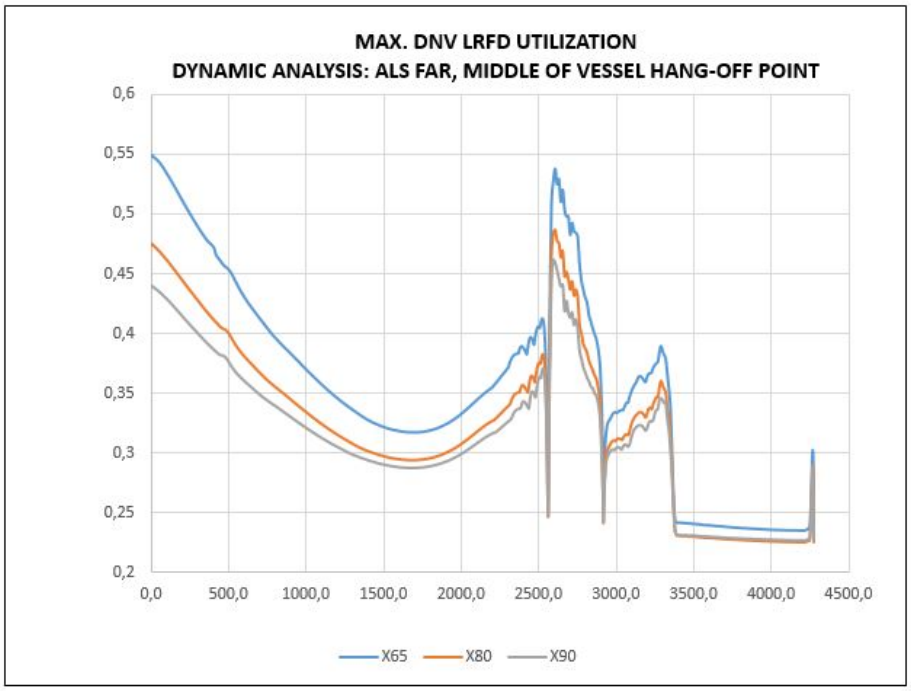

Figure 6.34: Maximum DNV LRFD Utilization, Dynamic Analysis-ALS Far, Middle of Vessel Hang-off Point

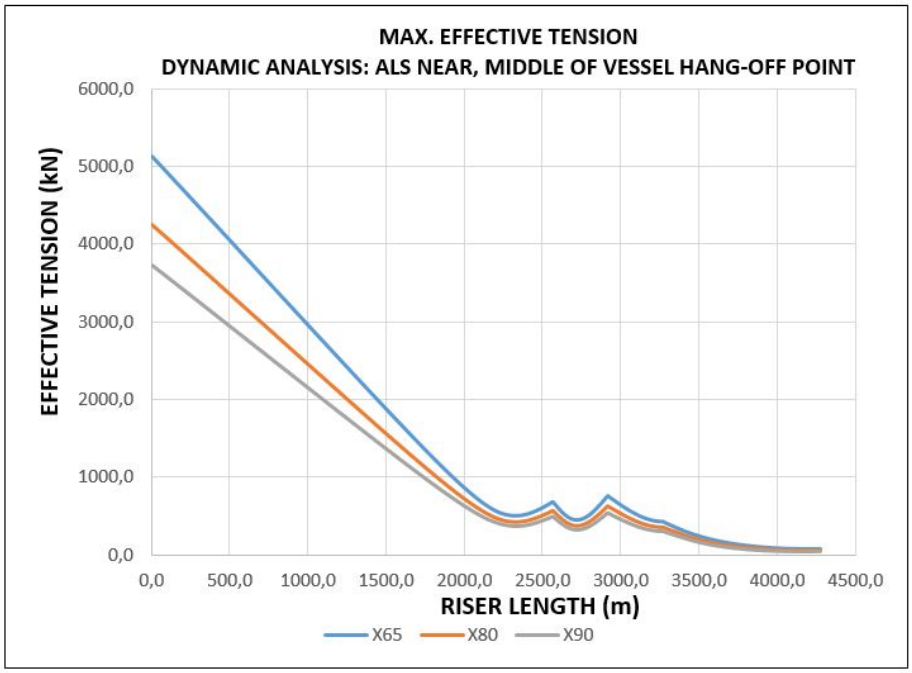

Figure 6.35: Maximum Effective Tension, Dynamic Analysis-ALS Near, Middle of Vessel Hang-off Point

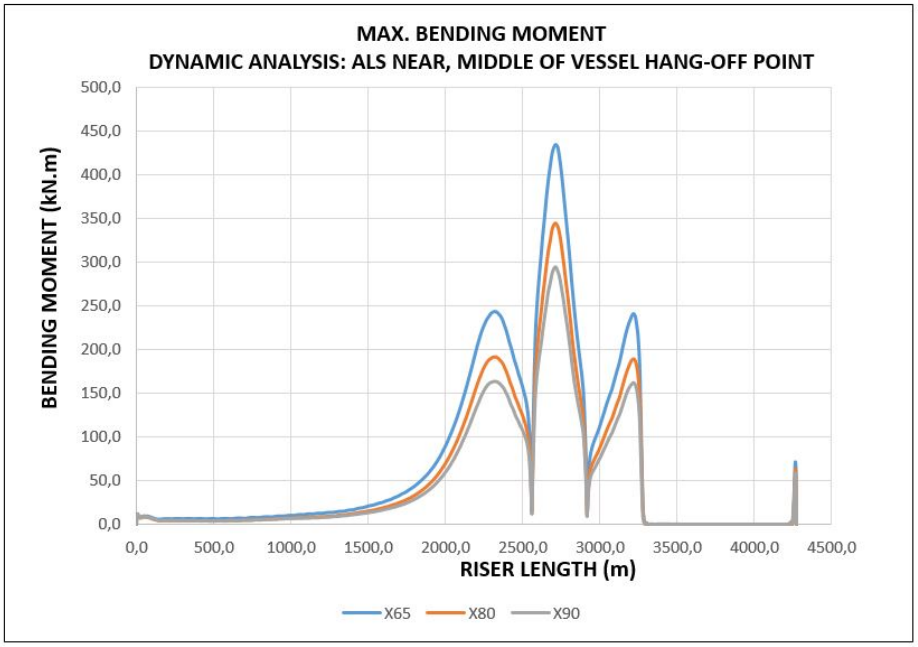

Figure 6.36: Maximum Bending Moment, Dynamic Analysis-ALS Near, Middle of Vessel Hang-off Point

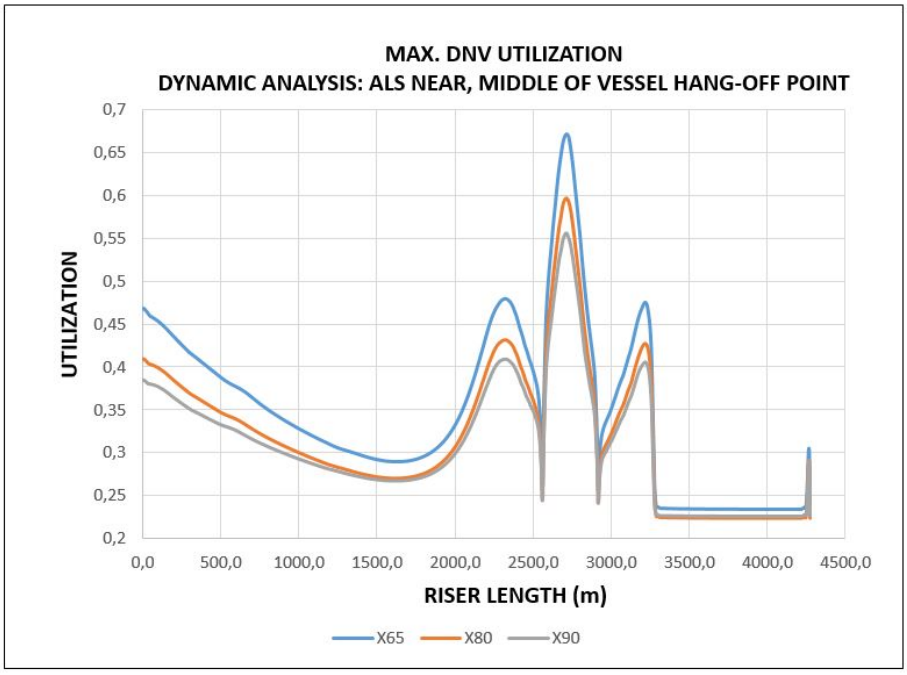

Figure 6.37: Maximum DNV LRFD Utilization, Dynamic Analysis-ALS Near, Middle of Vessel Hang-off Point

6.5.2.3 Comparison of Dynamic Analysis Results of the Portside and Middle of Vessel Hang-off Points

A comparison of the results of the dynamic analysis of the two hang-off points considered is presented in Table 6.11 and Figures 6.38, 6.39, 6.40.

From the results, the following was observed:

1. The maximum effective tension observed when the risers were connected to the hang-off point at the port side is greater than when they were connected to the hang-off point at the middle of the vessel. This maximum value occurred in the ALS far offset position.

2. The maximum bending moment observed is greater when the risers were connected to the hang-off point at the middle of the vessel than when they were connected to the hang-off point along the port side of the vessel. This maximum value occurred in the ULS near offset position.

3. The maximum DNV LRFD utilization observed is greater when the risers were connected to the hang-off point along the middle of the vessel than when they were connected to the hang-off point along the port side of the vessel. This maximum value occurred in the ULS near offset.

Riser Material	Maximum Effective Tension(kN)		Maximum Bending Moment (kN.m)		Maximum DNV LRFD Utilizaiton	
	Port Side	Middle	Port Side	Middle	Port Side	Middle
X65	6346	6139	427	435	0.70	0.71
X80	5336	5121	340	345	0.62	0.63
X90	4743	4530	290	295	0.58	0.59

Table 6.11: Hang-Off Points Comparison

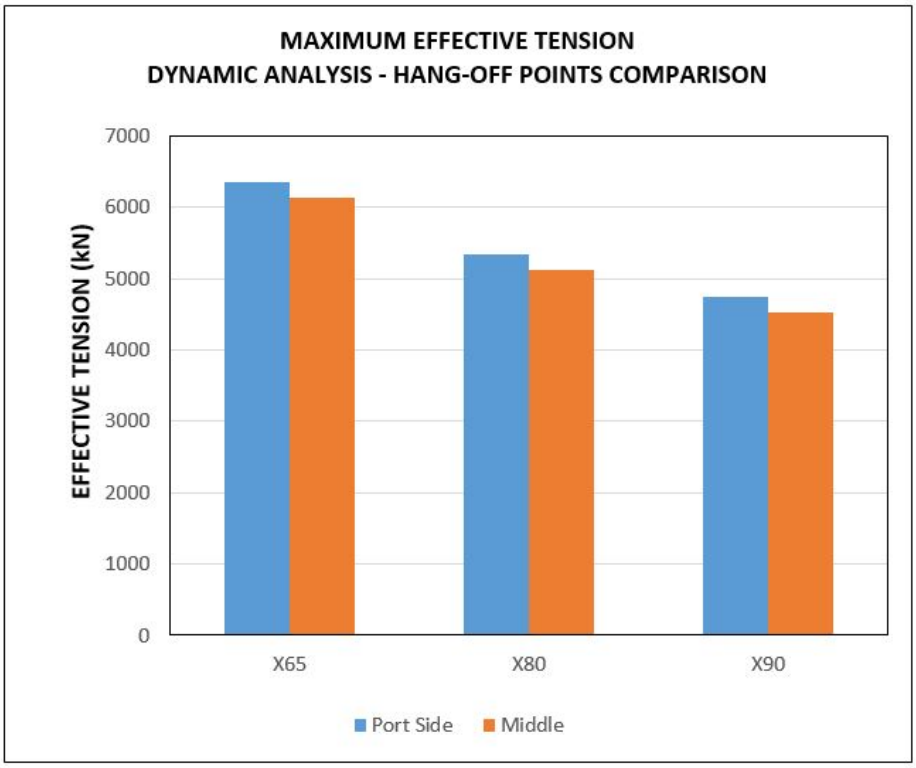

Figure 6.38: Maximum Effective Tension in Dynamic Analysis: Hang-off Points Comparison

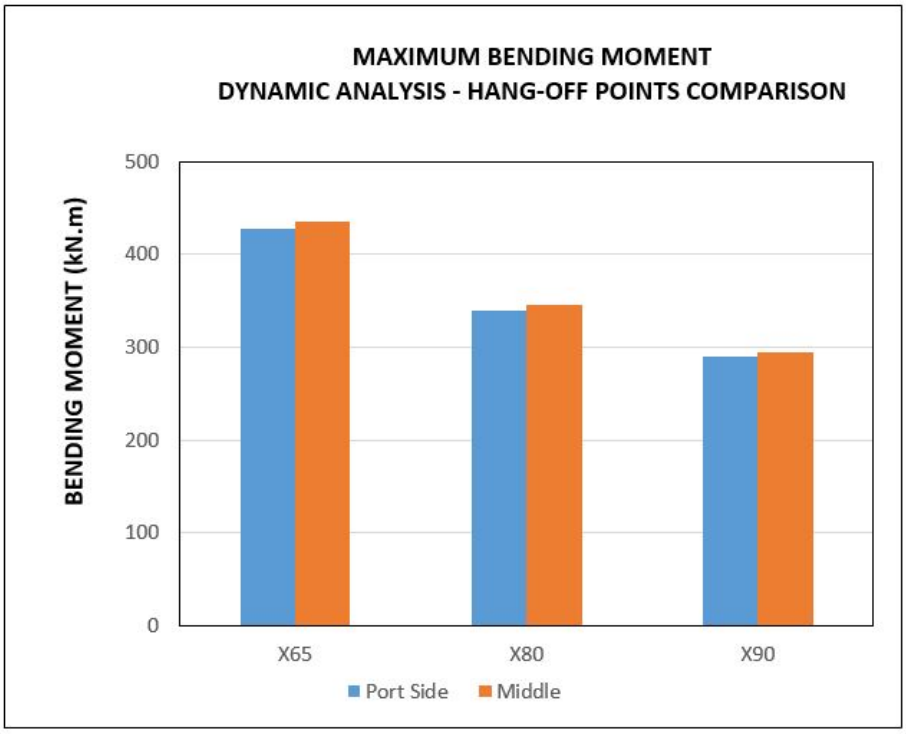

Figure 6.39: Maximum Bending Moment in Dynamic Analysis: Hang-off Points Comparison

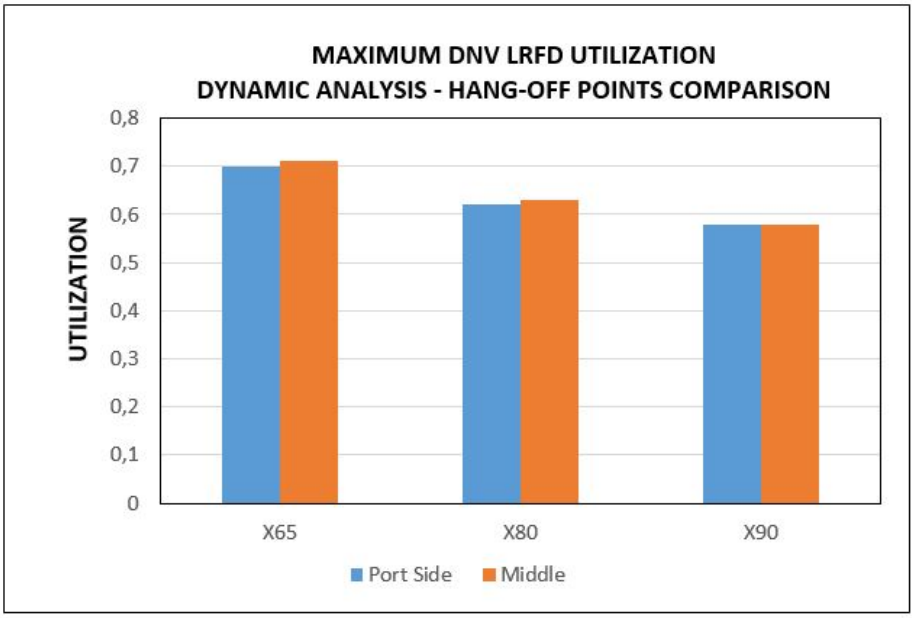

Figure 6.40: Maximum DNV LRFD Utilization in Dynamic Analysis: Hang-off Points Comparison

From Figures 6.39 and 6.40, it can be seen that the maximum bending moment and maximum DNV LRFD utilization were observed to be at their highest values when the risers were connected to the hang-off point at the middle of the vessel in the ULS near offset position.

These results were unexpected because the maximum downward velocities(see Table 6.12) experienced at the hang-off points as a result of the 100-year wave and 10 year-current from the West-NorthWest direction (wave and current direction that moves the vessel to the near offset position) are considerably lower than the maximum downward velocities experienced at the hang-off points as a result of the 100-year wave and 10-year current from the East-SouthEast direction (wave and current direction that moves the vessel to the far offset position).

Therefore, due to the larger maximum downward velocities the hang-off points experience in the far offset position, the maximum bending moment, maximum effective tension, and maximum DNV LRFD utilization should all occur when the risers are in the far offset position. Also, in the far offset position, the hang-off point at the port side experiences a larger maximum downward velocity than the hang-off point at the middle. For this reason, risers connected to the hang-off point at the port side of the vessel should experience a larger maximum down velocity than risers connected to the hang-off point at the middle of the vessel when the risers are in the far offset position

Riser Hang-off Point	**Max Downward Velocity(m/s) (West-NorthWest)**	**Max Downward Velocity(m/s) (East-SouthEast)**
A(30,0,11.6) Middle	-2.32	-3.69
D(30,31,11.6) Port Side	-1.77	-4.98

Table 6.12: Maximum Downward Velocities Experienced by the Riser Hang-off Points

Due to the unexpected results, the initial SLWR configuration determined in Section 6.4 was investigated. The results of the investigation showed that the use of excess buoyancy in the initial configuration caused the maximum utilization and maximum bending moment to be at their highest values in the near offset position when connected to the hang-off point at the middle even though the maximum downward velocities experienced were considerably lower than those experienced when the riser was in the far offset position connected to the hang-off point at the port side. Therefore, the results of the investigation suggested that the initial SLWR configuration selected in this study was not an optimal configuration.

As a result of this, an optimal configuration(see Figure 6.41) was determined and the parameters of this configuration are presented in Table 6.13.

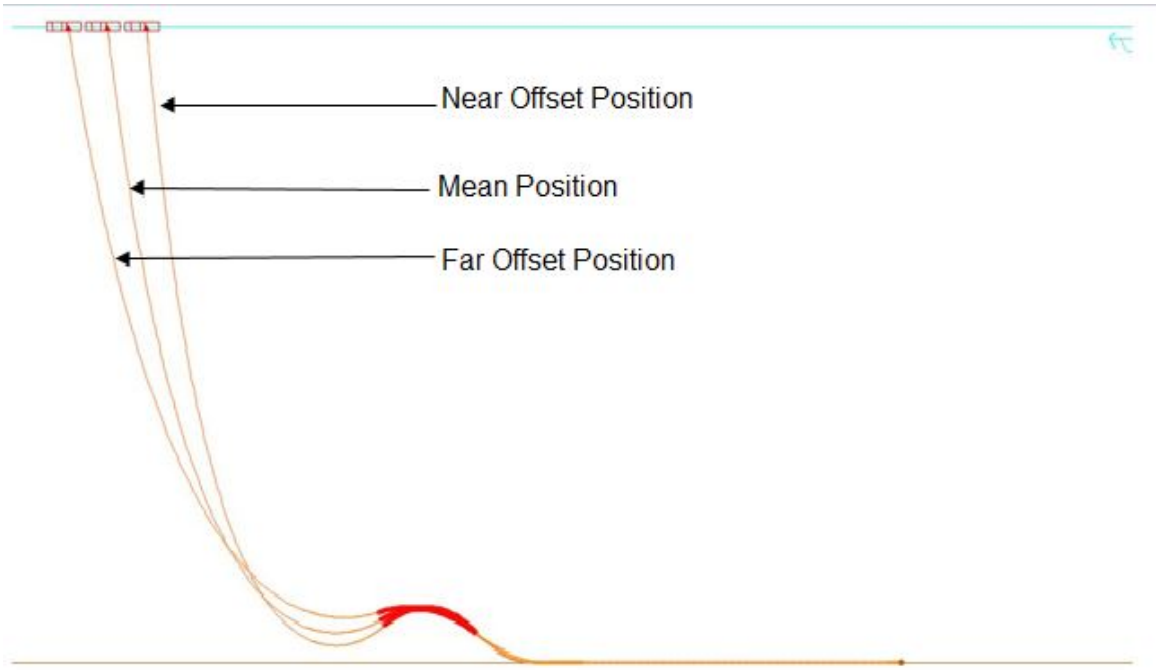

Figure 6.41: The Optimal SLWR Configuration

Description	**Value**	**Unit**
Hang-off Angle	8	°
Total Riser Length	4695	m
Upper Catenary Length	2595	m
Buoyancy Section Length	400	m
Lower Catenary Length	270	m
Bottom Section Length	1420	m
Sag-bend Height to Seabed	100	m
Hog-bend Height to Seabed	186	m
Lazy Wave Height	86	m
Net Buoyancy Force-X65 SLWR	156.4	kN
Net Buoyancy Force-X80 SLWR	127.9	kN
Net Buoyancy Force-X90 SLWR	111.4	kN

Table 6.13: Parameters of the Optimal SLWR Configuration

6.5.2.4 Dynamic Analysis of the Optimal SLWR Configuration

Dynamic analysis was conducted on the optimal configuration in the ULS and ALS far offset and the results are presented in this section. It should be noted only the results of the dynamic analysis of the X65 SLWR is presented in this section. The results of the X80 and X90 SLWR are presented in Appendix C.

The maximum effective tension, maximum bending moment, maximum DNV LRFD Utilization observed in the dynamic analysis of the optimal X65 SLWR when connected to either of the two hang-off points in the ULS and ALS far and near offset are presented below in Table 6.14.

DYNAMIC ANALYSIS: X65 SLWR	**Hang-Off Point**	
	Port Side	**Middle**
Maximum Effective Tension(kN)	6494	6332
Maximum Bending Moment(kN.m)	341	299
Maximum DNV LRFD Utilization	0.71	0.66

Table 6.14: Dynamic Analysis Results of the Improved X65 SLWR Connected to either of the Two Hang-off Points

From the results in Table 6.14, it can be seen that a maximum utilization of 0.71 was observed when the riser was connected to the hang-off point at the port side and 0.66 when the riser was connected to the hang-off point at the middle in the ULS Far offset. These were the expected results and it further verified that the configuration was optimal.

The difference in the maximum DNV LRFD utilization indicated that buoyancy could be saved by connecting the riser to the hang-off point at the middle instead of the hang-off point at the port side. To save buoyancy, a buoyancy reduction process was carried out on the riser connected to the hang-off point at the middle to push its maximum utilization from 0.66 to 0.71. It was observed that a buoyancy reduction of 7.5% pushed the maximum utilization to 0.69 and further reduction in buoyancy resulted in an unacceptable configuration.

Therefore, these results suggested that a riser connected to the hang-off point along the middle of the vessel will require 7.5% less buoyancy than a riser connected to the hang-off point at the port side of the vessel.

6.6 Fatigue Response Analysis

In this section, the fatigue response analysis is conducted on the optimal configuration and for this study, recommended practices in the DNV-RP-203: Fatigue Design of Offshore Steel Structures are adopted.

The DNV-RP-203 recommends the S-N curve methodology for estimating the fatigue response of offshore steel structures such as risers. The S-N curves, shown in Figure 6.42, have been derived from fatigue tests of small specimens in test laboratories and they are based on the mean-minus-two-standard-deviation curves for relevant experimental data. Therefore, S-N curves are associated with a 97.7% probability of survival (DNV, 2010b).

In this study, consideration is given to the C2 and D curves in Figure 6.42 based on the work of Karunakaran et al. (2013). The C2-curve is more tolerant than the D-curve and is expected to give a higher fatigue life for the same riser section (Orimolade, 2014).

According to DNV (2010b), the S-N curve is governed by:

$$\log N = \log \bar{a} - m \log \Delta\sigma \tag{6.1}$$

where:

N	Predicted number of cycles to failure for stress range $\Delta\sigma$
$\Delta\sigma$	Stress range with unit MPa
m	negative inverse slope of S-N curve
$\log \bar{a}$	Intercept of log N-axis by S-N curve

And

$$\log \bar{a} = \log a - 2 s_{\log N} \tag{6.2}$$

where:

$\log a$	Intercept of mean S-N curve with the log N axis
$s_{\log N}$	standard deviation of N

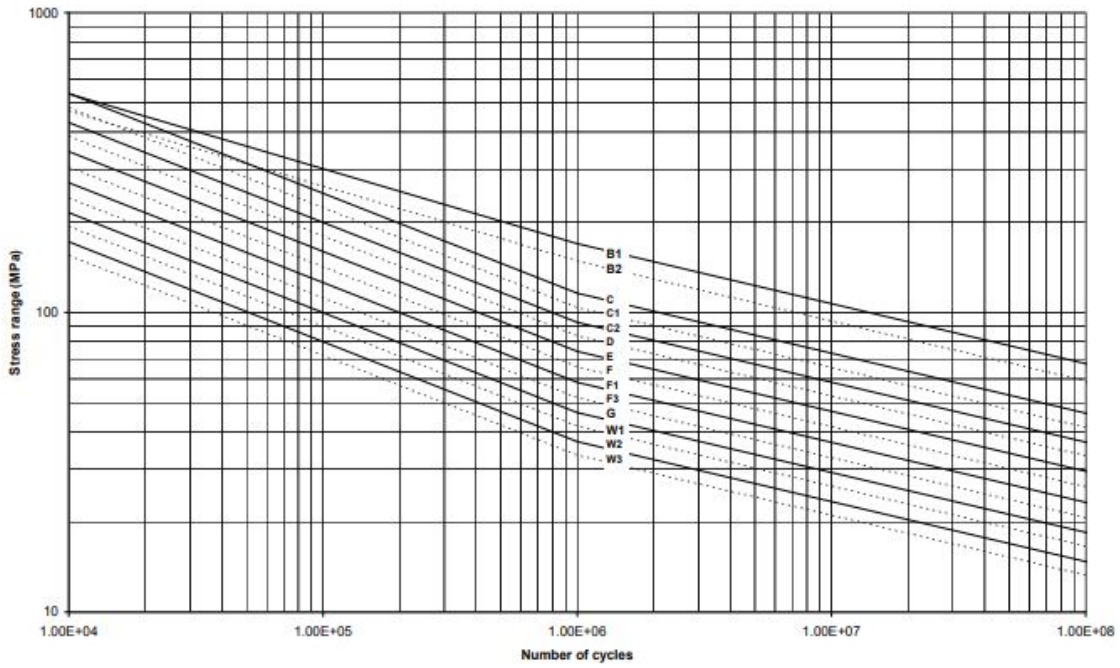

Figure 6.42: S-N Curves in Seawater With Cathodic Protection (DNV, 2010b)

The stress range is obtained by the use of stress concentration factor and thickness correction factor to the nominal stress range:

$$\Delta = \Delta_o \cdot SCF \cdot \left(\frac{t_3}{t_{ref}}\right)^k \tag{6.3}$$

where:

Δ_o	Nominal stress range
SCF	Stress Concentration Factor
$\left(\frac{t_3}{t_{ref}}\right)^k$	Thickness correction factor
t_3	Pipe wall thickness
t_{ref}	Reference wall thickness = 25 mm
k	Thickness exponent

The stress concentration factor(SCF) is used to account for uncertainties such as stress magnification arising from geometrical imperfections between adjacent joints. The SCF is obtained either by finite element analysis or the use of a closed-form expression. For welded riser joints, the expression below applies (DNV, 2010c):

$$SCF = 1 + \frac{3e}{t_3} exp\left(-\left(\frac{D}{t_3}\right)^{-0.5}\right) \tag{6.4}$$

where:

e eccentricity due to imperfections in geometry

Using the expression above, an approximated value of 1.2 is used as the stress concentration factor for the fatigue damage calculations in this study.

As recommended by DNV(2010c), the Miner-Palmgren rule is adopted for accumulation of fatigue damage from stress cycles and the rule is given by:

$$D_{fat} = \sum_i \frac{n(S_i)}{N(S_i)} \tag{6.5}$$

where:

D_{fat}	Accumulated Fatigue Damage
$n(S_i)$	Number of stress cycles with range S_i
$N(S_i)$	Number of stress cycles to failure

6.6.1 Wave-Induced Fatigue Damage

Wave-induced fatigue damage occurs as a result of vessel motions caused by sea states and it is highly dependent on a vessel's design and hang-off point location. Therefore, the wave induced fatigue damage calculations showed a clear difference in performance of the two hang-off points considered in this study.

In this section, the procedure adopted for the wave-induced fatigue damage calculations is presented first. Afterwards, the results observed in the calculations are presented and compared for each SLWR connected to the two different hang-off points considered in this study.

6.6.1.1 Wave-Induced Fatigue Damage Calculation Procedure

In this study, the wave-induced fatigue damage from a total of 9 wave directions and their frequencies of occurrence, as presented in Table 6.15, was considered. This resulted into 123 load cases for the wave-induced fatigue damage calculations.

According to DNV (2010c), the general approach for the calculation of wave-induced fatigue damage is based on the application of the following procedure:

1. Wave environment scatter diagram is subdivided into a number of representative blocks. In this study, the wave environment scatter diagram was divided into 12 representative blocks and is shown in Figure 6.43.

2. In each representative block, a single sea state(marked a red X in Figure 6.43) is selected to represent all the sea states within that block and the probabilities of occurrence for all sea-states within the block are lumped to the selected sea state.

3. Fatigue damage is computed for each of the selected sea state.

   In this study, OrcaFlex was used to compute the fatigue damage using the rain-flow cycle counting technique.

   Fatigue damage is calculated around the circumference of the riser at 16 equally spaced points for each weld along the entire length of the riser. The worst damage from the 16 points is then selected as the damage at that particular joint.

   The simulation time was set for each load case to 45 minutes in order to accurately capture the fatigue damage.

4. The weighted fatigue damage accumulation from all sea states is then calculated with:

$$D_L = \sum_{i=1}^{Ns} D_i P_i \tag{6.6}$$

   where:

D_L	Long-term fatigue damage
Ns	Number of discrete sea states in the wave scatter diagram
D_i	Short term fatigue damage
P_i	Sea state probability

This procedure is then repeated for all the wave directions considered and the total long-term fatigue damage is computed using Equation 6.6.

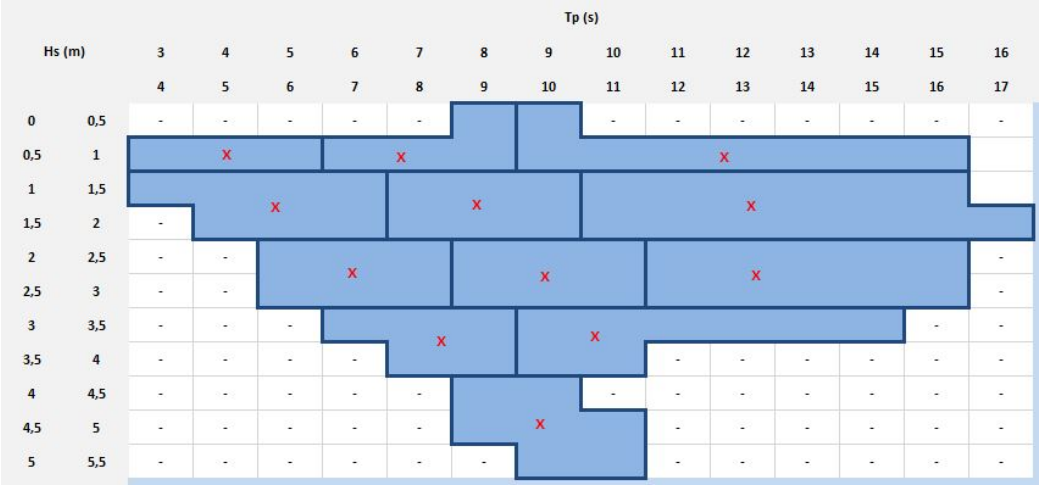

Figure 6.43: Subdivision of Wave Scatter Diagram into Representative Blocks

Wave Direction	**Frequency of Occurence(%)**
North East	20.37
East-NorthEast	14.87
East	6.69
Beam Port	11.28
East-SouthEast	2.7
South East	8.94
South-SouthEast	9.12
South	10.97
South-SouthWest	15.03
Total	100

Table 6.15: Considered Wave Directions and their Frequencies of Occurrence

6.6.2 Results of the Wave-Induced Fatigue Damage Calculations

The fatigue life at a point on the riser pipe is the time it takes for a crack to develop through the wall thickness of the riser pipe. Since the riser in this study is a production riser, the safety class is high and a safety factor of 10 is used for the fatigue calculation. Therefore, with a design life of 25 years, a minimum fatigue life of 250 years is required. This is in accordance with the recommendations of the DNV-OS-F201 reference standard.

The results for the total fatigue life observed at the critical sections of the X65, X80, X90 SLWRs when they are connected to either the hang-off point along the

middle of the vessel or the hang-off point along the port side of the vessel are presented in Table 6.16 and a clear comparison between the two hang-off points is shown in Figures 6.44 and 6.45. Also, the fatigue life over the entire riser length of the X65, X80 and X90 SLWRs is presented in Figures 6.46, 6.47,6.48,6.49,6.50,6.51.

From the Table 6.16, the following was observed:

1. The minimum fatigue life observed in the SLWRs are well above the required minimum fatigue life of 250 years. Hence, the fatigue performance of the risers are acceptable.

2. The minimum fatigue life (or worst fatigue damage) occurs at the top section in the risers irrespective of the hang-off points they are connected to. The top section has the minimum fatigue life because of the large top tension experienced by the risers.

3. The minimum fatigue life observed in the risers connected to the hang-off point at the middle is considerably larger than the minimum fatigue life observed in the risers connected to the hang-off point at the port side of the vessel.

4. An increase of 246%, 250% and 266% is observed in the D-curve when the risers are connected to the hang-off point at the middle rather than at the hang-off point at the port side. This indicated that risers connected to the hang-off point at the middle of the vessel would have a better fatigue performance than those connected to the port side.

5. It can also be seen that the minimum fatigue life reduces as the riser material is changed from X65 to X80 to X90. This is because the minimum fatigue life reduces with reducing wall thickness and steel weight.

6. As expected, the C-2 curve being more tolerant than the D-curve, gives a higher fatigue life in the risers.

Top Section:	**D-Curve (Years)**			**C2-Curve (Years)**		
10m below Hang-off Point	**Port Side**	**Middle**	**% Change**	**Port Side**	**Middle**	**% Change**
X65	1,794	6,203	246	3,089	10,927	254
X80	1,443	5050	250	2,380	8,479	256
X90	1053	3,849	266	1,735	6,403	269

Table 6.16: Minimum Fatigue Life in the X65, X80 and X90 SLWRs

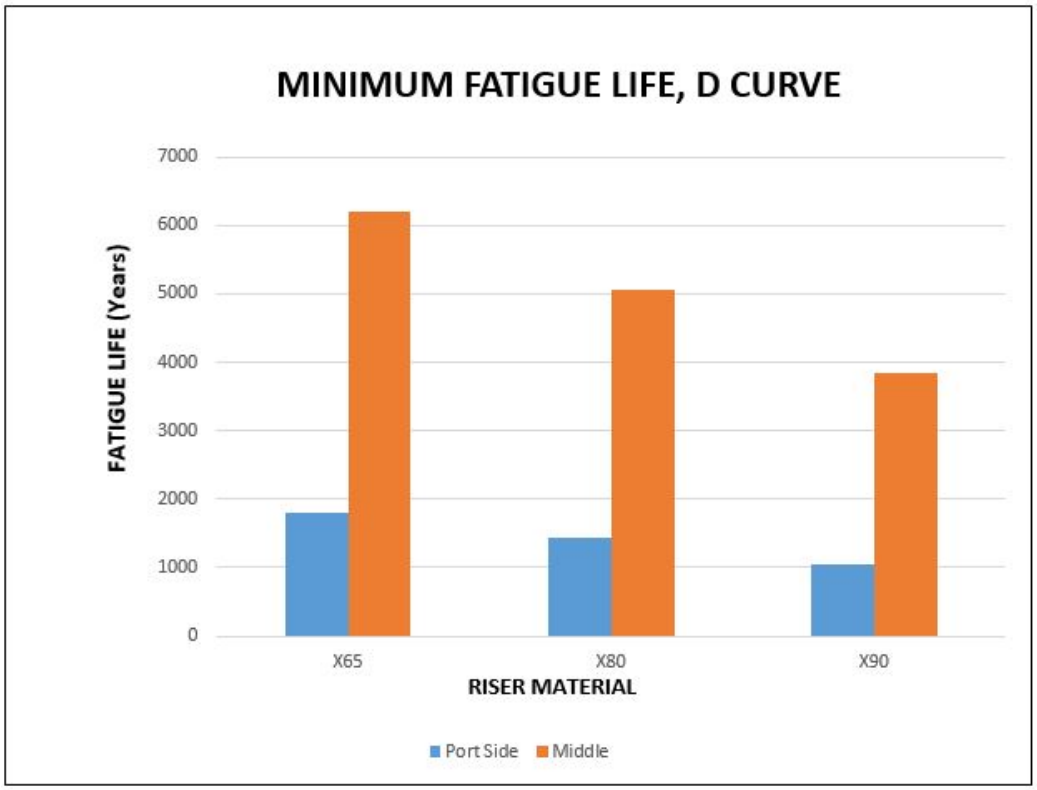

Figure 6.44: Minimum Fatigue Life, D-Curve Hang-off Point Comparison

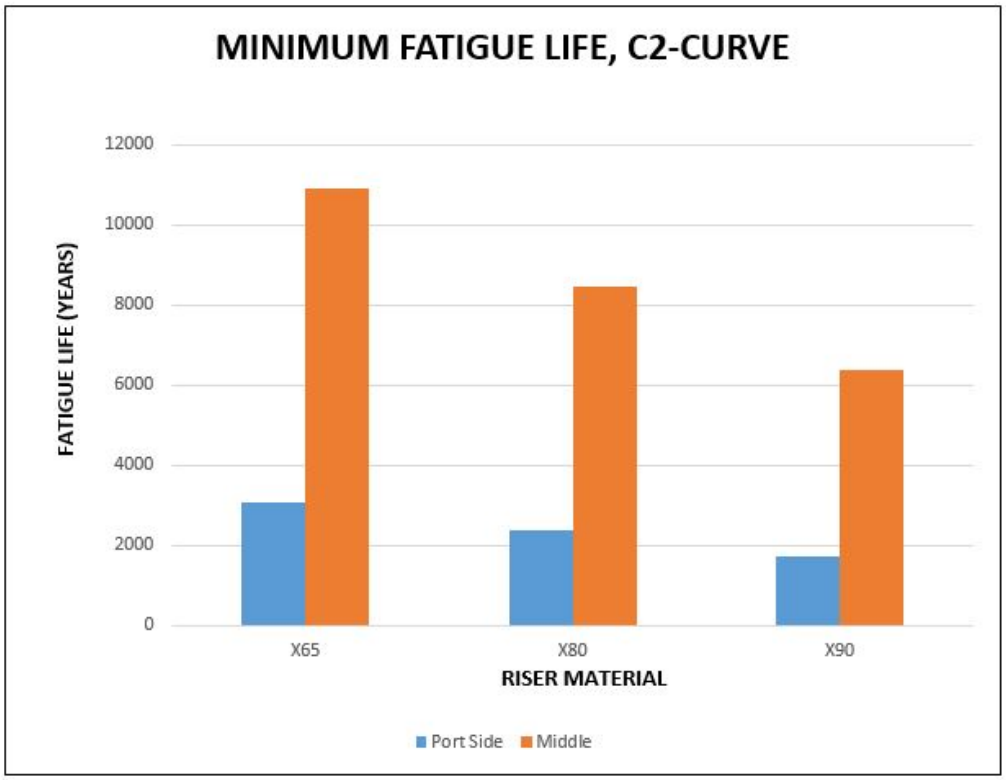

Figure 6.45: Minimum Fatigue Life, C2-Curve Hang-off Point Comparison

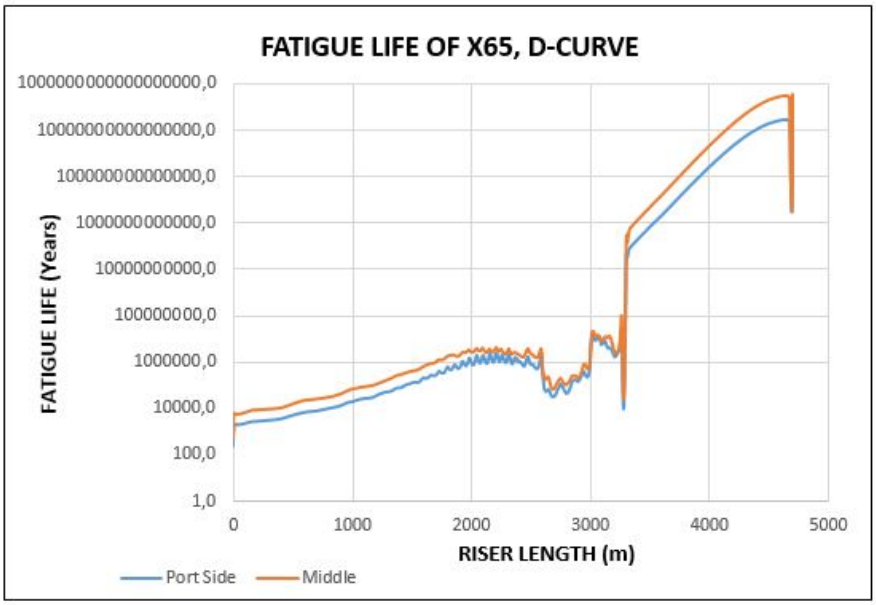

Figure 6.46: Fatigue Life Over The Entire X65 Riser Length, D Curve

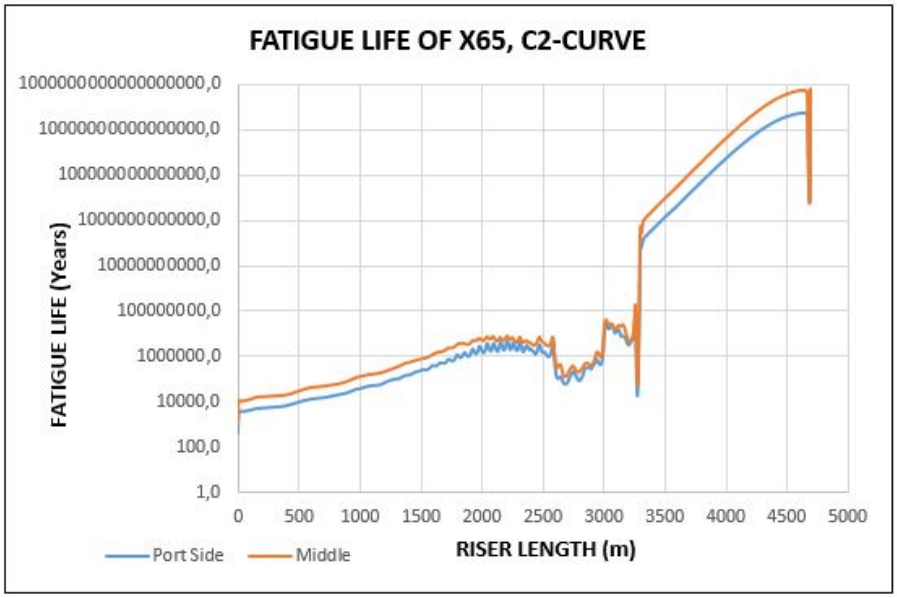

Figure 6.47: Fatigue Life Over The Entire X65 Riser Length, C2 Curve

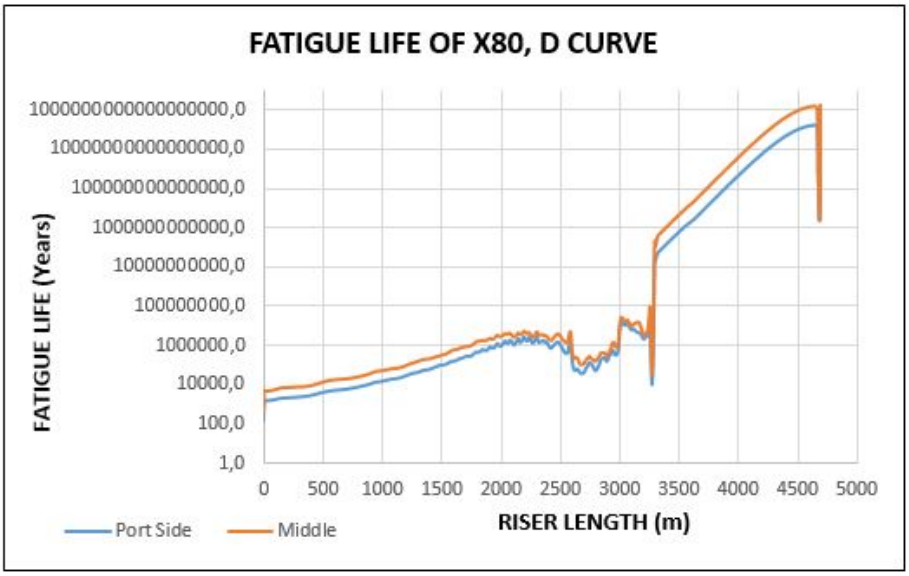

Figure 6.48: Fatigue Life Over The Entire X80 Riser Length, D Curve

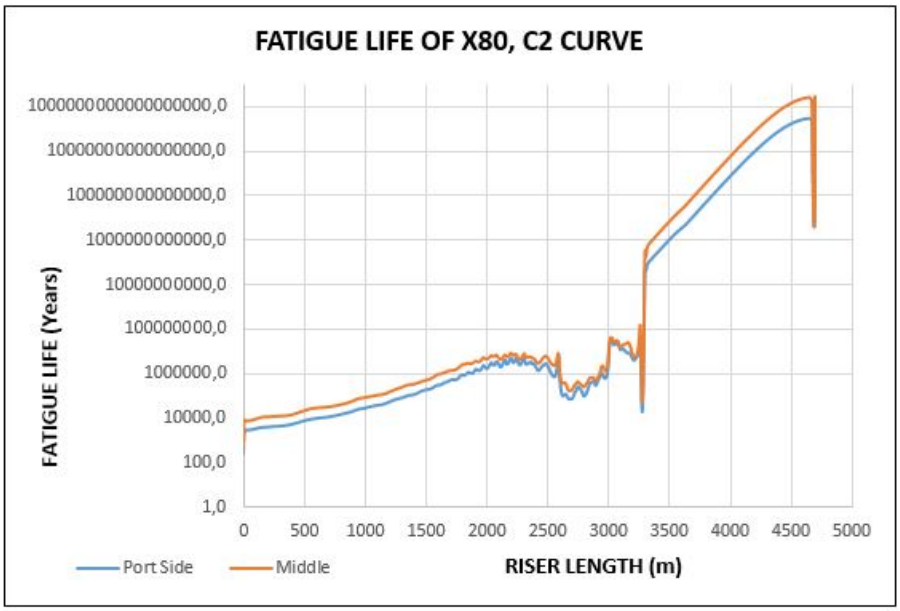

Figure 6.49: Fatigue Life Over The Entire X80 Riser Length, C2 Curve

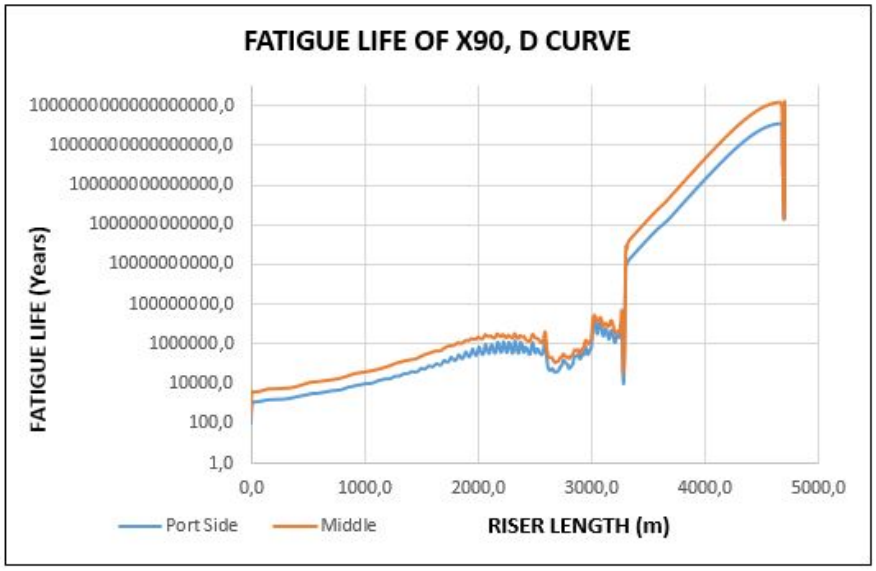

Figure 6.50: Fatigue Life Over The Entire X90 Riser Length, D Curve

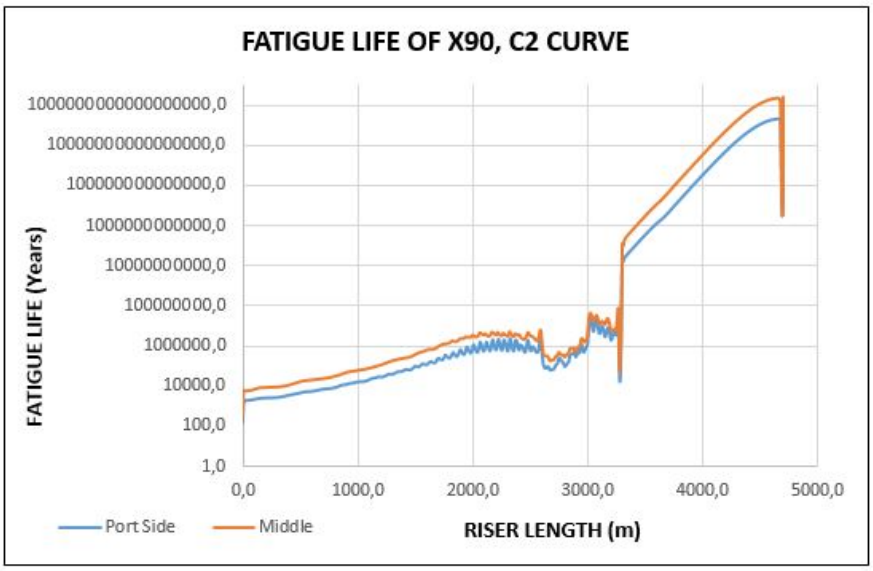

Figure 6.51: Fatigue Life Over The Entire X90 Riser Length, C2 Curve

Chapter 7

Conclusion and Recommendations

7.1 Conclusion

In this thesis work, the strength and fatigue performance of a SLWR connected to a spread-moored FPSO deployed in the Santos Basin, offshore Brazil at a water depth of 2200m has been presented.

The FPSO and SLWRs were modeled with OrcaFlex. In OrcaFlex, the vessel heading was set to 195° due to the environmental conditions of the region. In past SLWR deployments, the X65 carbon steel material was commonly used. In this study, risers made of X65, X80 and X90 carbon steel material were modeled in OrcaFlex in order to compare their strength and fatigue performance so as to suggest the best material among the three materials for future SLWR field applications.

The hang-off points of the SLWRs on the FPSO were determined by a vessel response analysis that subjected the FPSO to the 100-year waves and 10-year currents observed in this region. From the results of the vessel response analysis, two hang-off points (one along the port side and the other along the middle of the vessel) were selected and the worst sea state was determined.

With the SLWRs modeled, worst sea states determined, hang-off points selected, the strength and fatigue analysis were conducted to determine if the SLWRs met the DNV-OS-F201 LRFD utilization criteria and minimum fatigue life requirements. From the results of the strength analysis, it was seen that the maximum DNV LRFD utilization observed in the hang-off points along the middle of the vessel in the ULS near offset. This was not the expected result because the hang-off point at the middle of the vessel showed a lower maximum downward velocity during the vessel response analysis than the hang-off point at the port side of the vessel.

This unexpected result lead to the investigation of the initial SLWR modeled configuration. From the results of the investigation, it was observed that excess buoyancy was used in the initial SLWR configuration. As a result of this, the risers

experienced their maximum utilization at the hang-off point along the middle of the vessel instead of the hang-off point at the port side of the vessel. Hence, the initial SLWR configuration was not an optimal configuration.

An optimal configuration was then determined for the risers. Strength analysis was conducted on the optimal configuration and it was observed from the analysis that the maximum DNV LRFD utilization occurred when the riser was connected to the hang-off point along the port side of the vessel in the ULS far offset. This result was expected and a maximum DNV LRFD utilization value of 0.71, 0.61 and 0.55, was observed in the X65, X80 and X90 SLWRs. All these values met the utilization criteria (i.e utilization ≤ 1) and hence, the structural integrity of the risers was verified. In addition, the riser made of X90 had the lowest maximum DNV LRFD utilization and this indicated in that it had the best dynamic response when compared to all the other risers.

Strength analysis was also conducted on the optimal configuration when it was connected to the hang-off point at the middle of the vessel. A maximum DNV LRFD utilization value of 0.66 was observed in the X65 riser when it was in the ULS far offset position. The difference in the maximum values observed in the X65 riser as a result of connection to different hang-off points indicated that buoyancy could be saved in the riser connected to the middle of the vessel if the maximum utilization could be pushed from 0.66 to 0.71. To achieve this, a buoyancy reduction process was carried out.

It was observed from this reduction process that a buoyancy reduction of 7.5% pushed the maximum utilization to 0.69 and further reduction in buoyancy resulted in a configuration that was unacceptable. This suggested that a riser connected to the hang-off point along the middle of the vessel will require 7.5% less buoyancy than a riser connected to the hang-off point at the port side of the vessel.

Fatigue analysis was also conducted and a minimum fatigue life of 1794, 1443 and 1053 years in the D curve was observed in the X65, X80 and X90 SLWRs when they were connected to the hang-off point along the port side of the vessel. However, when they were connected to the hang-off point along the middle of the vessel, an increase of 246%, 250% and 266% was observed in the minimum fatigue life of the X65, X80 and X90 SLWRs respectively. This suggested that risers connected along the middle of the vessel will have a better fatigue performance than risers connected along the port side of the vessel. Therefore, if a suitable configuration does not meet the minimum fatigue requirements when connected to the port side of the vessel, it should meet the minimum fatigue life requirements if the hang-off point is changed to the middle of the vessel.

Based on the results of the strength and fatigue analysis conducted in this study, the X90 SLWR shows the best dynamic response. Also, it has the lowest minimum fatigue life. This is because of its reduced weight and wall thickness when compared

to the other risers. But with a minimum fatigue life of 1053 years, the X90 SLWR is well above the minimum requirements recommended by the the DNV-OS-F201 reference standard. In terms of cost, the X90 SLWR will be the cheapest option among all the riser materials also because of its reduced weight and low buoyancy requirements to achieve the same SLWR configuration.

According to the results observed in this thesis work, SLWRs made of X90 carbon steel material when connected to the hang-off point at the middle of the vessel appear to be the most option for deployment at a water depth of 2200m in the Santos Basin, offshore Brazil. However, further work is recommended to back-up up these results.

7.2 Recommendations for Further Work

For further work on this thesis, the following has been recommended:

1. Fatigue due to Vortex Induced Vibrations should also be calculated since a very large part of the risers will be exposed.
2. Hang-off angle variation should be performed to observe the impact of different angles on the strength and fatigue performance of the risers
3. Detailed installation analysis should be performed to ensure that designed risers can be installed easily.
4. SLWRs with larger internal diameters should be modeled and their integrity verified to further improve the production rate of the risers.

References

API, D. (2005). Analysis of stationkeeping systems for floating structures. *API RP 2SK, 3rd edition, American Petroleum Institute, Washington DC, USA*.

Bai, Y., & Bai, Q. (2005). *Subsea pipelines and risers*. Elsevier.

Barltrop, N. D. (1998). *Floating structures: a guide for design and analysis* (Vol. 1). Oilfield Pubns Inc.

Bax, J., de Werk, K., et al. (1974). A floating storage unit designed specifically for the severest environmental conditions. In *Spe european spring meeting.*

Brewer, J. H. (1975). The tension leg platform concept. *American Petroleum Institute*.

Brouard, Y., Seguin, B., Germanetto, F., Shah, V., et al. (2016). Riser solutions for turret moored fpso in arctic conditions. In *Arctic technology conference.*

Carter, B., Ronalds, B., et al. (1998). Deepwater riser technology. In *Spe asia pacific oil and gas conference and exhibition.*

Cheng, J., & Cao, P. (2013). Design of steel lazy wave riser for disconnectable fpso in the gulf of mexico. In *Asme 2013 32nd international conference on ocean, offshore and arctic engineering* (pp. V04BT04A010–V04BT04A010).

DNV. (2010a). Dnv-oss-302: Offshore service specification-offshore riser systems. *Det Norske Veritas Services, Research and Publications, Hovik, Norway*.

DNV. (2010b). Fatigue design of offshore steel structures. *No. DNV-RP-C203*, *30*.

DNV. (2010c). Offshore standard dnv os f201 dynamic risers. *Det Norske Veritas Services, Research and Publications, Hovik, Norway*.

England, L., Duggal, A., & Queen, L. (2001). A comparison between turret-and spread-moored f (p) so_s for deepwater field developments. In *Deep offshore technology symposium 2001.*

Fisher, & Berner, P. (1988). Non-integral production riser for green canyon block 29 development. In *Offshore technology conference.*

Fisher, F., & Spiess, F. (1963). Flip-floating instrument platform. *The Journal of the Acoustical Society of America*, *35*(10), 1633–1644.

Gemilang, G. M., & Karunakaran, D. (2017). Feasibility study of selected riser concepts in deep water and harsh environment. In *Asme 2017 36th international conference on ocean, offshore and arctic engineering* (pp. V05BT04A044–V05BT04A044).

Glanville, R., Paulling, J., Halkyard, J., Lehtinen, T., et al. (1991). Analysis of the spar floating drilling production and storage structure. In *Offshore technology conference.*

Halkyard, J. E. (1996). Status of spar platforms for deepwater production systems. In *The sixth international offshore and polar engineering conference.*

Hiller, D., Karunakaran, D., Cruz, I., Tadeu, M., et al. (2015). Developing an Innovative deepwater riser system: From concept to the full production of buoy supporting risers (bsr). In *Offshore technology conference.*

Hoffman, J., Yun, H., Modi, A., Pearce, R., et al. (2010). Parque das conchas pipeline, flowline and riser system design, installation and challenges. In *Offshore technology conference.*

Huang, S., & Hatton, S. (1996). Rigid bottom weighted large diameter risers–concept, analysis and design. *Technologies for Deep Hostile Seas*.

Jha, V., Latto, J., Dodds, N., Anderson, T. A., Finch, D., Vermilyea, M., et al. (2013). Qualification of flexible fiber-reinforced pipe for 10,000-foot water depths. In *Offshore technology conference.*

Karunakaran, & Baarholm, R. (2013). Cobra: An uncoupled riser system for ultradeep water in harsh environment. In *Offshore technology conference.*

Karunakaran, D., Dutta, A., Clausen, T., & Lund, K. (2002). Steel catenary riser configurations for large motion semi submersibles with lightweight coating. In *Deep offshore technology conference.*

Karunakaran, D., Legras, J.-L., & Jones, R. L. (2013). Fatigue enhancement of scrs: Design applying weight distribution and optimized fabrication. In *Offshore technology conference.*

Karunakaran, D., Nordsve, N., Olufsen, A., et al. (1996). An efficient metal riser configuration for ship and semi based production systems. In *The sixth international offshore and polar engineering conference.*

Karunakaran, D. N., Legras, J.-L., Jones, R. L., et al. (2013). Fatigue enhancement of scrs: Design applying weight distribution and optimized fabrication. In *Offshore technology conference.*

Katla, E., Mork, K., & Hansen, V. (2001). Dynamic risers: Introduction and background to the new dnv offshore standard (os-f201). In *Offshore technology conference.*

Legras, J.-L. (2013). Tethered catenary riser: A novel concept for ultradeep water. In *Offshore technology conference.*

Li, Y. (2012). Sensitivity study of scr fatigue at touch down point: effect of marine growth. In *The twenty-second international offshore and polar engineering conference.*

Lopez-Cortijo, J., Duggal, A. S., Van Dijk, R. R., Matos, S., et al. (2003). Dp fpso–a fully dynamically positioned fpso for ultra deep waters. In *The thirteenth international offshore and polar engineering conference. international society of offshore and polar engineers.*

Luppi, A., Cousin, G., O'Sullivan, R., et al. (2014). Deepwater hybrid riser systems. In *Offshore technology conference-asia.*

Orimolade, A. P. (2014). *Steel lazy wave risers from turret moored fpso* (Unpublished master's thesis). University of Stavanger, Norway.

Paik, J. K., & Thayamballi, A. K. (2007). *Ship-shaped offshore installations: design, building, and operation.* Cambridge University Press.

Sen, T. K., Hesar, M., et al. (2007). Riser soil interaction in soft clay near the touchdown zone. In *Offshore technology conference.*

Sparks, C. P. (2007). *Fundamentals of marine riser mechanics: basic principles and simplified analyses*. PennWell Books.

Standard, N. (2007). N-003. *Actions and Action Effects, Rev*, *1*.

Sworn, A. (2005). Hybrid riser towers from an operator's perspective. In *Offshore technology conference.*

Toro, L. F. B., Saraiva, T. C., Meroño, C. G., Vizcayno, P. L., Munáiz, M. M., Costa, R. D., et al. (2015). Floater concept selection for ultradeep waters in brazil. In *Offshore technology conference.*

You, J., Biscontin, G., Aubeny, C., et al. (2008). Seafloor interaction with steel catenary risers. In *The eighteenth international offshore and polar engineering conference.*

Appendix A

Wall Thickness Sizing

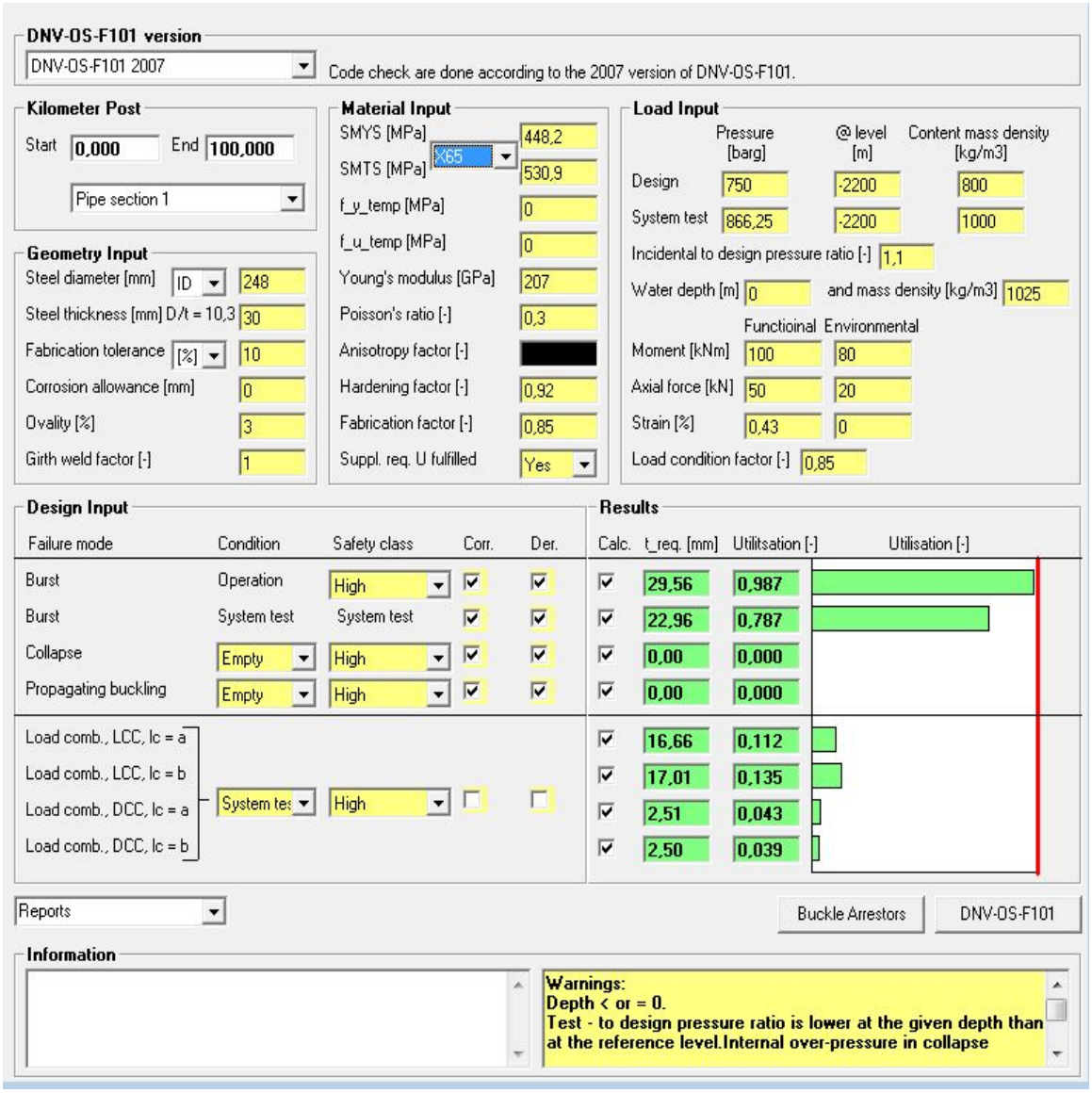

Figure A.1: Wall Thickness Calculation for X65 SLWR With the Pipeline Engineering Tool

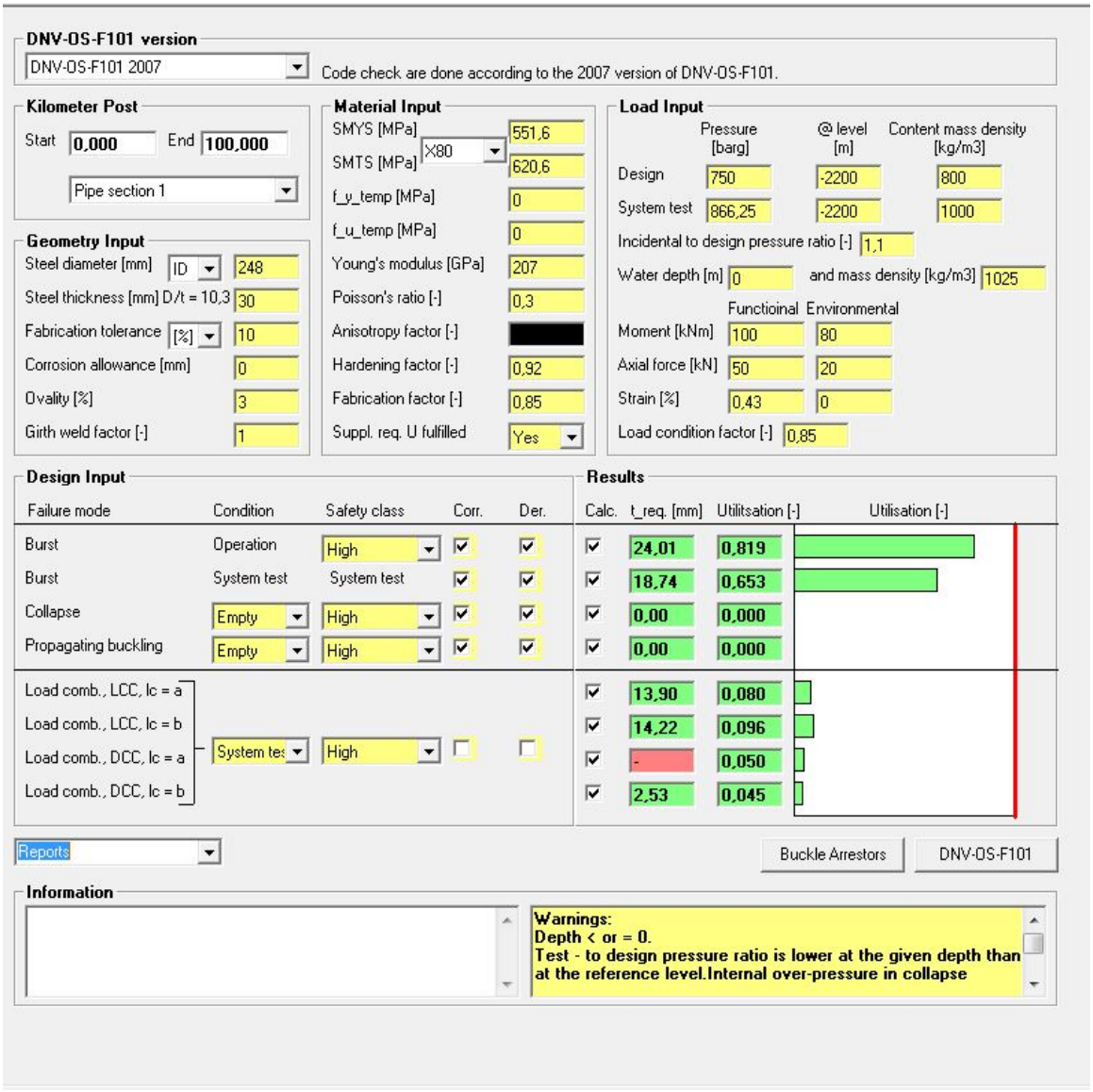

Figure A.2: Wall Thickness Calculation for X80 SLWR With the Pipeline Engineering Tool

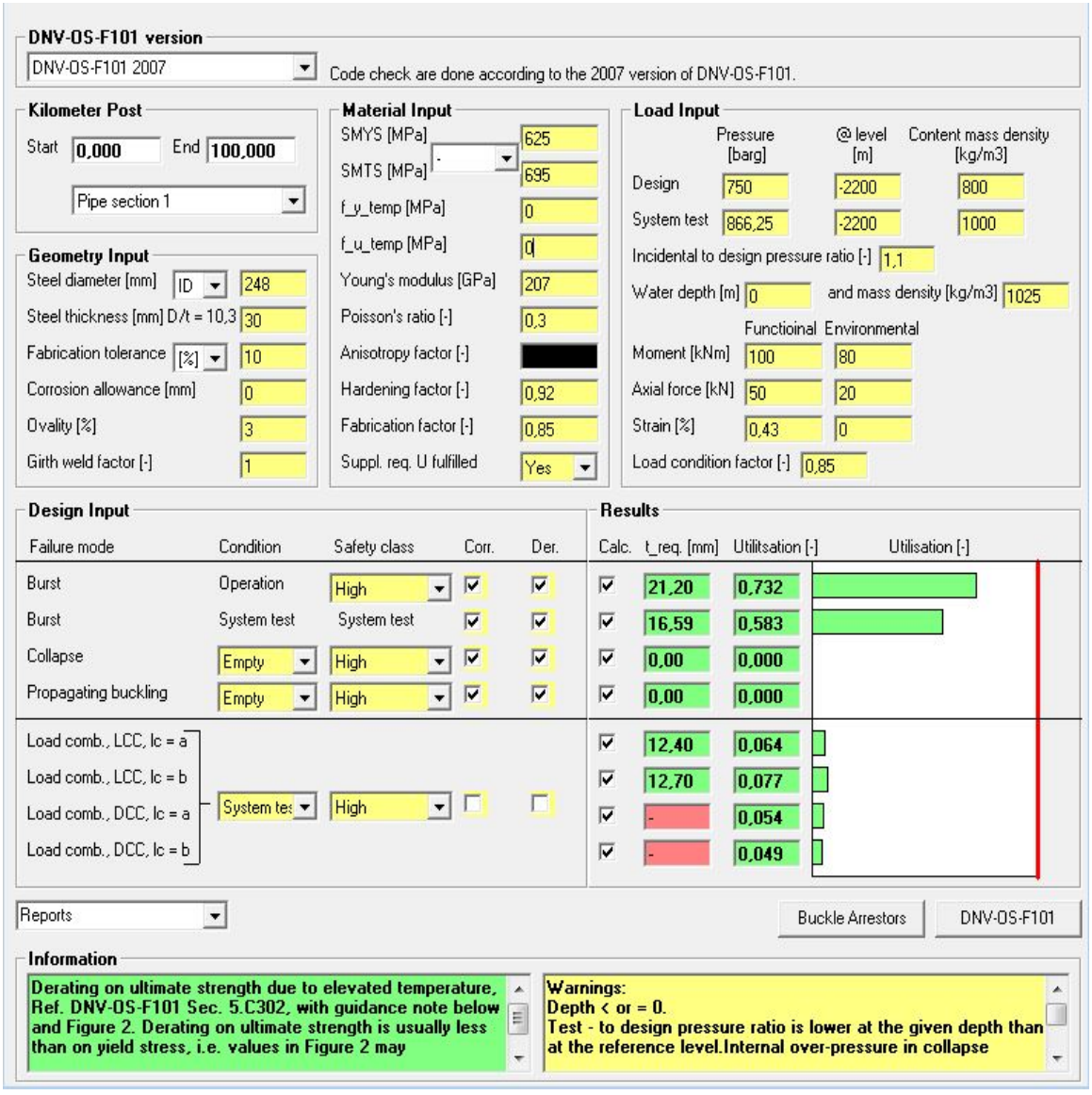

Figure A.3: Wall Thickness Calculation for X90 SLWR With the Pipeline Engineering Tool

Appendix B

Python Script Variation

A variation to the python script used for the vessel motion response analysis is given below:
< − − −Script Begins Here−− >

```
from OrcFxAPI import *

Vessel output
Critical parameter: Downward velocity
pos = (inserthangoffcoordinateshere)

modes = [
"X","GX-Velocity","GX-Acceleration",
"Y","GY-Velocity","GY-Acceleration",
"Z","GZ-Velocity","GZ-Acceleration",
"Roll","x-Angular Velocity","x-Angular Acceleration",
"Pitch","y-Angular Velocity","y-Angular Acceleration",
"Yaw","z-Angular Velocity","z-Angular Acceleration",
]

100yr contour
(Hs, TpLow, TpHigh)
contour_100yr = [

(6.6, 11.0, 11.5),
(6.5, 10.0, 12.5),
(6.3, 9.5, 13.0),
(6.2, 9.0, 9.0),
(6.1, 8.5, 13.5),
(6.0, 8.0, 8.0),
(5.8, 14.0, 14.0),
(5.7, 7.5, 7.5),
(5.4, 14.5, 14.5),
```

(5.2, 7.0, 7.0),
(4.8, 15.0, 15.0),
(4.5, 6.5, 6.5),
(3.8, 6.0, 6.0),
(3.7, 15.5, 15.5),]

dirs = [float(i)*15 for i in range(24)]

modelFileName = "insertfilenamehere"
vesselName = "insertvesselnamehere"

m = Model(modelFileName)

def getGamma(Hs,Tp):
return 6.4*Tp**-0.491

for sea in contour$_1$00yr :
$foriTpin[1, 2]$:
$m['General'].StageDuration[-1] = 10800.$
$m['Environment'].WaveType = "JONSWAP"$
$m['Environment'].WaveDirection = 0.$
$m['Environment'].WaveHs = sea[0]$
$m['Environment'].WaveGamma = getGamma(sea[0], sea[iTp])$
$m['Environment'].WaveTp = sea[iTp]$
$m[vesselName].ResponseNumberOfDirections = len(dirs)$
$m[vesselName].ResponseDirection = dirs$
$m[vesselName].ResponseNumberOfOutputPoints = 1$
$m[vesselName].ResponseOutputPointx[0] = pos[0]$
$m[vesselName].ResponseOutputPointy[0] = pos[1]$
$m[vesselName].ResponseOutputPointz[0] = pos[2]$
$m[vesselName].SaveSpectralResponseSpreadsheet("Draugth\%i$
$Hs\%004.1fTp\%004.1f.xls"\%(0, sea[0], sea[iTp]))$

$<---$Script Ends Here$-->$

Appendix C

Dynamic Response Analysis Results

The results of the dynamic analysis conducted on the optimized X65, X80 and X90 SLWRs in Section 6.5.2.4 are presented in this appendix.

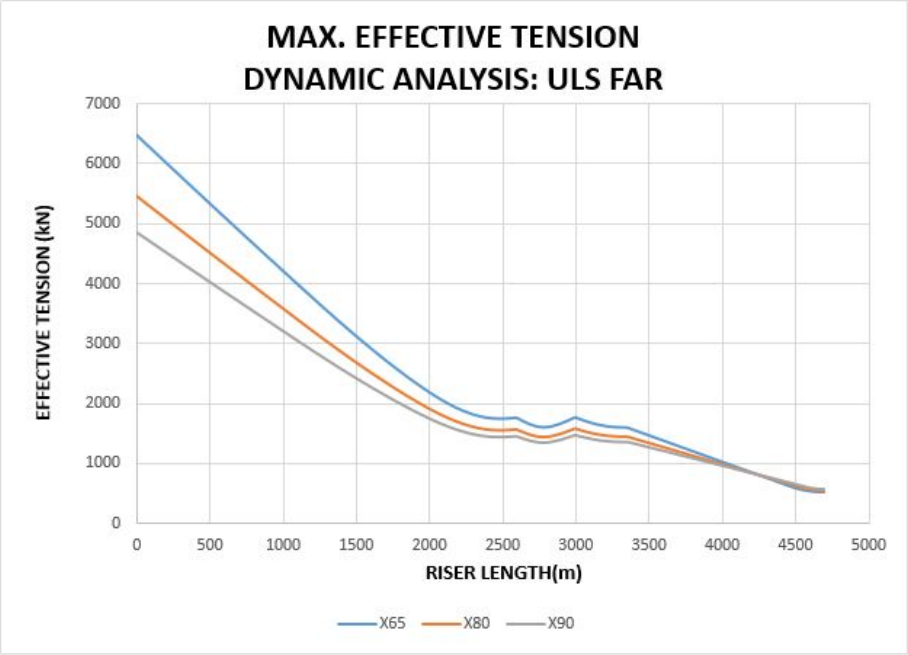

Figure C.1: Maximum Effective Tension, Dynamic Analysis-ULS Far, PortSide Hang-off Point

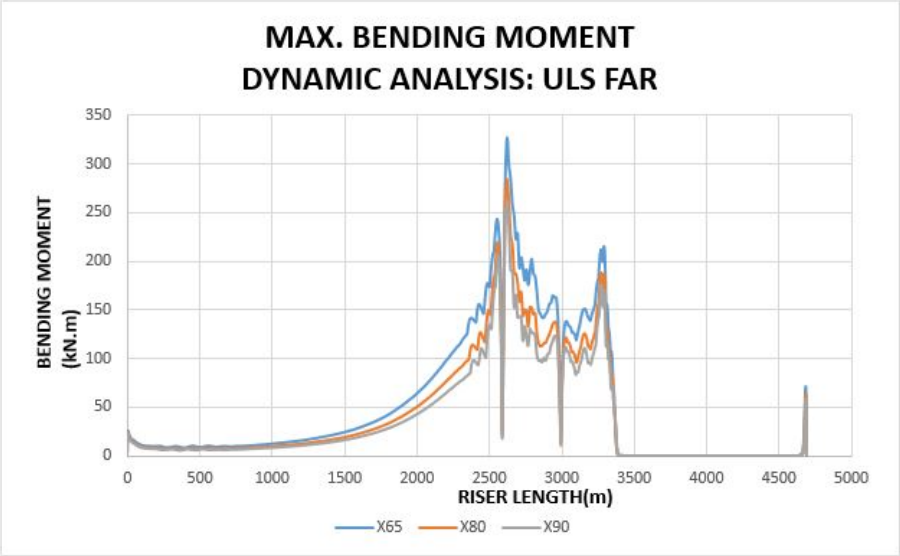

Figure C.2: Maximum Bending Moment, Dynamic Analysis-ULS Far, PortSide Hang-off Point

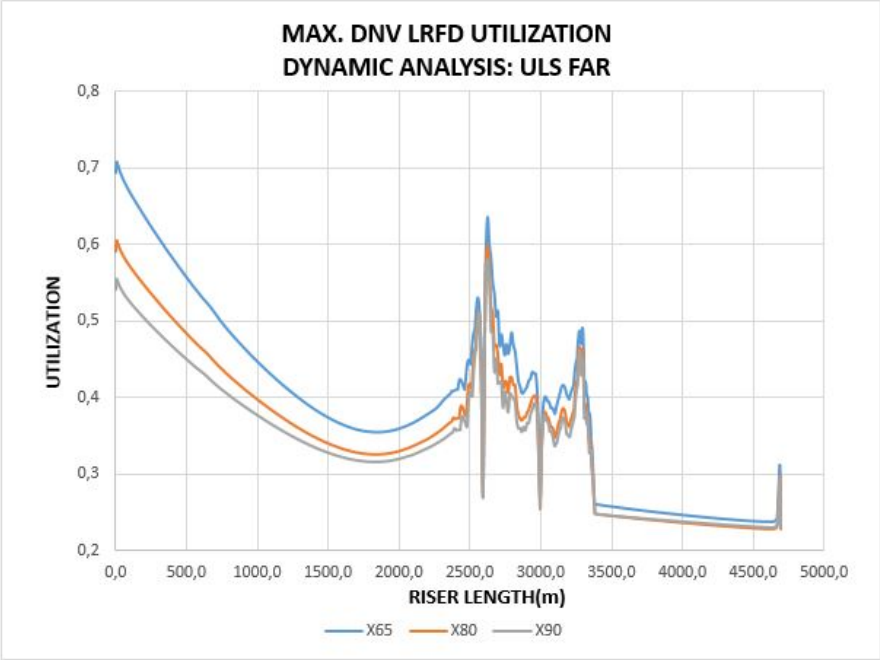

Figure C.3: Maximum DNV LRFD Utilization, Dynamic Analysis-ULS Far, PortSide Hang-off Point

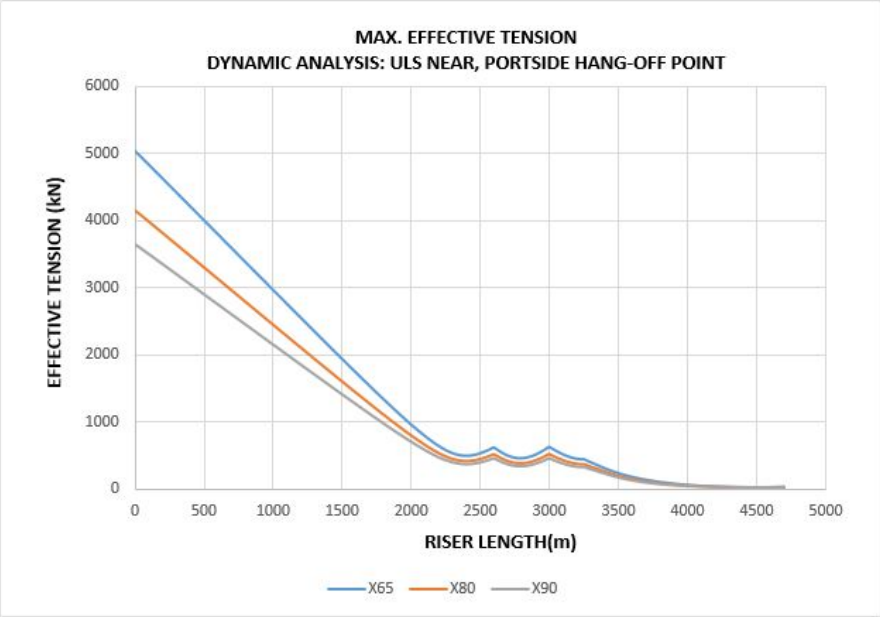

Figure C.4: Maximum Effective Tension, Dynamic Analysis-ULS Near, PortSide Hang-off Point

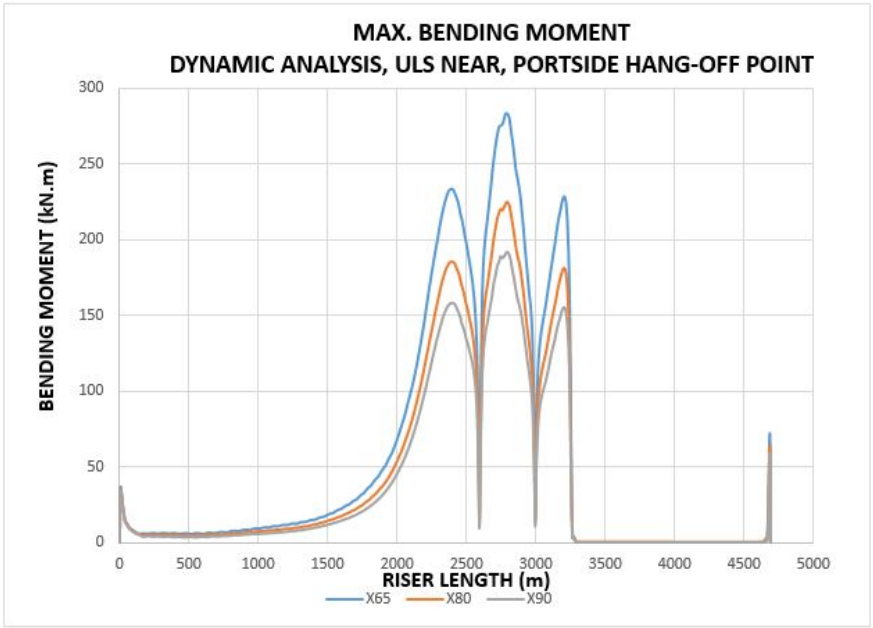

Figure C.5: Maximum Bending Moment, Dynamic Analysis-ULS Near, PortSide Hang-off Point

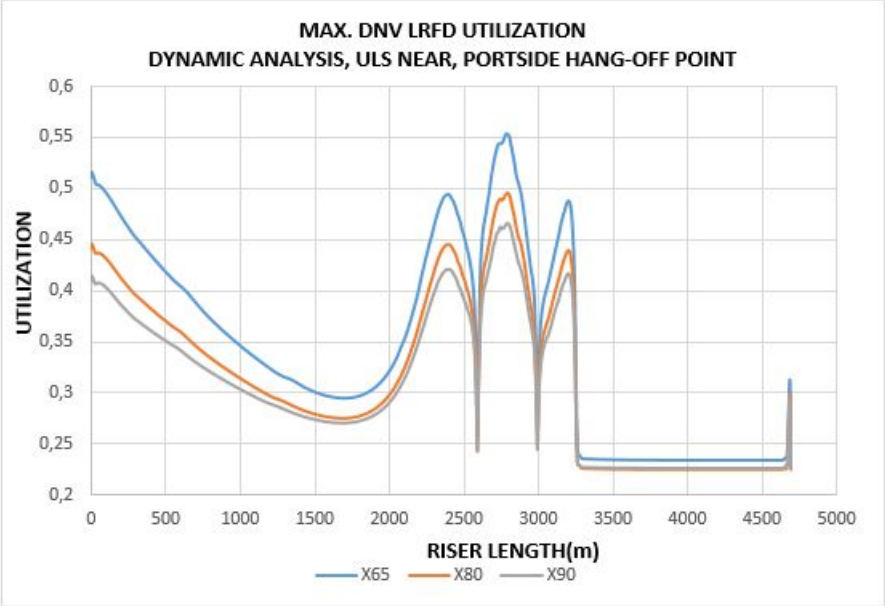

Figure C.6: Maximum DNV LRFD Utilization, Dynamic Analysis-ULS Near, PortSide Hang-off Point

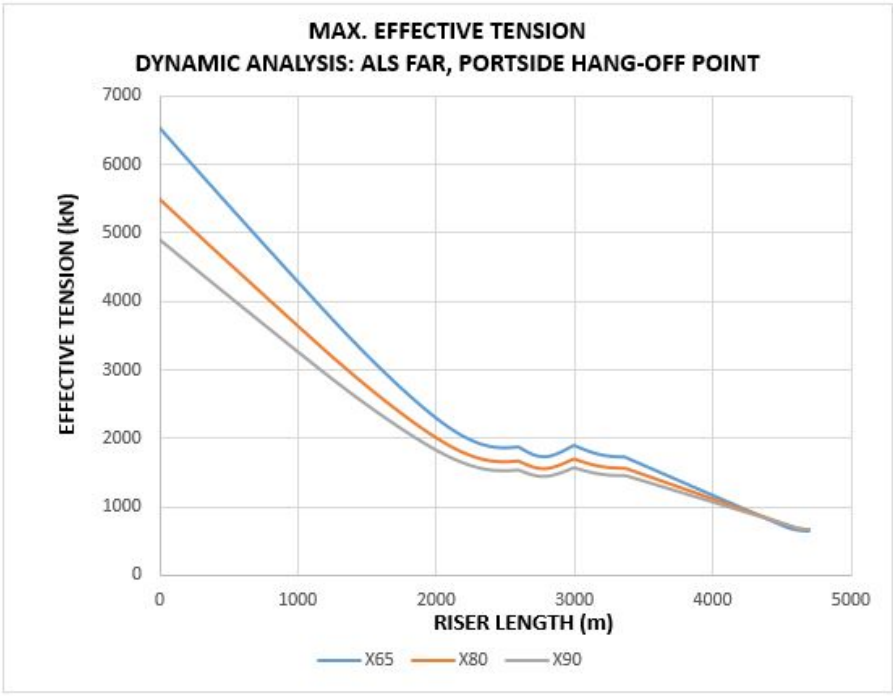

Figure C.7: Maximum Effective Tension, Dynamic Analysis-ALS Far, PortSide Hang-off Point

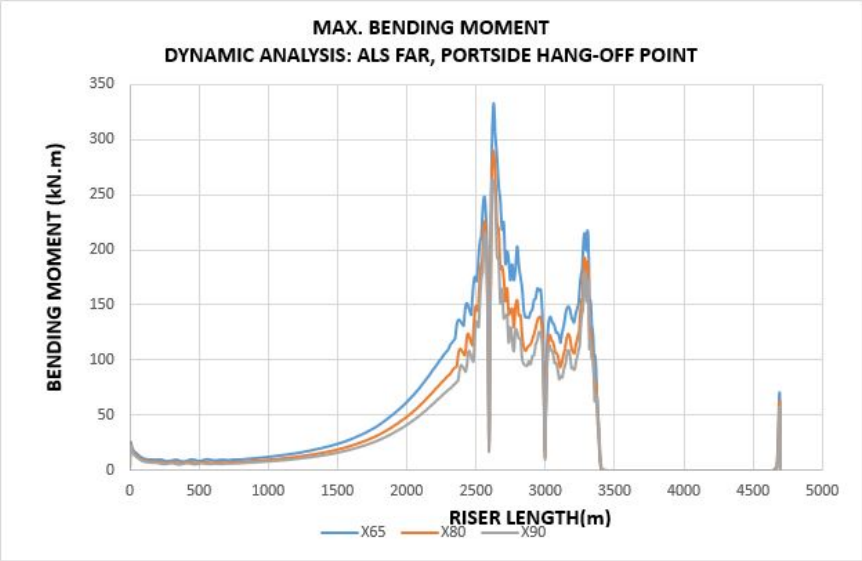

Figure C.8: Maximum Bending Moment, Dynamic Analysis-ALS Far, PortSide Hang-off Point

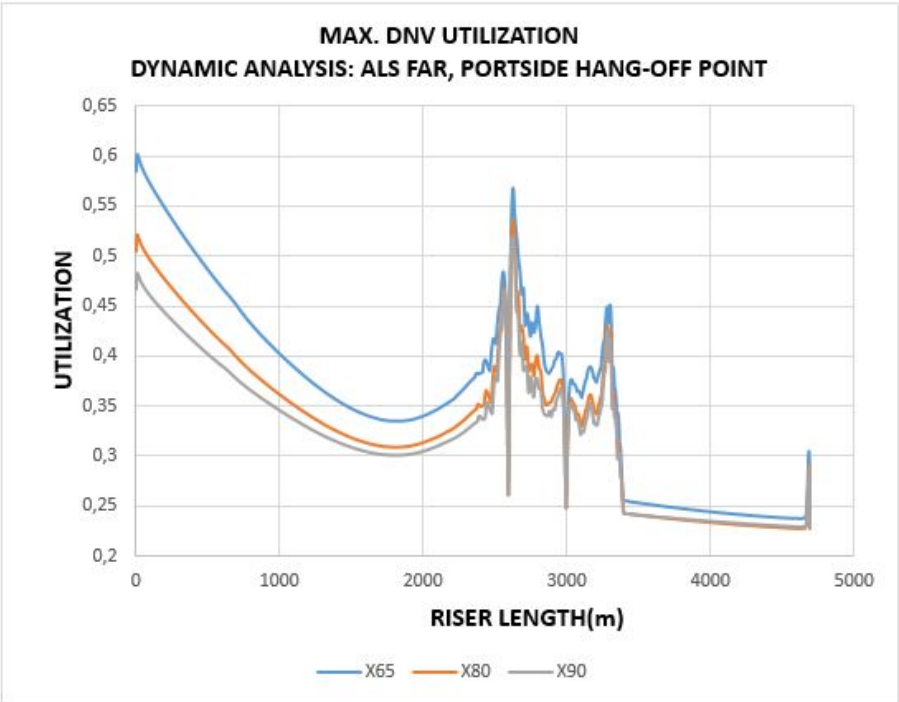

Figure C.9: Maximum DNV LRFD Utilization, Dynamic Analysis-ALS Far, PortSide Hang-off Point

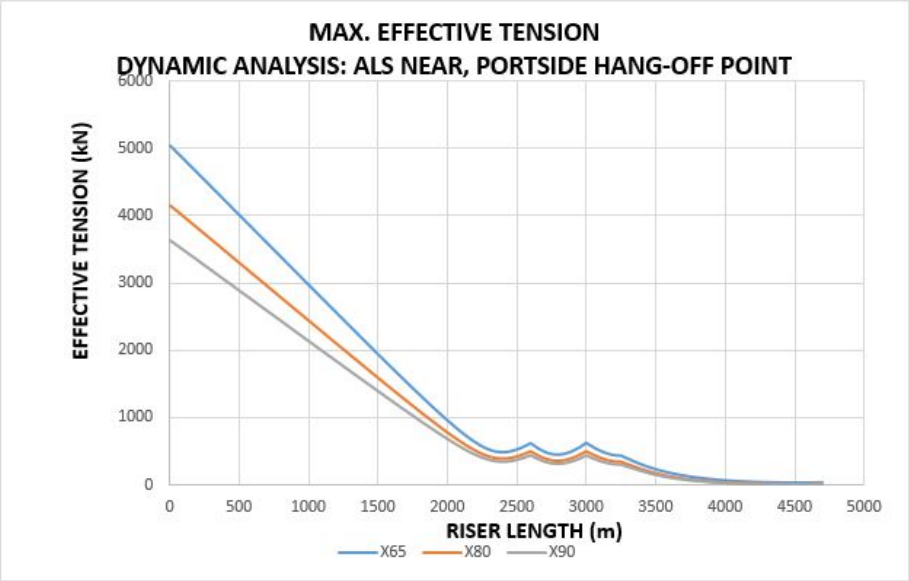

Figure C.10: Maximum Effective Tension, Dynamic Analysis-ALS Near, PortSide Hang-off Point

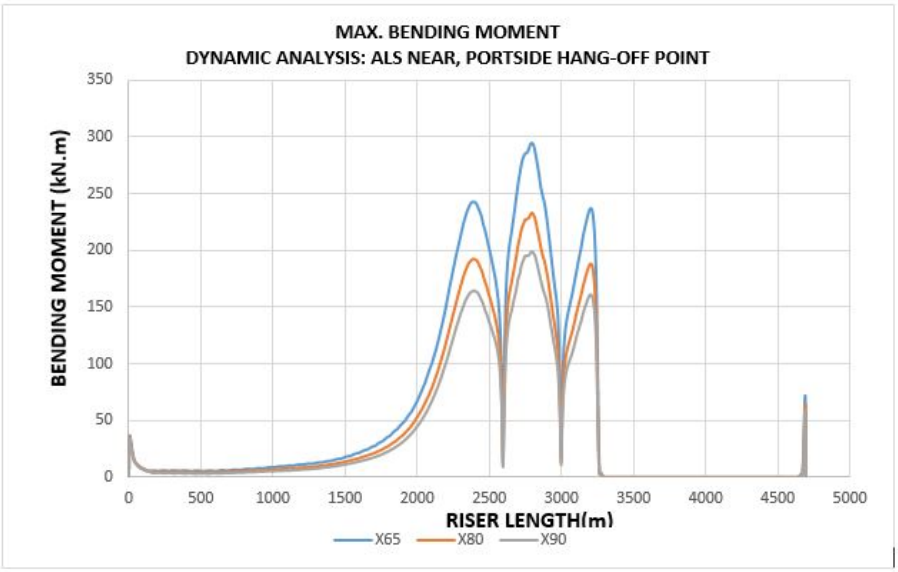

Figure C.11: Maximum Bending Moment, Dynamic Analysis-ALS Near, PortSide Hang-off Point

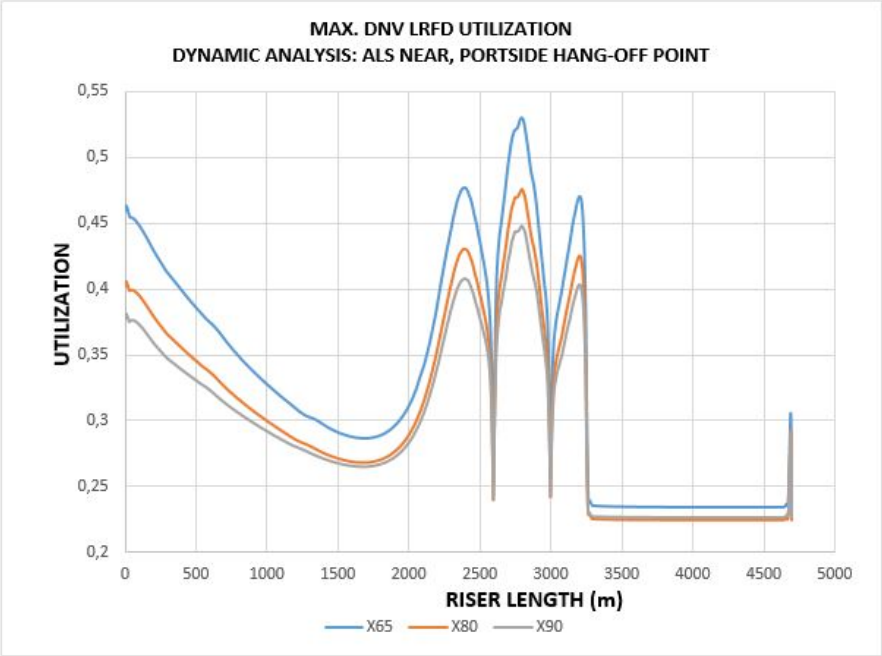

Figure C.12: Maximum DNV LRFD Utilization, Dynamic Analysis-ALS Near, PortSide Hang-off Point

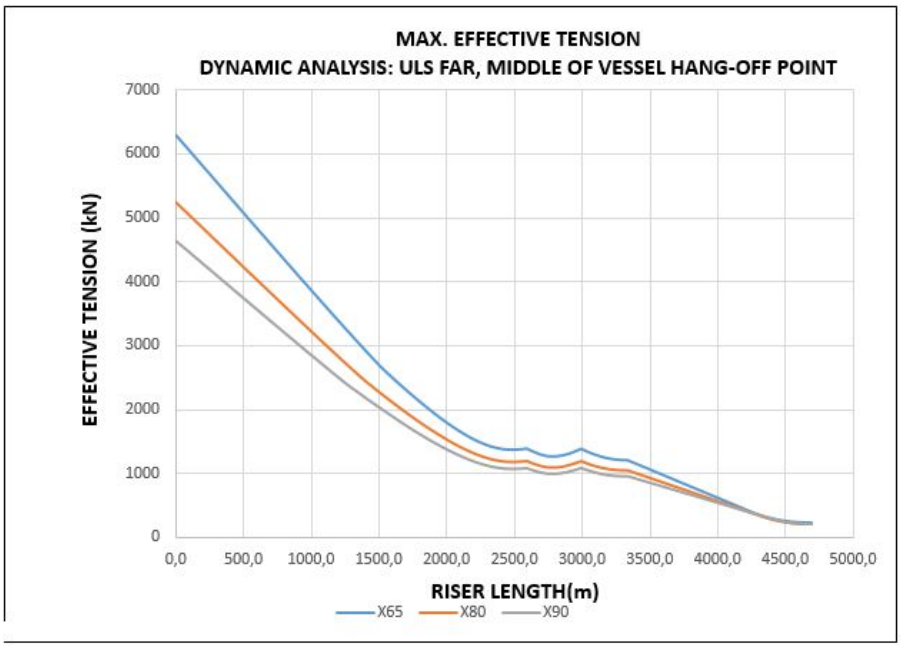

Figure C.13: Maximum Effective Tension, Dynamic Analysis-ULS Far, Middle of Vessel Hang-off Point

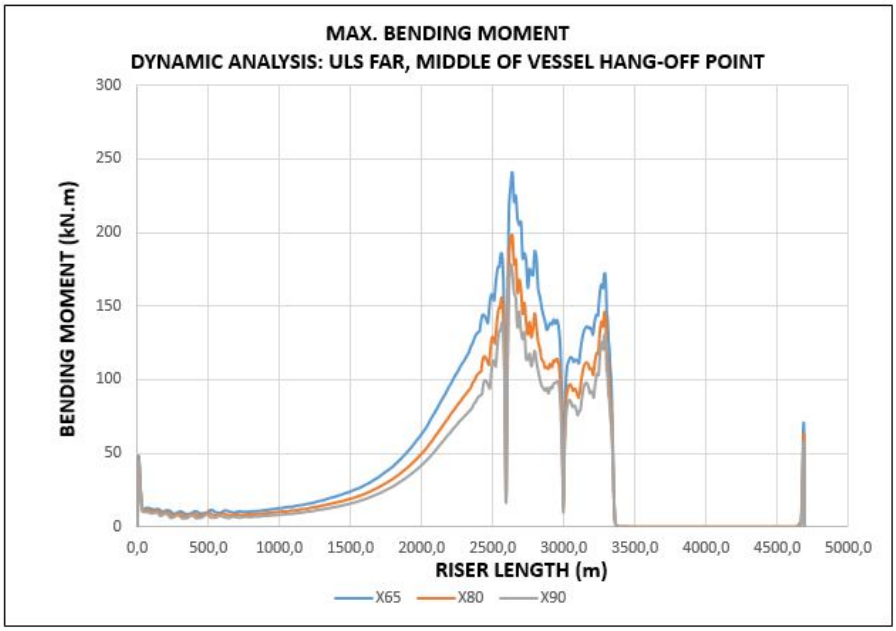

Figure C.14: Maximum Bending Moment, Dynamic Analysis-ULS Far, Middle of Vessel Hang-off Point

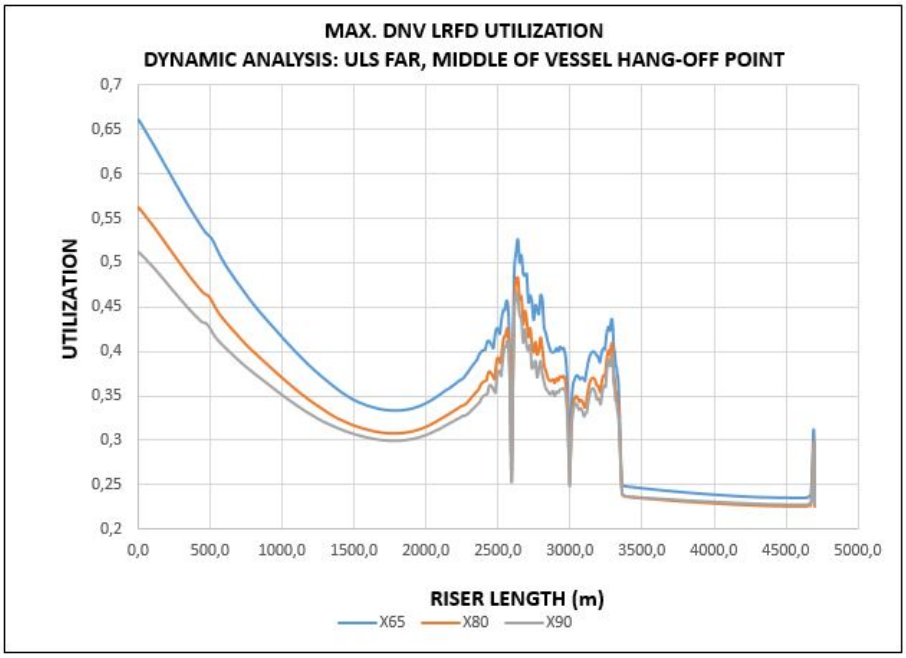

Figure C.15: Maximum DNV LRFD Utilization, Dynamic Analysis-ULS Far, Middle of Vessel Hang-off Point

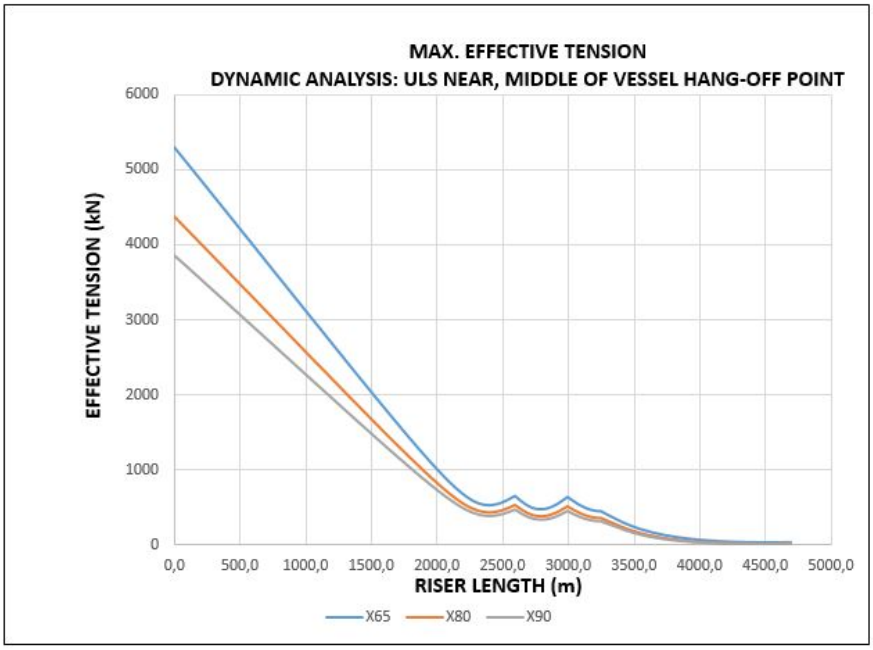

Figure C.16: Maximum Effective Tension, Dynamic Analysis-ULS Near, Middle of Vessel Hang-off Point

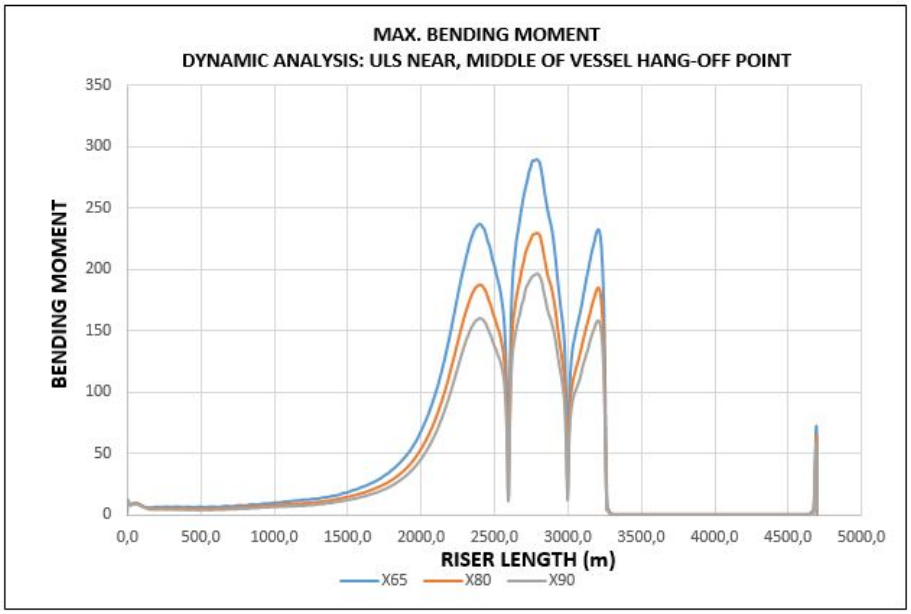

Figure C.17: Maximum Bending Moment, Dynamic Analysis-ULS Near, Middle of Vessel Hang-off Point

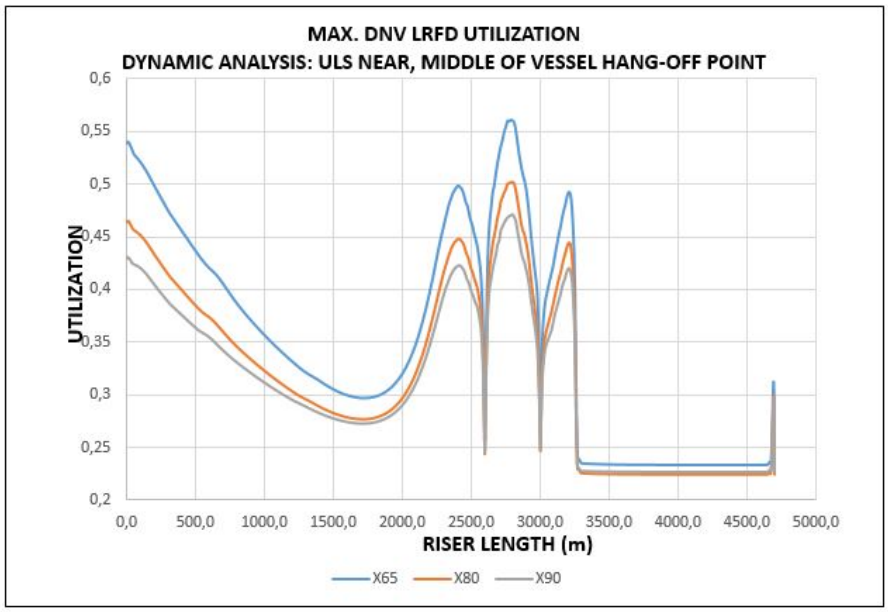

Figure C.18: Maximum DNV LRFD Utilization, Dynamic Analysis-ULS Near, Middle of Vessel Hang-off Point

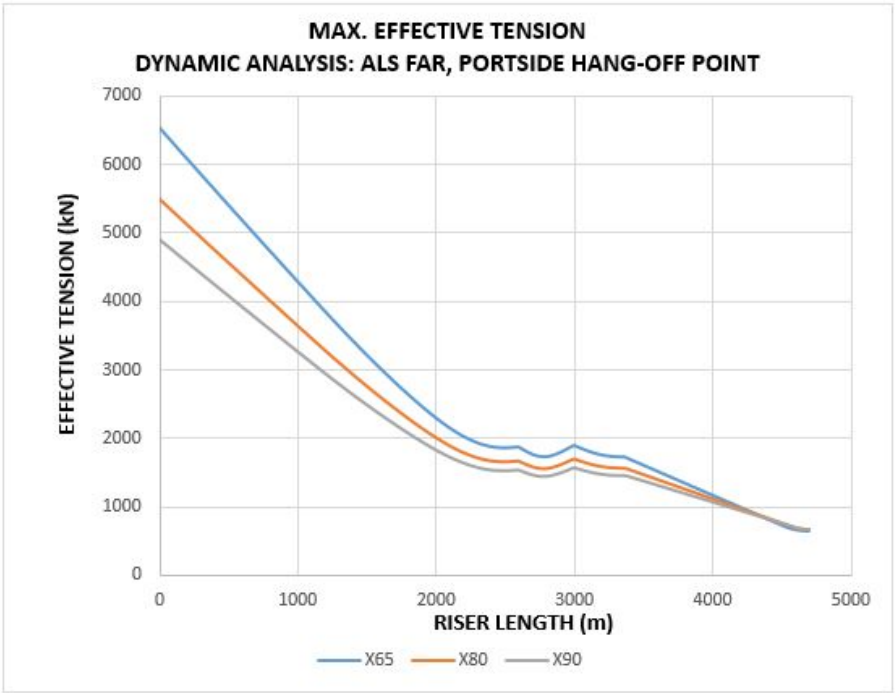

Figure C.19: Maximum Effective Tension, Dynamic Analysis-ALS Far, Middle of Vessel Hang-off Point

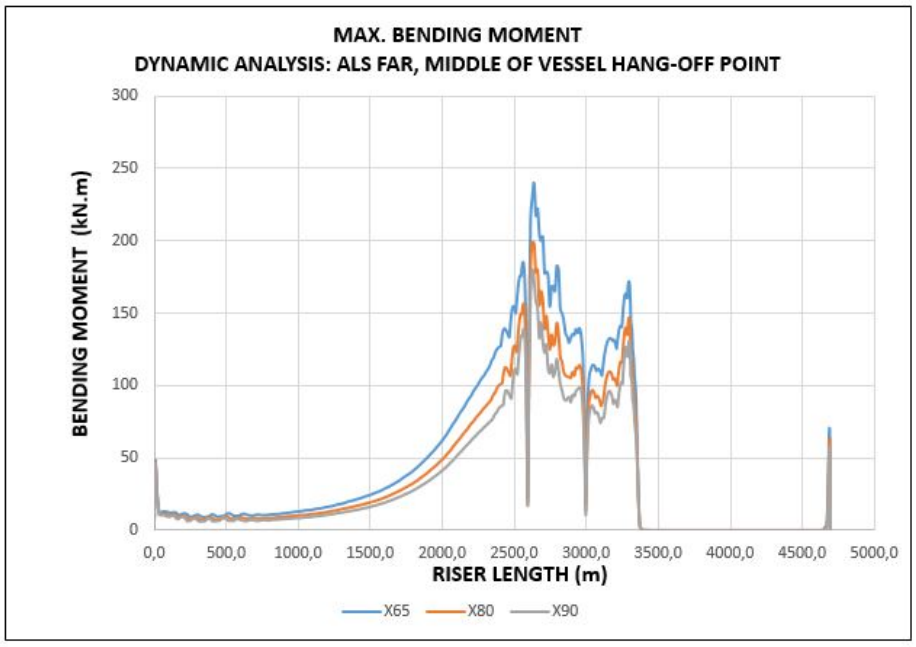

Figure C.20: Maximum Bending Moment, Dynamic Analysis-ALS Far, Middle of Vessel Hang-off Point

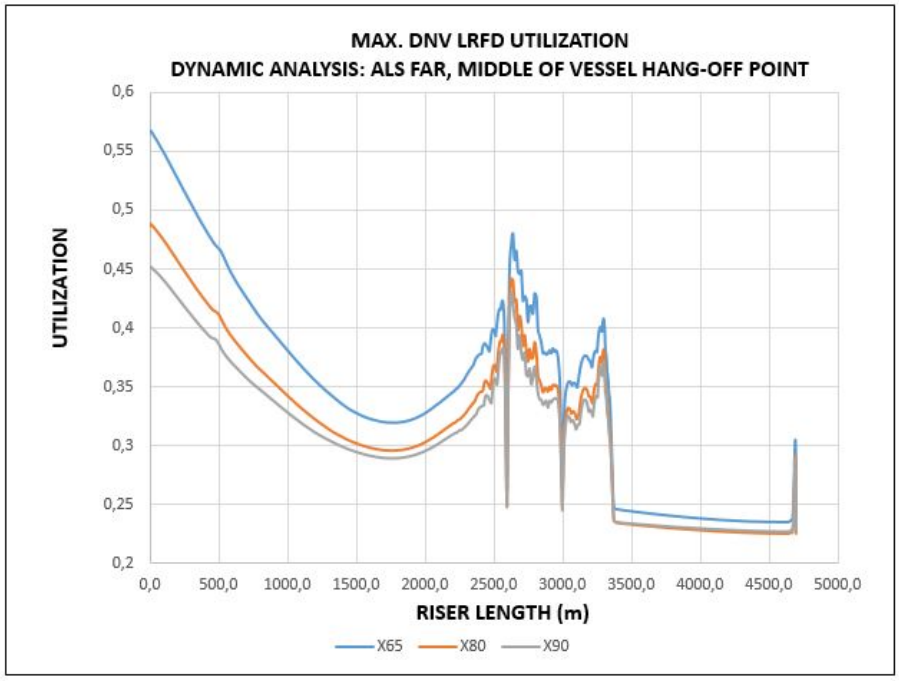

Figure C.21: Maximum DNV LRFD Utilization, Dynamic Analysis-ALS Far, Middle of Vessel Hang-off Point

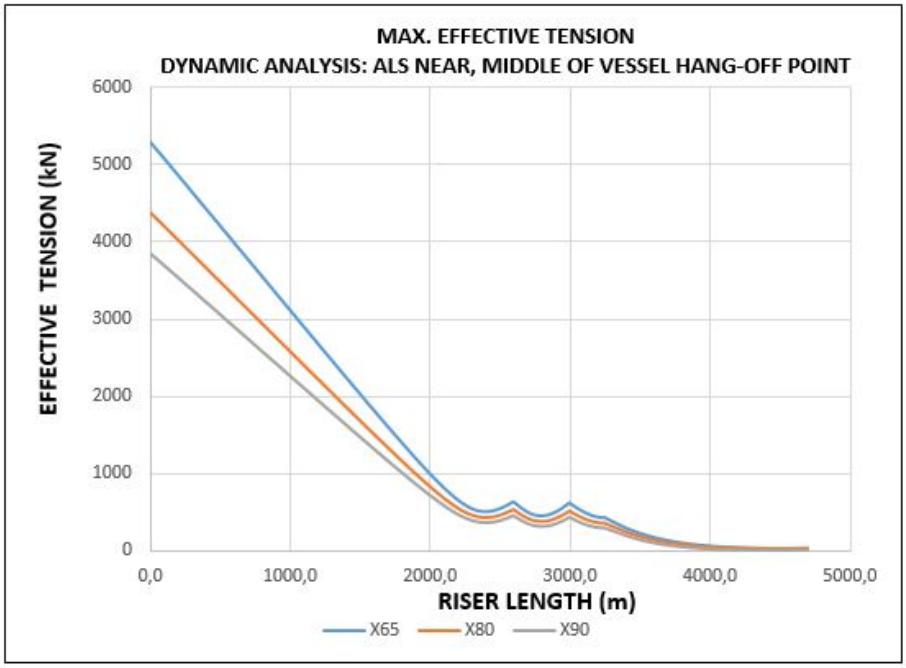

Figure C.22: Maximum Effective Tension, Dynamic Analysis-ALS Near, Middle of Vessel Hang-off Point

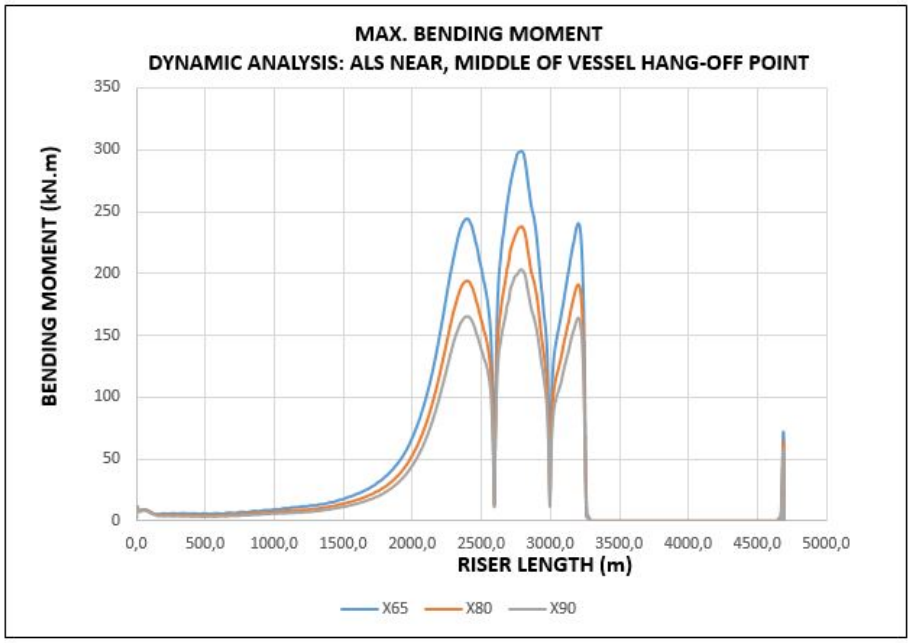

Figure C.23: Maximum Bending Moment, Dynamic Analysis-ALS Near, Middle of Vessel Hang-off Point

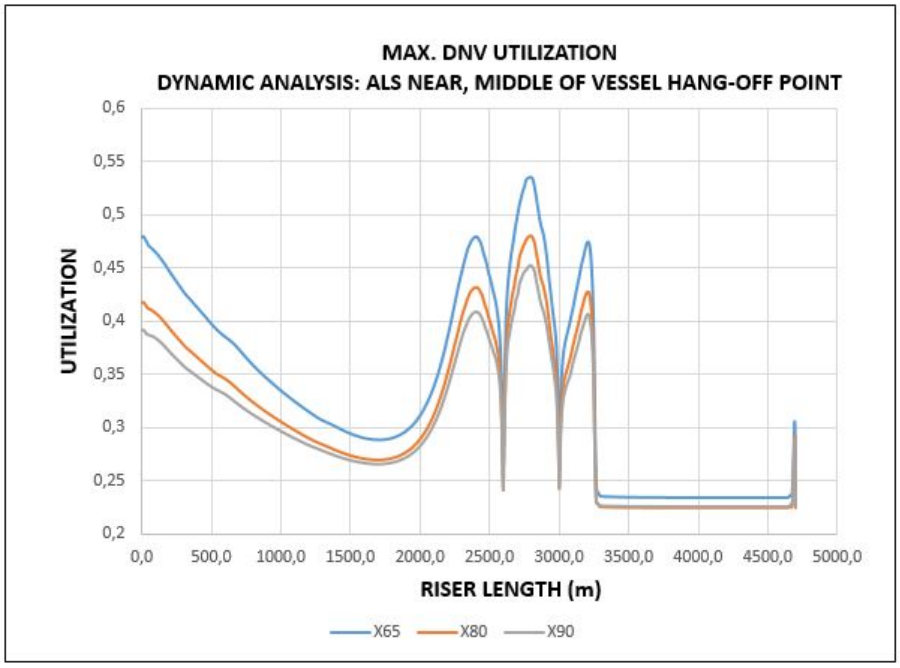

Figure C.24: Maximum DNV LRFD Utilization, Dynamic Analysis-ALS Near, Middle of Vessel Hang-off Point